Mantle dynamics in the Mediterranean

Claudio Faccenna, Thorsten W. Becker, Ludwig Auer, Andrea Billi, Lapo Boschi, Fabio A. Capitanio, Francesca Funiciello, Ferenc Horvàth, Laurent Jolivet, Claudia Piromallo, et al.

AGU PUBLICATIONS

Reviews of Geophysics

REVIEW ARTICLE
10.1002/2013RG000444

Key Points:
- Subduction drives the evolution of the Mediterranean
- Tyrrhenian and Hellenic subduction zones induce a large-scale return flow
- Surface deformation is coupled to and drived by upper mantle return flow

Correspondence to:
C. Faccenna,
claudio.faccenna@uniroma3.it

Citation:
Faccenna, C., et al. (2014), Mantle dynamics in the Mediterranean, *Rev. Geophys.*, *52*, doi:10.1002/2013RG000444.

Received 9 OCT 2013
Accepted 16 APR 2014
Accepted article online 23 APR 2014

Mantle dynamics in the Mediterranean

Claudio Faccenna[1], Thorsten W. Becker[2], Ludwig Auer[3], Andrea Billi[4], Lapo Boschi[5], Jean Pierre Brun[6], Fabio A. Capitanio[7], Francesca Funiciello[1], Ferenc Horvàth[8], Laurent Jolivet[9], Claudia Piromallo[10], Leigh Royden[11], Federico Rossetti[1], and Enrico Serpelloni[10]

[1]Dip. Scienze, Università Roma TRE, Rome, Italy, [2]Department of Earth Sciences, University of Southern California, Los Angeles, California, USA, [3]Eidgenössische Technische Hochschule Zürich, Zürich, Switzerland, [4]Consiglio delle Nazionale Ricerche, IGAG, Rome, Italy, [5]ISTEP, UPMC-CNRS, Paris, France, [6]Géosciences Rennes, Université de Rennes 1, CNRS, Rennes, France, [7]School of Geosciences, Monash University, Clayton, Victoria, Australia, [8]Institute of Geography and Earth Science, Eötvös University, Budapest, Hungary, [9]Univ d'Orléans, ISTO, Orléans, France, [10]Istituto Nazionale di Geofisica e Vulcanologia, Italy, [11]Department of Earth, Atmospheric, and Planetary Sciences, Massachusetts Institute Technology, Cambridge, Massachusetts, USA

Abstract The Mediterranean offers a unique opportunity to study the driving forces of tectonic deformation within a complex mobile belt. Lithospheric dynamics are affected by slab rollback and collision of two large, slowly moving plates, forcing fragments of continental and oceanic lithosphere to interact. This paper reviews the rich and growing set of constraints from geological reconstructions, geodetic data, and crustal and upper mantle heterogeneity imaged by structural seismology. We proceed to discuss a conceptual and quantitative framework for the causes of surface deformation. Exploring existing and newly developed tectonic and numerical geodynamic models, we illustrate the role of mantle convection on surface geology. A coherent picture emerges which can be outlined by two, almost symmetric, upper mantle convection cells. The downwellings are found in the center of the Mediterranean and are associated with the descent of the Tyrrhenian and the Hellenic slabs. During plate convergence, these slabs migrated backward with respect to the Eurasian upper plate, inducing a return flow of the asthenosphere from the back-arc regions toward the subduction zones. This flow can be found at large distance from the subduction zones and is at present expressed in two upwellings beneath Anatolia and eastern Iberia. This convection system provides an explanation for the general pattern of seismic anisotropy in the Mediterranean, first-order Anatolia, and Adria microplate kinematics and may contribute to the high elevation of scarcely deformed areas such as Anatolia and eastern Iberia. More generally, the Mediterranean is an illustration of how upper mantle, small-scale convection leads to intraplate deformation and complex plate boundary reconfiguration at the westernmost terminus of the Tethyan collision.

1. Introduction

Squeezed between two converging large plates, the Alpine-Mediterranean mobile belt presents intriguing tectonic features that have been the focus of decades of geological study. Mountain edifices, narrow arcuate belts, extensional basins, active volcanoes, violent earthquakes, and tsunamis have given the *Mare Nostrum* a distinctive geological fingerprint, attracting the attention of generations of Earth scientists since the early masterpiece of *Argand* [1924]. Over the years, the Mediterranean has provided a unique and manifold geological instance to test, improve, and even challenge the foundations of plate tectonic theory. *Argand* [1924], first, and *Carey* [1955], later, pointed out that the tectonic evolution of the Mediterranean was characterized by oroclinal bending, that is the process leading to the curvature of an originally linear collisional zone and defined its relationship to block rotations and opening of back-arc basins, that is the opening of a basin located to the back of the volcanic arc (e.g., Sardinia-Corsica microblock and opening of the Liguro-Provençal basin; see Figure 1 for major geological features, respectively). *McKenzie* [1970, 1972, 1978] presented the first detailed map of active deformation in the Mediterranean region, showing the importance of extensional and strike-slip tectonics within the overall convergence. These works also first introduced the "extrusion" or "escape" mechanism, to define the motion of continental material away from collision zone related to forces due to continental buoyancy. The evolution of the Alpine structure in the Mediterranean framed within the Africa-Eurasia convergence system was analyzed from the early 1970s [e.g., *Smith*, 1971; *Dewey et al*., 1975], and *Alvarez et al*. [1974] recognized that the Alpine chain translated and split

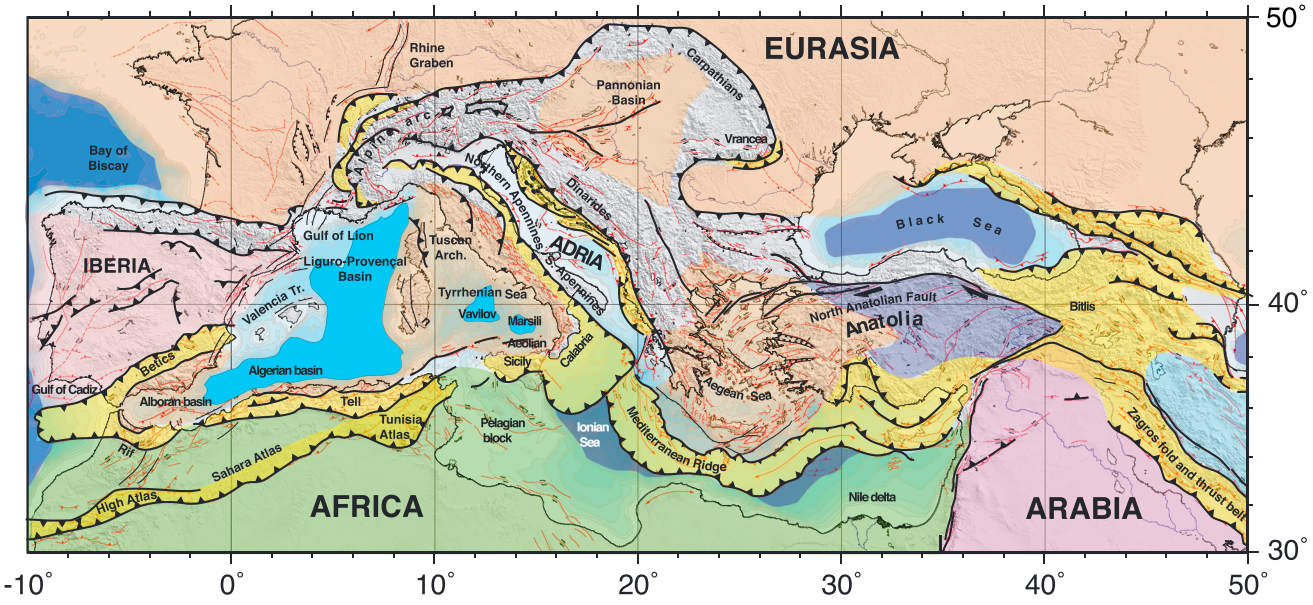

Figure 1. Plate tectonic setting of the Mediterranean.

apart during the back-arc extensional process. *Horvath and Berckhemer* [1982], and later *Dewey et al*. [1989], provided the basis for a more quantitative analysis of the Africa-Eurasia shortening.

The conceptual model of trench rollback was originally applied to the Mediterranean. This mechanism was first introduced by *Dewey* [1980] to illustrate the backward/oceanward motion of the trench with respect to the upper plate. This kinematic analysis was mainly based on the fundamental concept that old oceanic lithosphere is negatively buoyant, and therefore, it may be pulled downward producing a retrograde motion [e.g., *Elsasser*, 1971; *Molnar and Atwater*, 1978; *England and Wortel*, 1980] and leading to rollback if the subduction is larger than the convergence rate. The opening of the Mediterranean Basin as a back-arc or marginal basin was first suggested in the Mediterranean by *Boccaletti and Guazzone* [1974] for the Apennines, *Le Pichon and Angelier* [1981] for the Aegean, and later made clear by *Malinverno and Ryan* [1986] for the Apennines-Tyrrhenian system. The analysis of foredeep structure by *Royden et al*. [1987] and *Royden* [1993] quantifies the role of a sublithospheric load to flex the subducting lithosphere, further developing the concepts of slab pull and of trench rollback, even for the case of continental lithosphere. Another important step in the quantitative understanding of the role of mantle dynamics in this area comes from the contributions of the Utrecht University group, summarized in the seminal paper by *Wortel and Spakman* [2000], whose core idea consisted in coupling deep tomography with shallow tectonics to better understand mantle geodynamics. This study introduced the concept that the disruption of lithospheric slab during subduction can be the cause of differential trench migrations. The Mediterranean, its arcs, and their polarity provided a test for models considering the role of global mantle flow on subducting slabs and their potential impact on surface kinematics [*Doglioni et al*., 1999]. Far from being complete, this short overview highlights the relevance of the Mediterranean as a natural laboratory and source of inspiration for understanding global geodynamic processes.

Our aim here is to discuss the role of mantle convection on the tectonics of the Mediterranean and, more generally, how and if the deep mantle processes may be expressed on the surface.

The paper is divided in two parts to separate data from models. In the first part, we provide a summary of the present-day to recent deformation from geology and geodesy (section 2), review the crustal (section 3) and mantle structure (section 4), illustrate the tectonic evolution of the region over the last 30 Ma (section 5), and end by pointing out outstanding questions (section 6). In the second part, we discuss the role of mantle convection in Mediterranean deformation. This includes a discussion of the consistency between tomography and tectonics models (section 7), and a reconstruction of the subduction history and related models (section 8). We then explore the results of mantle convection models, to understand if and how

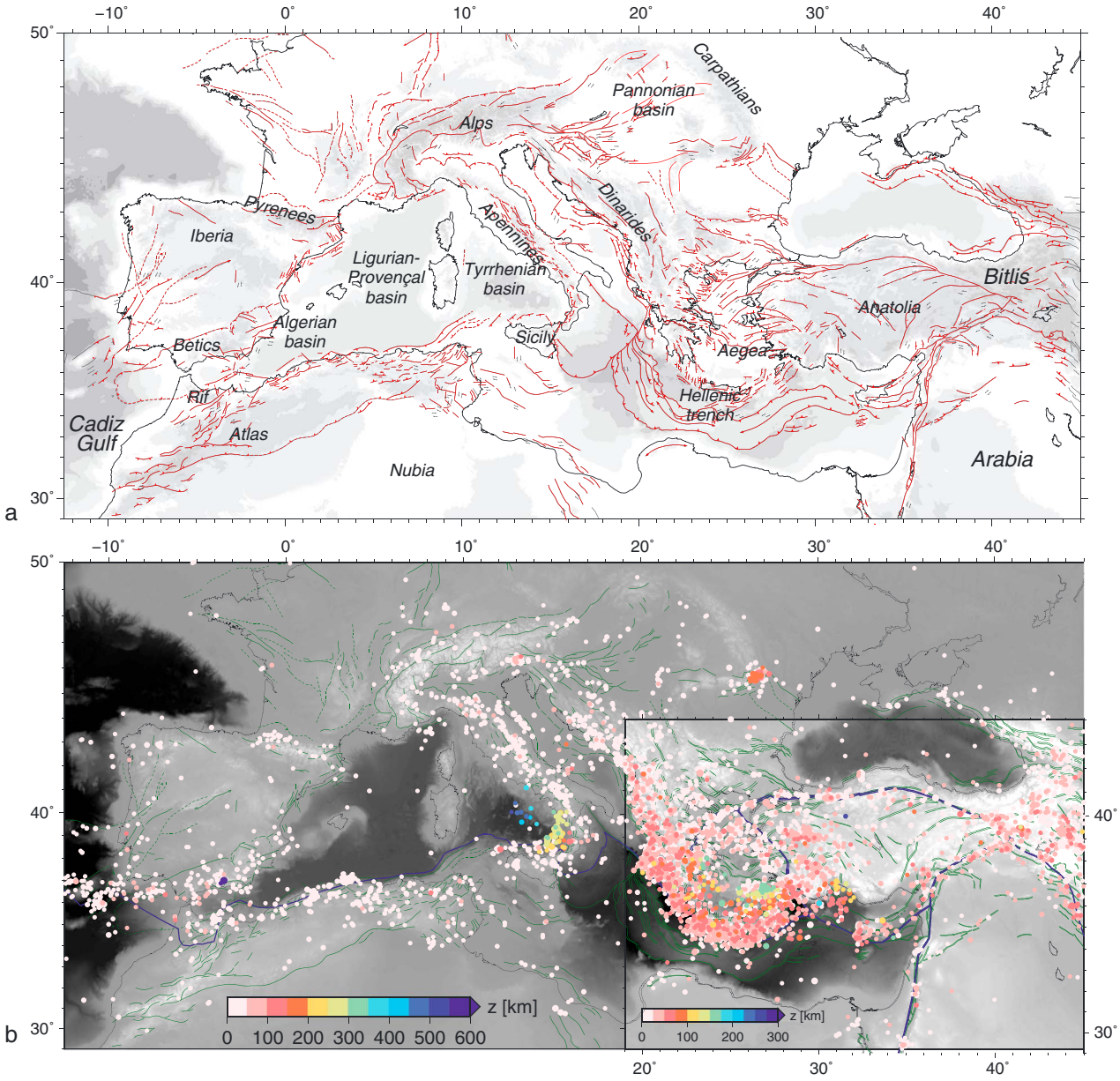

Figure 2. Tectonic, seismic, and geodetic indicators of lithospheric deformation. (a) Large-scale topography and active fault zones within the study region. Quaternary to active faults from *Barrier et al.* [2004] are represented as solid red lines where well located, and by dashed lines where approximately located or inferred. Fault are distinguished between reverse (barbs on the upper side), strike slip (arrows along fault indicate direction of lateral movement), and normal (ticks on downthrown side). (b) Seismicity color-coded by hypocentral depth (International Seismological Centre catalog, magnitude range > 4).

mantle dynamics may explain the motion of Adria, Anatolia, and Aegean microplates (section 9), the patterns of seismic anisotropy (section 10), and the role of the mantle on shaping the topography features of the Mediterranean (section 11). We end by presenting the most likely scenario for the present-day pattern of mantle circulation.

The study area extends to the Middle East and the Pannonia-Carpathian systems (Figure 1); the latter is considered more for its tectonic affinity rather than geographical pertinence. We do not investigate the Alpine evolution of the region; we will rather concentrate on the formation of the most recent tectonic features, however, without disregarding the structural grain inherited from the collisional history of the Mediterranean. We will also address briefly the volcanological-geochemical aspects of the region but refer the reader to more detailed works on this topic [e.g., *Carminati et al.*, 2012; *Lustrino and Wilson*, 2007, and references therein].

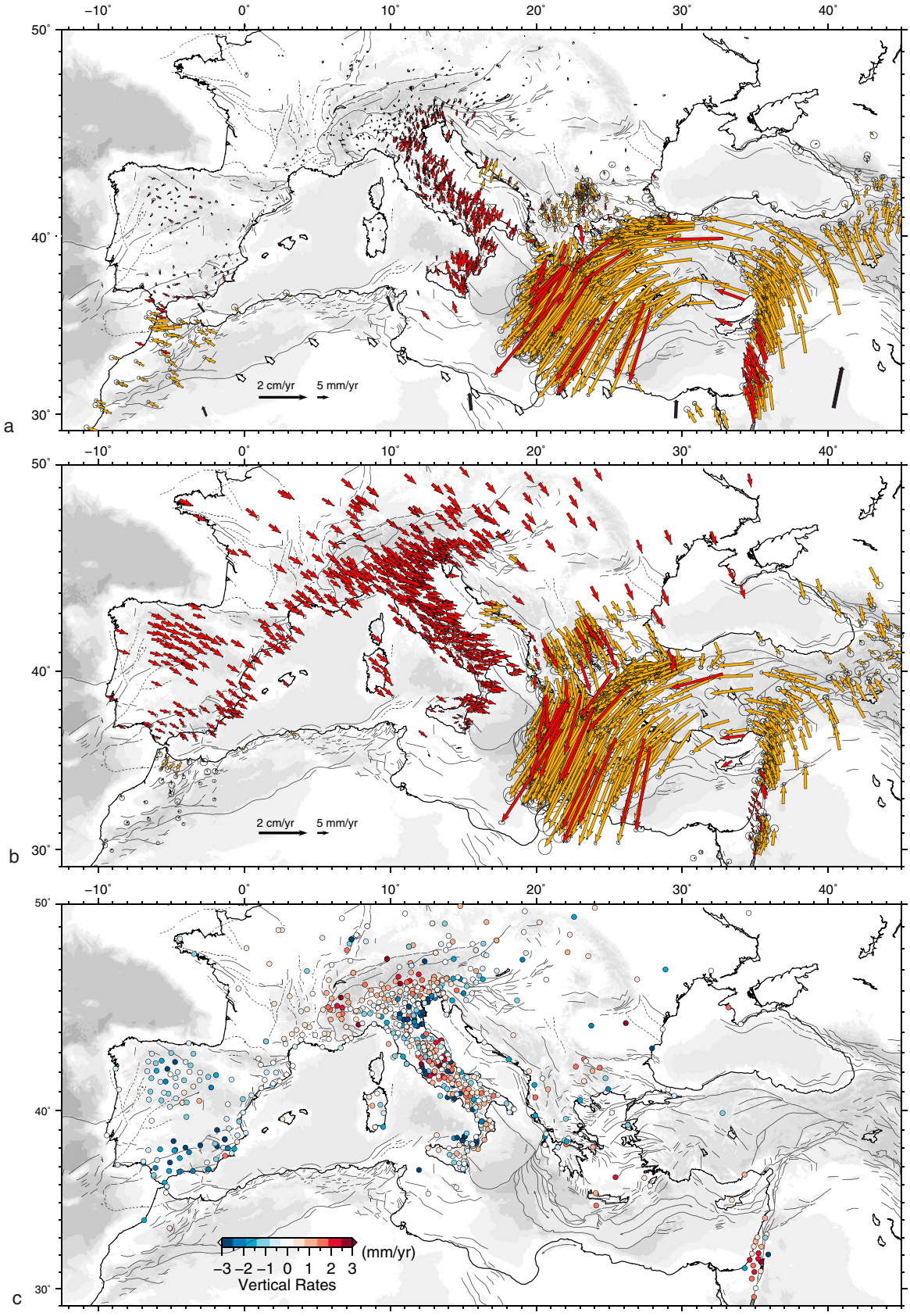

Figure 3

2. Present-Day to Recent Deformation

2.1. Crustal and Deep Seismicity

Active tectonics and seismicity in the Mediterranean is diffuse over vast areas and elongated belts (Figure 2). Seismicity is characterized by the occurrence of frequent low-to-moderate magnitude events and occasionally large (>7) magnitude earthquakes [e.g., *McKenzie*, 1972; *Jackson and McKenzie*, 1988; *Vannucci et al*., 2004; *Guidoboni et al*., 2007; *Serpelloni et al*., 2007; *Brandmayr et al*., 2010; *Godey et al*., 2013]. As illustrated in Figure 2, seismicity mainly localizes along the plates and microplates boundaries (i.e., Nubia, Eurasia, Adria, Arabia, and Anatolia). Shallow earthquake occurrence is widespread in the whole Mediterranean (Figure 2b), whereas deep and intermediate-depth events mainly cluster below the Hellenic Arc (depth ≤ 180 km), Cyprus Arc (depth ≤ 130 km), Calabrian Arc (depth ≤ 500 km), Betic-Rif (depth ≤ 160 km and a few isolated events at ~600 km depth), and eastern Carpathians (depth ≤ 220 km). Deeper seismicity is limited, mostly confined beneath the inner portion of the orogenic arcs. The deepest seismic zone is found beneath the Calabrian Arc, where a 70°-dipping Wadati-Benioff zone is found from 50 down to 450 km [e.g., *Gutenberg and Richter*, 1954; *Peterschmitt*, 1956; *Isacks and Molnar*, 1971; *Giardini and Velona*, 1991; *Selvaggi and Chiarabba*, 1995].

The map of instrumental seismicity of the Mediterranean and adjacent areas well illuminates the shallow seismicity zones where most elastic energy is released mainly through low-to-intermediate magnitude earthquakes (Figure 2b). We will briefly illustrate the style of active and seismic deformation from west to east. The Moroccan and Algerian coastal areas along the Mediterranean Sea display seismicity on faults accommodating, with compressional and strike-slip mechanisms, the oblique convergence between Africa and Eurasia (Figures 3a and 4a). This deformation belt extends to the east to northern Sicily and is localized along the southern margin of the Alboran, Algerian, and Tyrrhenian Sea [*Goes et al*., 2004; *Dévèrchere et al*., 2005; *Stich et al*., 2006, *Billi et al*., 2007; *Mauffret*, 2007; *Serpelloni et al*., 2007; *Doglioni et al*., 2012]. The onset of this compressional belt produced the tectonic "inversion" of the basin margins, from extension to compression, and propagated eastward from the Alboran (~8 Ma) to the Tyrrhenian margin (younger than ~2 Ma), following the progressive cessation of northward subduction of the African Plate [*Billi et al*., 2011] (see also section 5). Among other important recent and historical events here, the 2004, M_w 6.3, Al Hoceima (Morocco), the 1980, M_w 7.1, El Asnam, and the 2003, M_w 6.9, Boumerdès (Algeria) earthquakes [*Meghraoui et al*., 2004; *Stich et al*., 2005] are representative of the active tectonics in this sector of the Mediterranean. Active compressional structures are also described on the Ligurian margin and in southern France (Provence), where earthquake occurrence indicates that active compression occurs along south-verging thrusts. The 1909, M_s 6.2, Provençe earthquake represents the strongest latest thrust reactivation [*Chardon and Bellier*, 2003].

Active tectonics in the Italian Peninsula is heterogeneous (Figures 2–4). The south-Tyrrhenian compressional domain terminates in northeast Sicily [*Pondrelli et al*., 2004; *Billi et al*., 2007; *Serpelloni et al*., 2010], as the Tyrrhenian side of the Calabrian Arc and central-southern Apennines is dominated by extension (Figure 4) [*Montone et al*., 2004; *Serpelloni et al*., 2007; *D'Agostino et al*., 2011; *Presti et al*., 2013]. In the Calabrian Arc and eastern Sicily, southern Italy, several strong earthquakes rupturing normal faults under NE-SW extension (Figure 3a) have repeatedly caused damage and casualties in historical and recent times. Among the most destructive ones, the 1908, M_w 7.1, Messina Straits and the 1693, M_w 7.4, Hyblean earthquakes [*Valensise and Pantosti*, 1992; *Bianca et al*., 1999] were both followed by strong tsunamis in the Ionian Sea [*Billi et al*., 2008, 2010]. The central and southern Apennines (Italy) are sites of numerous earthquakes rupturing along NW-SE striking normal faults up to M_w 7, including, for instance, the 1857, M_w 7, Agri Valley, the 1915, M_w 7, Avezzano, and the 1980, M_w 6.9, Irpinia destructive events. The eastern boundary of the Adria microplate (Figures 1 and 2) is surrounded by active compression. Active compression normal to fold-thrust belts is found along the northern Apennines [*Bennett et al*., 2012], in the eastern Alps [*Bennett et al*., 2012; *D'Agostino et al*., 2005], and on the eastern side of the Adriatic Sea, along the Dinarides-Albanides orogenic system. Two destructive earthquakes of M_w ~7.1 and ~7.3 occurred in 1348 in Karinthia and Friuli (Austrian and Italian Alps,

Figure 3. Geodetic velocities. We show horizontal velocities, with 68% error ellipses, given with respect to (a) the Eurasian and (b) the Nubian Plate. Red and orange arrows show velocities from *Serpelloni et al*. [2013] and published solutions, respectively (see text for references). Grey tick arrows show Nubia-Eurasia plate motions, form the relative Nubia-Eurasia Euler pole and black arrows are long-term plate velocities from MORVEL [*DeMets et al*., 2010] (both in Eurasia-fixed reference frame); (c) vertical velocities of continuous GPS sites from *Serpelloni et al*. [2013], the color scale is saturated at ±3 mm/yr. Positive (red) and negative (blue) values show uplift and subsidence, respectively.

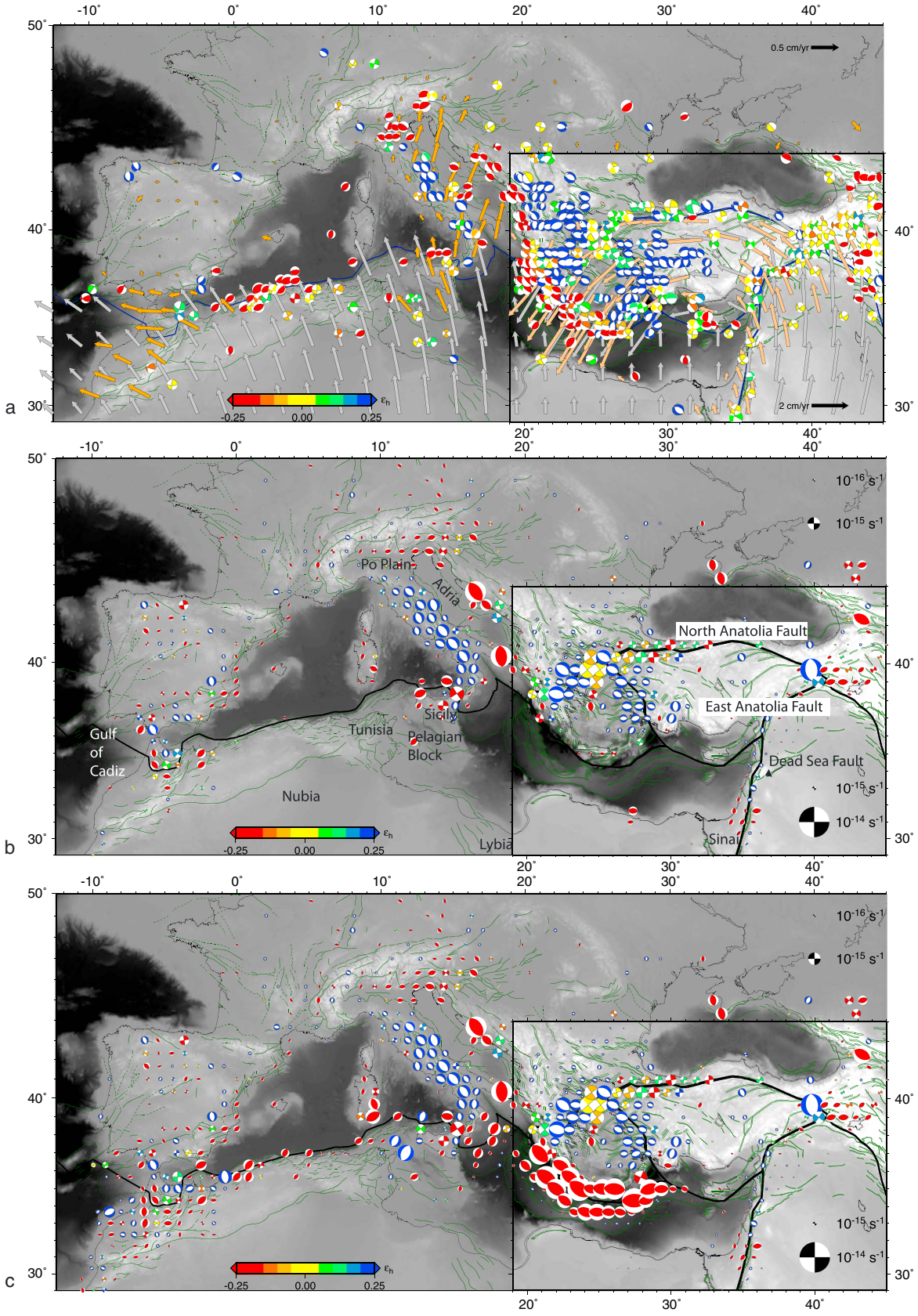

Figure 4

respectively) are representative of active seismicity rupturing active thrust with NS bearing compression (Figure 4a). The Dalmatian coastline of the Dinarides shows high seismicity rates with events of magnitude up to 6 along NW-SE striking thrust faults. Energy release increases toward the southeast, and a $M_w = 7.2$ event was recorded in 1979 in Montenegro [*Kuk et al*., 2000]. To the south, along the active subduction of the Ionian Sea beneath Calabria (Figures 2 and 3), compression [*Minelli and Faccenna*, 2010; *Polonia et al*., 2013] is also active but is not associated to a significant seismic moment release, likely because of low "coupling" at the subduction interface [*Serpelloni et al*., 2010].

Recent and active tectonics of the eastern Mediterranean is likewise complex and characterized by some of the world's most intense seismicity. The eastern Mediterranean has been recently and historically struck by strong to very strong earthquakes on the seismically capable faults in the Hellenic Arc, Cyprus Arc, North Anatolian and East Anatolian Faults, and Dead Sea Transform Fault. A few events of these historical earthquakes reached M_w 7, such as the 1170, M_w 7.7, Syria-Lebanon and the 1202, M_w 7.6, Lebanon earthquakes [*Guidoboni et al*., 2007], and rarely M_w 8, such as the 1068, M_w 8.1, Elat (Israel), and the 365 and 1303, $M_w \geq 8$, Crete earthquakes.

The North Anatolian Fault and the Dead Sea Transform Fault are among the most seismically active faults of all the Mediterranean region and adjacent areas. Global Position System (GPS) measurements give a rate of 24 ± 1 mm/yr of right-lateral slip along the North Anatolian Fault and a less well-constrained rate of ~10 mm/yr of left-lateral slip on the East Anatolian Fault [*Barka and Reilinger*, 1997; *Reilinger and McClusky*, 2011; *Kurt et al*., 2013] (Figure 3a). Geological estimates for the North Anatolian arrive at slightly lower rates (for a summary, see *Molnar and Dayem* [2010]; *Hubert-Ferrari et al*. [2002]: between 12.5 mm/yr and 23 mm/yr; *Kozacı et al*. [2007]: 20.5 ± 5.5 mm/yr; *Kozacı et al*. [2009]: $18.6^{+3.5}_{-3.3}$ mm/yr; and *Pucci et al*. [2008]: 15.0 ± 3.2 mm/yr on a separate splay). Recent and active tectonics of the eastern Mediterranean is likewise complex and characterized by some of the world's most intense seismicity. The North Anatolian Fault generated several large earthquakes such as the 1999, M_w 7.4, Izmit event. The Holocene slip rate determined through marine studies and ^{14}C dating (~10 mm/yr) is smaller than the GPS-determined rate [*Polonia et al*., 2004]. The Dead Sea Transform Fault in the Middle East is a major left-lateral strike-slip fault [*Garfunkel*, 1981] accommodating ~1 to 5 mm/yr of slip rate, depending on the fault segment [*McClusky et al*., 2003; *Westaway*, 2003, 2004; *Karabacak et al*., 2010]. GPS data give sinistral motion at rate between 3 and 5 mm/yr [*Wdowinsky et al*., 2004; *Gomez et al*., 2007; *Le Beon et al*., 2008; *Reilinger et al*., 2006, *Molnar and Dayem*, 2010]. This fault system has a long history of strong and often destructive historical earthquakes. As the Middle East has been inhabited for millennia, archeological evidences of historical earthquakes are numerous [e.g., *Meghraoui et al*., 2003]. Cities such as Jericho, the oldest city in the world, were repeatedly hit and severely damaged by strong earthquakes [*Ben-Avraham et al*., 2005]. *Khair et al*. [2000] compiled a seismic catalog of historical earthquakes with estimated magnitude (M_s and M_l) larger than 5.0 along the Dead Sea Transform Fault. This catalog includes 82 earthquakes between 2150 B.C. and 1997 A.D. During the last millennium, the strongest earthquakes (M_s 7.4–7.5) occurred in 1822, 1759, 1201, and 1170. The August 1822 event, in particular, destroyed 60% of Aleppo and was felt in all of the Middle East.

2.2. Geodesy and Kinematics

Starting in the early 1990s, the increasing number of Global Positioning System measurements in the Euro-Mediterranean region has provided denser and more accurate surface velocity fields. It is now possible to image crustal deformation and, in well-sampled regions, resolve slip rates on major faults. A review of the kinematics revealed by two decades of GPS measurements from campaign acquisitions across the Mediterranean area has been recently presented in *Nocquet* [2012].

Here we combine a new three-dimensional geodetic velocity solution [*Serpelloni et al*., 2013], obtained from the analysis of more than 800 continuous GPS (cGPS) stations, with velocities published in the recent literature, aiming to fill some of the gaps in the heterogeneous distribution of cGPS sites around the

Figure 4. (a) Interpolated GPS velocities (orange vectors, a smoothed representation of data in Figure 3a, obtained by first averaging velocities weighted by their uncertainties on a $1° \times 1°$ grid, and then using spline-in-tension interpolation [*Smith and Wessel*, 1990]), NNR-MORVEL56 [*Argus et al*., 2011] long-term plate velocities (gray vectors, both in Eurasia-fixed reference frame), and Kostrov summed Harvard/gCMT moment tensor solutions (depth < 75 km), colored by their mean horizontal strain, and normalized by the tensor norm. (b) Horizontal strain rate field inferred from the interpolated geodetic velocities shown as moment tensors, where blue, red, and green indicate extensional, compressional, and strike-slip types of deformation state. (c) Same plot as in Figure 4b but allowing for rigid plate motions within the Nubia Plate away from where there is GPS data, minimum distance for infill is 150 km.

Mediterranean area. In particular, we used velocities from *Reilinger et al*. [2006], *Le Beon et al*. [2008], *Alchalbi et al*. [2010], and *Floyd et al*. [2010] for the eastern Mediterranean and Middle East, from *Burchfiel et al*. [2006] and *Bennett et al*. [2008] for the Balkans, and from *Serpelloni et al*. [2007] and *Koulali et al*. [2011] for northern Africa and the western Mediterranean. The published velocities considered are originally defined in different realization of the stable Eurasian Plate and can be aligned to a common reference frame by estimating the six parameters (three rotations and three translations) of a Helmert transformation using stations that are in common between the different solutions and a reference solution. We first estimate the absolute Eurasian pole of rotation starting from *Serpelloni et al*. [2013] horizontal velocities, defined in the International Global Navigation Satellite Systems Service (IGS) realization of the International Terrestrial Reference Frame 2008 [*Altamimi et al*., 2011; *Rebischung et al*., 2011], which is located at 97.9°E/55.6°N, and rotates at angular velocity of 0.261°/Myr, and then align the published solutions to this Eurasian-fixed reference frame. We also show the combined velocity field in a Nubia-fixed reference frame, defined by a rotation pole, estimated from *Serpelloni et al*. [2013] absolute velocities, and located at 79.9°E/49.6°N, rotating at angular velocity of 0.270°/Ma with respect to IGS08.

Although geodetic solutions show some differences in the definition of the instantaneous Nubia/Eurasia relative rotation pole (see *Serpelloni et al*. [2007] and *Nocquet* [2012] for a summary), most of the recent studies [e.g., *Serpelloni et al*., 2010; *D'Agostino et al*., 2011; *Reilinger and McClusky*, 2011; *Altamimi et al*., 2012; *Saria et al*., 2013] agree as to a pole of rotation located offshore west of Africa (25 ± 5°W, 5 ± 5°S) with an angular velocity of ~ 0.06°/Myr. Such a pole predicts a convergence rate of ~5.5 mm/yr in a N25 ± 5°W azimuth at the longitude of Cyprus, with its magnitude westward slowly decreasing toward the west as directions swing from nearly north-south to northwest-southeast, changing to pure right-lateral strike-slip motion along the Gloria fault in the Atlantic and predicted NE-SW extension along the Terceira ridge, near the Azores triple junction. These trends are in general agreement with seismotectonic observations [*Vannucci et al*., 2004; *Serpelloni et al*., 2007], although the Arabia/Eurasia relative motion remains still debated [*Vernant et al*., 2004; *Vigny et al*., 2006; *Reilinger et al*., 2006; *Reilinger and McClusky*, 2011].

Figures 3a and 3b show horizontal velocities with respect to the Eurasian and Nubian plates, which delineate how the relative motions between the three major tectonic plates, Nubia, Eurasia, and Arabia, are accommodated within the Mediterranean and the surrounding Alpine belts. This figure highlights how domains of deformation are notably independent from the motion of the major tectonic plates. The most spectacular aspect of the GPS velocity field is in the eastern Mediterranean, where the zone of interaction of the Arabian and Eurasian plates indicates the counterclockwise rotations of a broad area of the Earth's surface including the Arabian Plate, adjacent parts of the Zagros and central Iran, Turkey, and the Aegean/Peloponnesus relative to Eurasia at rates in the range of 20–30 mm/yr [*Reilinger et al*., 2006; *Hollenstein et al*., 2008; *Floyd et al*., 2010; *Le Pichon and Kreemer*, 2010]. Rates increase toward the Hellenic Trench system. There, the Nubian lithosphere subducts beneath the continental lithosphere of the Aegean at a velocity close to 4 cm/yr, which contrasts with the slow (~6 mm/year) Nubia/Eurasia convergence rate. At the eastern end of this region, focused deformation occurs along well-defined and narrow (approximately few tens of kilometer) boundaries (the Dead Sea fault system, the East and North Anatolia Fault, and the Gulf of Corinth) and wider areas (western Turkey, and to a less extent the Aegean). Localized deformation appears clearer in the velocity field with respect to Nubia (Figure 3b). The increase of velocities toward the Hellenic Trench is westward, from Anatolia to the Aegean, and directed northward, reaching as far north as the southeastern Carpathians and Balkans mountains.

The second striking feature of the GPS velocity field is the abrupt decrease in the motion rates west of 20°E. In the central and western Mediterranean, velocities with respect to Eurasia are of the order of few millimeter per year, and show two patterns, the first spanning from northern Africa and Sicily, where sites move NW-ward at few mm/yr, and the second located in the circum-Adriatic area, where sites move NE-ward to northward at similar rates. Velocities with respect to Nubia highlight two "African" domains, the Pelagian/Sicily and the Moroccan Rif, where systematic deviations from the predicted Nubia-Eurasia plate motions are apparent (Figure 3a). Here direction of motion rotates and large strain rates occur [*Serpelloni et al*., 2010; *Koulali et al*., 2011]. Along the Italian Peninsula, the velocity field has two distinct main trends. Sites located on the Tyrrhenian side of the Apennine chain move toward the northwest, whereas sites located on the Adriatic side of the chain move toward the north-northeast. This differential motion results in the SW-NE oriented extensional deformation that characterizes the Apennines chain. In the northern Adriatic region, material comprising the northern Adriatic microplate rotates counterclockwise about an axis in northwestern

Italy [*Battaglia et al*., 2004; *D'Agostino et al*., 2008], resulting in NS shortening along the southeastern Alps. In the Pannonian Basin, velocities are NE-ward oriented, with decreasing rates toward the east. In the Balkans, GPS velocities show mainly southward motion, with increasing rates toward Greece [e.g., *Burchfiel et al*., 2006].

The third relevant and original aspect of the geodetic field is its vertical component. Newly emerging evidence of vertical ground deformation comes from the increasing number of cGPS stations over Europe. Figure 3c shows vertical velocities from *Serpelloni et al*. [2013] and highlights the presence of spatially coherent patterns of uplift and subsidence. In the western Mediterranean, Iberia shows a general pattern of regional subsidence, but with varying rates. Uplift is localized in central Iberia, and in southeastern Spain, whereas the fastest subsidence rates are close to −3 mm/yr and are located in southern Spain. The Alps show a general uplift, with fast rates (~2 mm/yr) in the western and central Alps, which decrease toward the eastern Alps turning to stable or negative values in the Slovenian Alps. Toward Eastern Europe, the Pannonian-Carpathians region shows slow subsidence in the Hungarian plain and stable or slow uplift in the Carpathians. Fast subsidence characterize the Po Plain in northern Italy, while the Apennines show differences in the vertical velocity pattern both along and normal to the mountain range, with the positive signal localized along the chain axis, characterized by the higher topographic relief, and fastest uplift rates in the central Apennines (~2 mm/yr). Calabria shows subsidence in its western (Tyrrhenian) side and uplift in its eastern (Ionian) side. The fastest subsidence rates (down to −10 mm/yr) of the Mediterranean are in the southern Tyrrhenian Sea. Eastern Mediterranean vertical deformation is less constrained by a smaller number of sites. The Balkan mountains of Bulgaria shows a rather coherent pattern of uplift, at rates of ~1.5 mm/y, and also Crete and the Cyclades show uplift at ~1 mm/yr. Continental Greece and the Gulf of Corinth subside at rates down to 2 mm/yr. The Levantine shows an increasing rate of uplift, up to 2 mm/yr, closer to the Dead Sea fault trace. The most striking feature of vertical deformation over Europe and the Mediterranean is the presence of undulations of the vertical velocity patterns, at different spatial scales, occurring both in tectonically active regions, such as the eastern Alps, Apennines, and eastern Mediterranean, and in regions characterized by a low or negligible tectonic activity, such as central Iberia and western Alps. These undulations correlate with topographic features in general.

The match between coseismic strain and geodetic strain rates is illustrated in Figure 4. Figure 4a shows an interpolated and smoothed horizontal geodetic velocity field, in the Eurasia-fixed reference frame, based on the GPS velocities shown in Figure 3a. For comparison, it also illustrates the velocity field estimated from NNR-MORVEL56 model [*Argus et al*., 2011] and the summed moment tensors from the gCMT catalog for depths < 75 km. Figures 4b and 4c show the horizontal strain rates inferred from the interpolated geodetic velocities of Figure 3a, and visualized as moment tensors in analogy to Figure 4a. Geodetic strain rates match the style of seismic strain from moment tensor summation, although the scarcity of GPS data in northern Africa prevents any reliable comparison between geodetic and seismic deformation styles along the seismically active belts of northern Algeria, Tunisia, and Libya (Figure 4b). Figure 4c shows geodetic strain rates based on GPS augmented with plate motion vectors in northern Africa obtained from a Nubia-Eurasia relative rotation pole located at 27°E/9.9°N and rotating counterclockwise at a rate of 0.057°/Ma. This solution, although based on the assumption that large part of northern Africa and the Ionian and Aegean seas move as part of a rigid Nubia plate, provides a more complete image of crustal deformation along the plate boundary. Along the northern Africa plate boundary crustal strain rates show E-W extension in the Gulf of Cadiz (Spain), N-S shortening along the Moroccan Rif, transtension in the Gulf of Cadiz (Spain), and approximately N-S shortening along the Moroccan Rif and Atlas, and change to NW-SE oriented shortening and strike-slip associated to the oblique Nubia-Eurasia convergence in northern Algeria [*Meghraoui and Pondrelli*, 2013]. Shortening, from geodetic and seismic data, is also present in southeastern Spain, whereas the Betics shows E-W extension, which continues in the Alboran Sea [*Stich et al*., 2006]. Strike-slip tectonics is present in Tunisia and Libya, representing a rather diffuse NW-SE trending shear zone, decoupling the Pelagian and Sicily block (southern Italy) from the Nubian Plate [*Serpelloni et al*., 2007, 2010]. Shortening is then transferred along the southern Tyrrhenian seismic belt, where geodesy indicates increasing shortening rates toward the central Aeolian region (southern Italy) and a transition to NW-SE extension in the Messina Straits [*Argnani et al*., 2007]. A good agreement between geodetic and seismic style of crustal strains is also found along the Hellenic Trench (Figure 4). Overall, geodetic deformation matches seismic deformation along the Italian Peninsula [e.g., *Hunstad et al*., 2003; *Angelica et al*., 2013], with extension normal to the Apennines

chain axes well imaged by divergence of the geodetic velocities (Figures 3b and 4a), decreasing from south to north. The northern Apennines show a transition from extension to compression toward the Po Plain (Italy), where active shortening is present along the mountain front and in the Po Plain [*Bennett et al*., 2012]. Approximately N-S shortening along the eastern Alps is well imaged by seismic and geodetic strains, and is associated with the NW-ward convergence between Adria and Europe [*D'Agostino et al*., 2005; *Devoti et al*., 2011; *Bennett et al*., 2012]. The NE-oriented collision between Adria and the Balkans is the cause of NE-SW oriented shortening along the eastern coasts of the Adriatic Sea (Figure 4). Geodetic deformation rates increase toward Ionian Greece, where strike-slip deformation mainly accommodates the southward motion of the Hellenic and Aegean areas with respect to Eurasia and the Adriatic region. Greece and Anatolia show the highest deformation and seismicity rates of the Mediterranean region, mainly along the Hellenic arc and the North Anatolia Fault (NAF) system (Figure 2b). The North Anatolia Fault is outlined by a narrow zone of pure dextral strike slip that widens within the North Aegean Sea and dies out abruptly at its western end (Figure 4). Geodetic and earthquake data agree in NE-SW oriented extension in continental Greece and western Anatolia, as a response to the increasing velocity from Anatolia to Aegea. The average rate of extension within most of the inner south Aegean is small, and an order of magnitude smaller than the extension rates within western Anatolia and continental Greece. Central Anatolia shows lower deformation rates than its northern and southern boundaries. The relative motion of Arabia, Anatolia, and the Sinai blocks is well recorded by seismic and geodetic deformation (Figures 3 and 4), with active thrusting and strike-slip tectonics along the East Anatolian Fault and the Dead Sea Fault.

These 3-D geodetic features are set within the framework of the slowly converging plate Eurasian and Nubian plates, pointing to the simultaneous interplay of different geodynamic processes needed to explain the complex kinematics [e.g., *McKenzie*, 1972; *Jackson and McKenzie*, 1988; *Faccenna and Becker*, 2010; *Le Pichon and Kreemer*, 2010; *Reilinger and McClusky*, 2011].

3. Crustal Structure

Several published compilations constrain the structure of the crust in the Mediterranean. Most of them use seismic data where active source reflection/refraction data and receiver function analysis serve mainly to detect the Moho discontinuity, and surface wave tomography can sense the associated velocity gradients for short period waves. Gravity analysis can also be used, although such work typically involves assumptions about isostatic compensation. Despite these long-standing efforts, crustal complexities and the lack of data in specific regions are apparent in the disagreement between different published models. In addition, there are a number of recent regional contributions investigating in detail specific areas that are not included in those compilations.

Figure 5 shows the crustal thickness from four larger scale models: (a) EuroMoho [*Grad et al*., 2009], (b) EuCrust07 [*Tesauro et al*., 2008], (c) EpCrust [*Molinari and Morelli*, 2011], and (d) CRUST1.0 [*Laske et al*., 2013]. They all are based on a mix of active source seismic profiles, body and surface waves, receiver functions as well as gravity data, and, as such, not independent estimates. In particular, EpCrust is mainly based on EuroMoho data, and CRUST1.0 used an averaging approach based on a range of regional models.

Consistent features of Moho structure include the following: (i) a thicker crustal beneath most of the orogenic belts, with peaks of more than ~50 km beneath the Alps, Pyrenees, and northern Hellenides; (ii) 10 to 20 km thin crust in the Liguro-Provençal, Tyrrhenian, and Ionian basins; (iii) a crustal thickness of ~25 km for the stretched continental domains such as the Alboran, Northern Tyrrhenian, and Aegean Sea and as thin as 15 km for the Cretan Sea; and (iv) a ~30 km thick crust in undeformed domains such as Iberia and France.

The detailed structure shows, however, relevant differences, in particular in areas of orogenic belts and in the Middle East. Beneath mountain belts, for example, the Moho is often doubled, with the Moho from the downgoing and upper plates being superposed and difficult to distinguish. Such complexities are usually smoothed out in large-scale models. The maps also show different crustal thicknesses for the Alps, from more than 50 to less than 40 km, in particular on the western part. For example, receiver function analysis shows a much thicker crust in the western Alps with respect to other models, more than ~50 km [*Di Stefano et al*., 2011]. The Moho depth beneath the Apennines is well constrained by active source seismic data [*Scrocca et al*., 2003, and references therein], receiver functions [*Piana Agostinetti and Amato*, 2009; *Di Stefano et al*., 2011; *Miller and Piana Agostinetti*, 2012], and shallow tomography studies [*Di Stefano et al*., 2009]. These

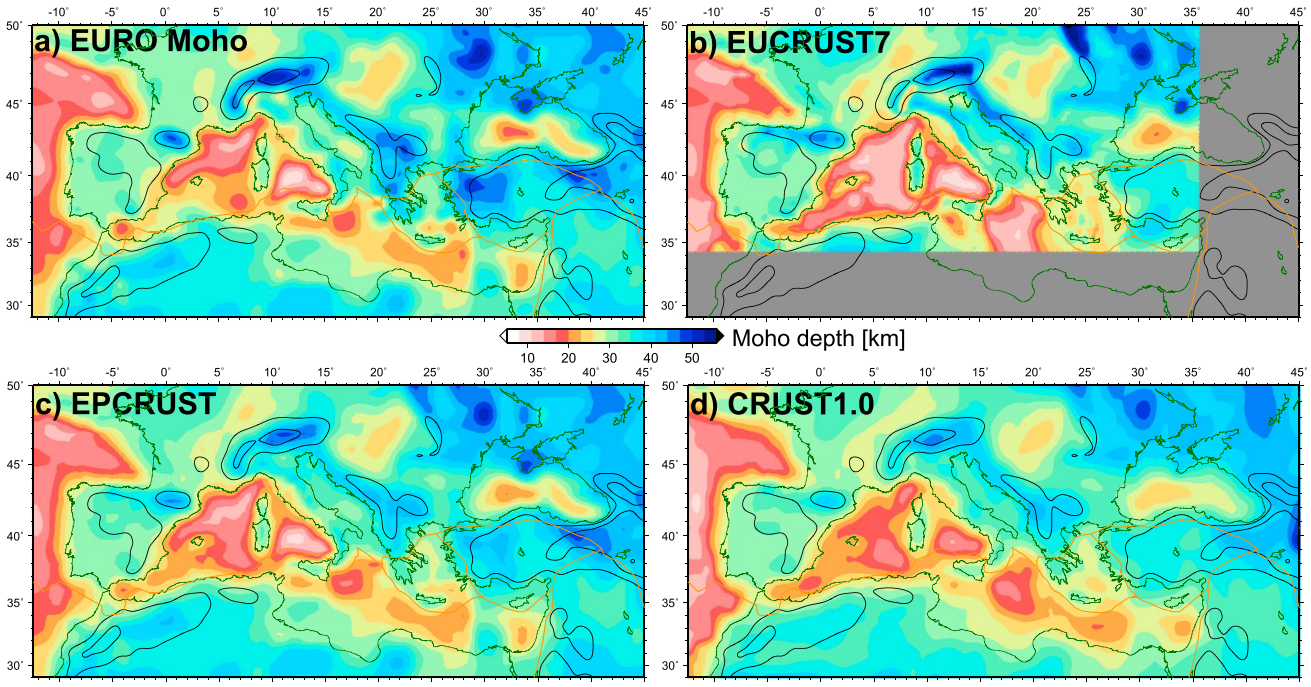

Figure 5. Comparison of crustal models for Moho depth. (a) EuroMoho [*Grad et al.*, 2009], (b) EuCrust07 [*Tesauro et al.*, 2008], (c) EpCrust [*Molinari and Morelli*, 2011], and (d) CRUST1.0 [*Bassin et al.*, 2000; *Laske et al.*, 2013]. Contours show long-wavelength (300 km Gaussian filter) smoothed, positive topography in 750 m contours to allow visual association of regions where high topography is mirrored by isostatically thickened crust.

studies show that the Adriatic crust is on average ~30–35 km thick and is flexed to a depth of ~40–50 km beneath the Tyrrhenian Sea, where the Moho is ~20–25 km thick (western Italy). Beneath the northern Apennines (northern Italy) and Calabria (southern Italy), the maximum crustal thickness is ~50 km, whereas beneath the central-southern Apennines, it is nowhere deeper than ~40 km. This trend is not clearly expressed in some of the large-scale model shown here. Crustal thicknesses in other orogens, such as the Bitlis or the Betics-Rif, are still poorly constrained.

Another region where discrepancies are large is western Anatolia. EuroMoho and EpCrust overestimate the thickness of the western and northwestern Anatolia compared to EuCrust07 which provides average values of ~30 km. However, the latter is in agreement with recent receiver function measurements, showing an average crust over western Anatolia ranging from 25 to 30 km [*Karabulut et al.*, 2013; *Vanacore et al.*, 2013].

As we will discuss later on, the uncertainties in crustal thickness will of course have consequences on the shallow structure imaged by seismic tomography, and on the estimate of the crustal component of isostatically supported topography.

4. Mantle Structure

4.1. Mantle Tomography

The detection of high- and low-seismic wave speed regions through seismic tomography has become a fundamental tool for linking tectonics and mantle geodynamics. The Mediterranean represents a key site where, from the early 1990s, tectonics models have been mutually compared and validated against seismic tomography models [e.g., *De Jonge and Wortel*, 1990; *Spakman*, 1990; *Wortel and Spakman*, 1992, 2000; *Spakman et al.*, 1993; *De Jonge et al.*, 1994; *Panza et al.*, 2007].

Seismic wave propagation is primarily sensitive to two resolvable parameters, the *P* and *S* wave velocity. Potential sources for seismic velocity anomalies imaged by tomography are temperature anomalies, compositional variations, the presence of partial melt, and anisotropy [see, e.g., *Nolet et al.*, 2007]. Given the strong sensitivity of upper mantle velocities to temperature variations [e.g., *Goes et al.*, 2000], velocity anomalies are here simply interpreted in terms of temperature anomalies in a first pass, as alternative interpretations, e.g., in terms of composition, would require further constraints.

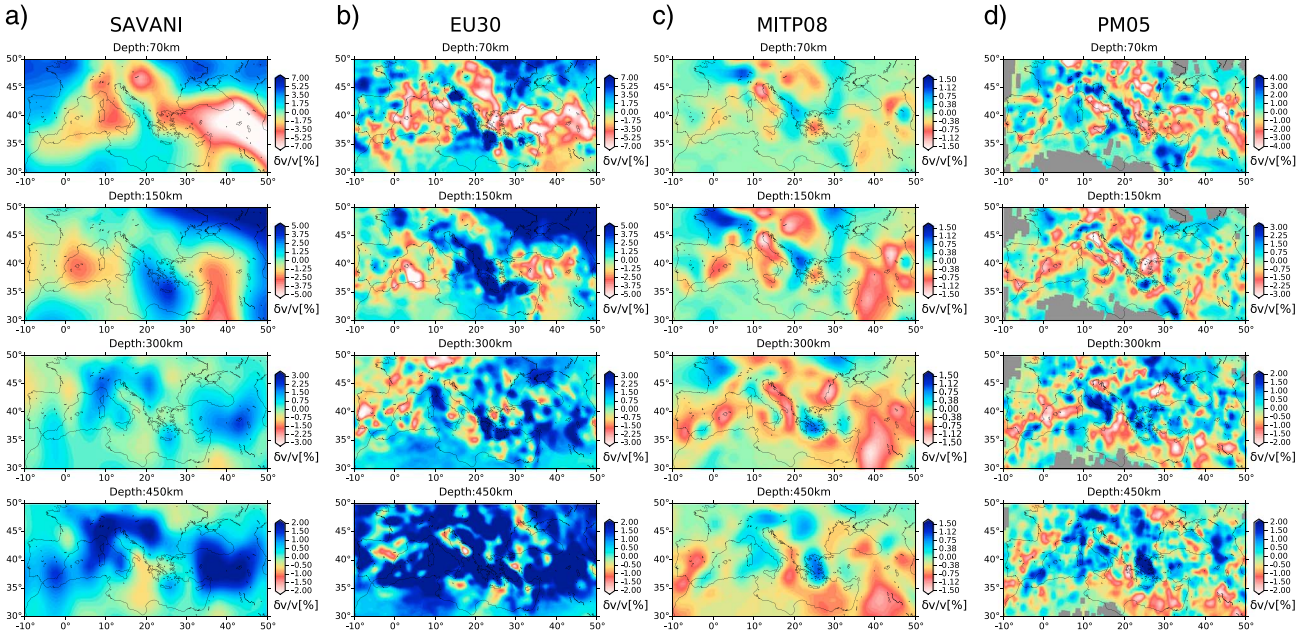

Figure 6. Comparison of tomographic models: *S* wave models (a) SAVANI [*Auer et al*., 2014] and (b) EU30 [*Zhu et al*., 2012] and *P* wave models (c) MITP08 [*Li et al*., 2008] and (d) PM0.5 [*Piromallo and Morelli*, 2003]. Horizontal layers in the upper mantle at 70, 150, 300, and 450 km. Seismic velocities are expressed as percent differences in wave speeds with respect to a reference model; note the difference in color scale for each panel.

The structure of the Mediterranean mantle is rather well illuminated by many different tomographic models. We show in Figures 6 and 7 a selection of representative *P* and *S* wave velocity models in the region of interest, expressed as percent differences with respect to their reference models. As expected, *P* and *S* models differ in terms of resolution, mainly because the former are based on body wave data only, while the latter also include surface wave observations. Generally, teleseismic *P* waves, which constitute the bulk of most data sets, are numerous but limited in depth resolution as they travel in the vertical direction over most of the upper mantle; this problem is only partially made up by using observations which improve crossing ray coverage, such as regional [e.g., *Piromallo and Morelli*, 2003] or shallow phases (*pP*, *pwP*, and *PP*, e.g., *Li et al*. [2008]), which are more difficult to measure than direct *P*. Body wave *S* data are less numerous than *P* data, but surface waves (fundamental modes and overtones), which are primarily sensitive to shear velocity, are strongly affected by the uppermost mantle structure and enhance vertical resolution in this depth range. The observed longer wavelength character of *S* [e.g., *Boschi et al*., 2009; *Schivardi and Morelli*, 2009] with respect to *P* [e.g., *Bijwaard et al*., 1998; *Piromallo and Morelli*, 2003; *Li et al*., 2008] models in the Mediterranean was first ascribed to sparser sampling (epicentral distances of *S* models often larger than ~10°). However, recent results obtained, e.g., by *Schmandt and Humphreys* [2010] based on USArray data indicate that, with a sufficiently dense sampling, resolution differences between body wave and surface wave-based models tend to be reduced (see, e.g., the comparison in *Becker* [2012]). In the case of the Mediterranean, this can be observed in Figures 6b and 6d, comparing model EU30 [*Zhu et al*., 2012] and the *P* model PM0.5 [*Piromallo and Morelli*, 2003], clearly characterized by heterogeneities of similar scale. The former represents a step forward in tomography resolution; it is obtained inverting the whole waveform by means of a numerical description of wave propagation and is clearly characterized by significant signal at short wavelengths compared, for example, to the *S* model SAVANI [*Auer et al*., 2014], obtained from a joint inversion of fundamental modes, overtones, and body wave data. Mapped anomaly amplitudes often vary widely among published tomographic models that, nevertheless, show similar patterns [e.g., *Becker*, 2012]. For example, *P* and *S* models of Figures 6 and 7 share a similar long- to intermediate-wavelength component (at scales larger than ~400 km), while discrepancies emerge at shorter wavelength.

The main large-scale tomographic structures at 70 km depth are the relatively high wave speeds of the East European Platform, Armorican Massif, east-Mediterranean sea and Adriatic Plate and the low velocities of central and eastern Europe, western Mediterranean and Tyrrhenian basins, Pannonian Basin and Anatolian

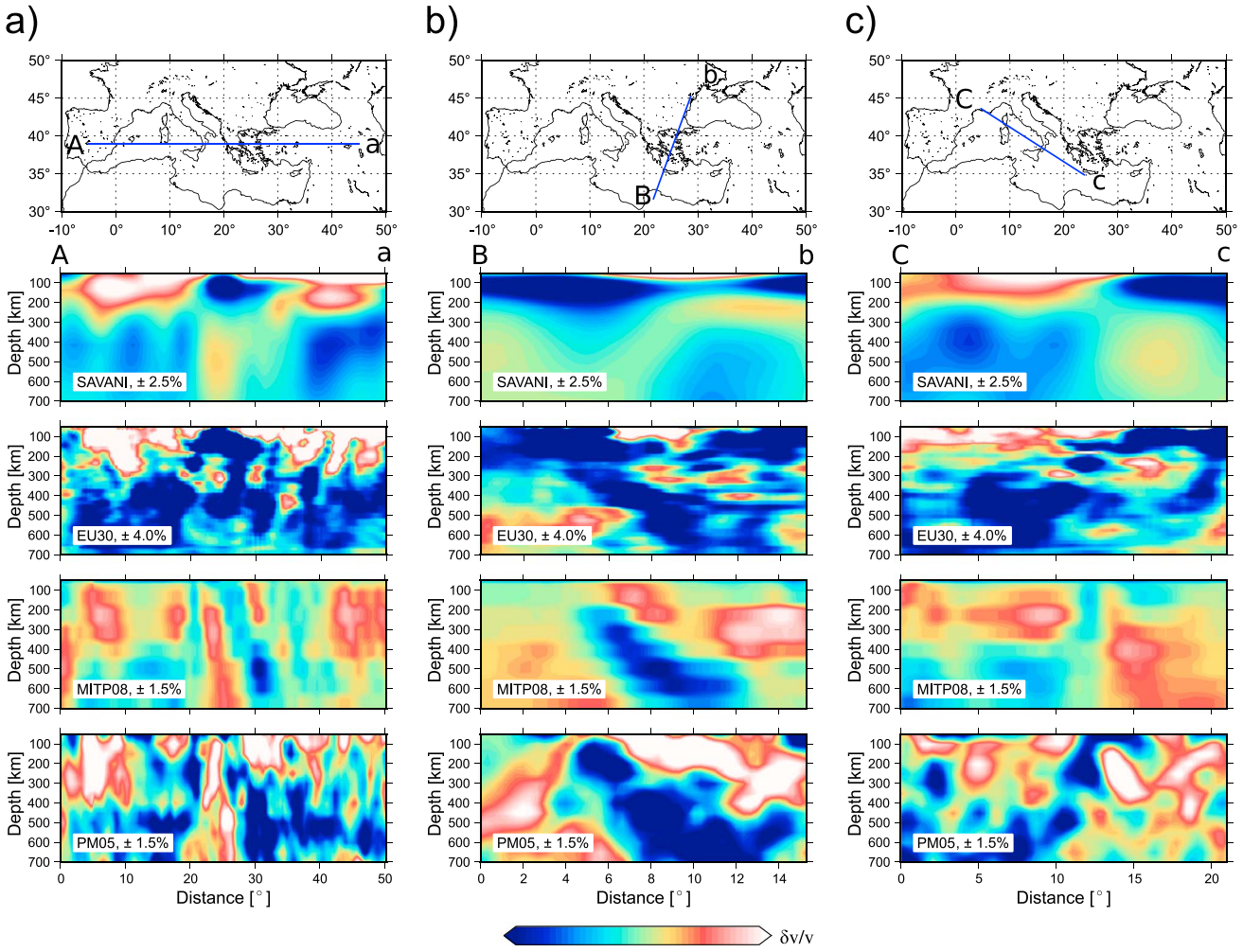

Figure 7. Vertical cross sections (length of cross sections is ~50° for AA′ and ~15° for BB′ and CC′) of tomographic *S* wave models SAVANI [*Auer et al*., 2014] and EU30 [*Zhu et al*., 2012] and *P* wave models MITP08 [*Li et al*., 2008] and PM0.5 [*Piromallo and Morelli*, 2003]. See text for details about the different models and description of imaged features. Note the difference in color scale for each panel.

Plate. At smaller spatial scales, models EU30 and PM0.5 (Figure 6) depict a discontinuous belt of high-velocity anomaly located beneath the Alpine-Mediterranean orogenic belt, extending from the Maghrebides, to the Calabrian Arc, (the Apennines, the Alps, and the Carpathians) to the Dinaric-Hellenic arc (also visible in MITP08 by *Li et al*. [2008]), commonly interpreted as subducted lithosphere [see, e.g., *Wortel and Spakman*, 2000]. Low wave speeds characterize areas related to the Cenozoic Rift System of Central and Western Europe. The fragmented signature of the Alpine subduction persists down to 150 km beneath the entire Alpine-Mediterranean belt (models EU30 and PM0.5), while at 300 km, it spreads in a more continuous and larger scale structure. These broader anomalies at 300 km depth are a common pattern among the four models. From this depth downward, models show pronounced differences, likely due to differences in the data and vertical resolution of the various models. High-velocity anomalies become dominant from 450 km, entering the transition zone, where subducted lithosphere stagnates atop the 660 km discontinuity [e.g., *Wortel and Spakman*, 2000; *Piromallo et al*., 2001; *Piromallo and Faccenna*, 2004; *Dando et al*., 2011; *Mitterbauer et al*., 2011; *Ren et al*., 2012]. All models show high wave speed heterogeneities accumulated below central-western Europe and the Aegean, with the exception of EU30 where high velocities cover the whole region of interest.

Cross sections in Figure 7 run along an EW oriented, longer profile (AA′) and two shorter profiles cutting the Aegean (BB′) and Calabrian (CC′) subduction zones roughly perpendicular to the arcs. The longer profile AA′ captures the anomaly pattern of alternating high and low velocities below the Mediterranean. Here it is

possible to detect high-velocity anomalies in correspondence of the deep inclined seismic zone at depth beneath the Aegean and Calabrian arcs plunging into the mantle in opposite directions (at ~20° and ~25° distance along AA'), separated by an elongated slow anomaly which in *P* models is consistently imaged from about 100 km depth downward. While EU30 detects a slow anomaly of much limited vertical extent (in the depth range 200–400 km), SAVANI depicts a smoother and deeper structure (from about 250 to 300 km downward). Both high-velocity slabs are identified as anomalies down to the transition zone and, more clearly by shorter wavelength models EU30, MITP08, and PM0.5; the Hellenic slab anomaly is thicker and particularly prominent. The slab continuity with depth, however, differs among models. Along profile BB', the Aegean anomaly in MITP08 is anticorrelated to EU30/PM0.5 above 200 km. The *S* model SAVANI seems to suggest a detachment along BB': in the depth range 300–400 km, the slab might be too thin to be resolved by the long-period surface waves which constitute the bulk of data on which SAVANI is based. The Calabrian high-velocity anomaly in EU30 shows a gap at about 300 km depth on profiles AA' and BB', which the authors interpret as slab detachment [*Zhu et al*., 2012], while the MITP08 and PM0.5 models suggest only limited thinning. The western Mediterranean and Tyrrhenian mantle are underlain by low wave speed anomalies slightly shallower in SAVANI and EU30 (down to ~200–300 km) than in MIT08 and PM0.5 (down to ~300–400 km) models. Differently, the Aegean supraslab mantle appears layered in the *S* models, with a high velocity sandwiched between a shallower and a deeper low velocity, a feature not seen in *P* models which image widespread slow anomalies. Overall, low wave speed anomalies in the supraslab and subslab mantle seem to be dominant (in size and amplitude relative to high velocities) in *P* with respect to *S* models; these important discrepancies could hint at a nonthermal origin of some anomalies (i.e., possible compositional or partial melting variations) or a trade-off with seismic anisotropy, which needs to be further analyzed.

4.2. Seismic Anisotropy

Seismic anisotropy is widespread in the Earth and provides information about dynamics, in particular for the uppermost mantle where we expect that anisotropy is mainly caused by the alignment of intrinsically anisotropic olivine crystals in mantle convection (LPO (lattice-preferred orientation) type of anisotropy; see, e.g., *Silver* [1996], *Montagner* [1998], *Savage* [1999], and *Long and Becker* [2010] for reviews). LPO-induced anisotropy is expected to be a record of recent (~5 Ma, *Becker et al*. [2006]) asthenospheric flow, and the most direct measurement of seismic anisotropy is split *S* phases. Those arise when a single pulse is split into two quasi *S* waves propagating at different speeds upon traversing an azimuthally anisotropic medium. A shear wave splitting measurement can detect the polarization orientation of the fast pulse ("fast azimuth") and the delay time between the two pulse arrivals as proxies for the overall alignment of the symmetry axis and the strength of anisotropy along the raypath.

Compared to the orientation of fast azimuths, delay time estimates are less reproducible, somewhat analysis method dependent, and show larger variations with back azimuth [e.g., *Savage*, 1999]. This makes the interpretation of station-averaged delay time values complicated, particularly in continental regions where shallow, frozen-in anisotropy from past deformation may overprint deeper, shear-induced LPO fabrics related to the present-day asthenospheric flow [e.g., *Fouch and Rondenay*, 2006]. Compared to the end-member case of a single olivine layer that is uniformly sheared to saturation fabric strength, there are several mechanisms that can reduce average *SKS* delay times, including the following: (i) orientation of symmetry axes out of the horizontal (e.g., by radial flow and pure, rather than simple shear deformation), (ii) strong rotations of horizontally aligned fast axes with depth due to complex flow, and (iii) superposition of differently aligned shallow (e.g., lithospheric fabrics) with deeper asthenospheric shearing. One interpretation of delay times, then, is of being indicative of the degree of consistent shear deformation as recorded in the uppermost mantle rock column, roughly underneath the station.

LPO anisotropy caused by mantle flow in the upper mantle will also be expressed in differences in *SH* and *SV* polarized seismic wave velocities, i.e., radial anisotropy. Those anomalies are typically imaged using surface waves, and radial anisotropy patterns have been used to constrain mantle flow on global scales [*Becker et al*., 2008]. Radially anisotropic tomography is generally of lower lateral resolution than the inferences that are possible from shear wave splitting. Regional work for the Mediterranean by *Schaefer et al*. [2011] indicated general consistency between seismological imaging and geodynamic modeling, but detailed tectonic inferences on the scales we attempt here have to await future seismological model refinement [cf. *Auer et al*., 2014].

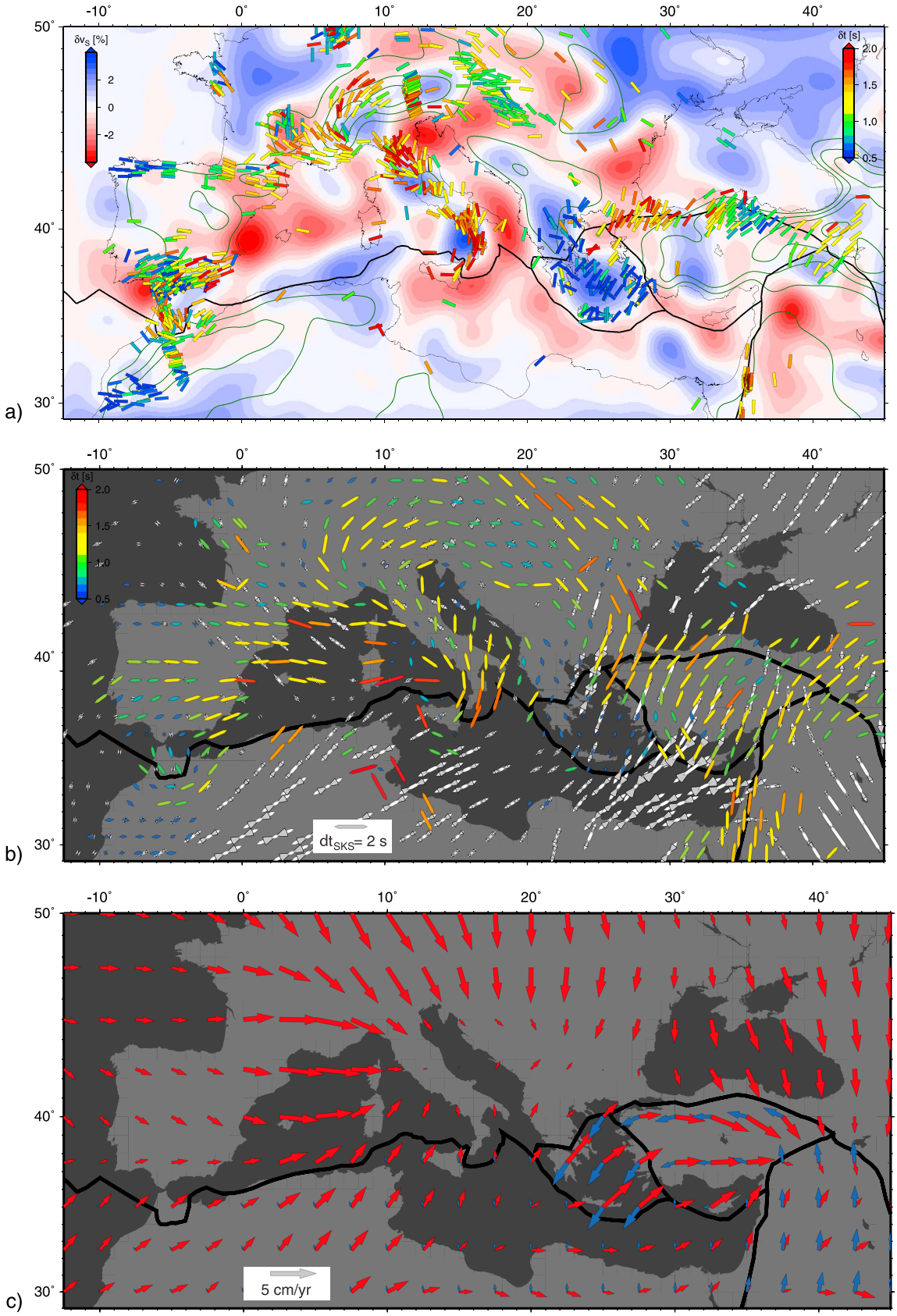

Figure 8

Figures 8a and 8b show a compilation of the nonnull shear wave splitting measurements in the Mediterranean from the compilations of *Wuestefeld et al*. [2009] and *Becker et al*. [2012], both updated May 2013 based on the analysis of *SKS* and *SKKS* arrivals [e.g., *Barruol and Souriau*, 1995; *Barruol et al*., 1998, 2004, 2011; *Hatzfeld et al*., 2001; *Barruol and Granet*, 2002; *Margheriti et al*., 2003; *Sandvol et al*., 2003; *Civello and Margheriti*, 2004; *Schmid et al*., 2004; *Diaz et al*., 2006; *Lucente et al*., 2006; *Plomerová et al*., 2006; *Baccheschi et al*., 2007; *Buontempo et al*., 2008; *Diaz et al*., 2010; *Evangelidis et al*., 2011; *Kovács et al*., 2012; *Bokelmann et al*., 2013; *Miller et al*., 2013]. The color-coding of sticks indicates delay time for station-averaged splits, and orientation the fast azimuth. Average values of delay times in the central Mediterranean (~1.2, …, 2 s) are much larger than in the Aegean (~ 0.5 s) region where anisotropy is complex and strongly depth variable [e.g., *Endrun et al*., 2011]. Anisotropy is also small in southwestern Morocco where the cratonic lithospheric signature may overprint asthenospheric shear [*Miller et al*., 2013].

Splitting measurements in Figure 8a are shown on top of the *P* wave velocity anomalies from model PM0.5 [*Piromallo and Morelli*, 2003]. The map is a vertical average of velocity anomalies between 100 and 400 km depth, based on the assumption that anisotropy is mainly caused by asthenospheric flow roughly in those depth regions. This simple comparison highlights that azimuthal anisotropy strikes parallel to the high-velocity zones along the Alpine-Mediterranean belt, and perpendicular to the direction to the high-velocity zones in the back-arc region [*Jolivet et al*., 2009].

Overall, the region shows a range of intriguing patterns of fast azimuths, and presumably mantle shear (cf. Figure 8c), where relatively homogeneous patterns over length scales of approximately thousands of kilometer are interrupted by smaller scale features, associated with the Alboran domain, the Alps, as well as the Tyrrhenian and Hellenic subduction zones, for example (Figures 8a and 8b). In particular, over the central and western Mediterranean, we see a dominance of EW direction turning progressively toward NW in the north (southern France) and toward WSW to the south (Morocco). This large-scale pattern also shows a westward increase in delay times toward the Tyrrhenian trench; the fast azimuths strike parallel to the stretching direction of the back-arc basin and have been related to back-arc extension [*Lucente et al*., 2006; *Jolivet et al*., 2009].

In the eastern Mediterranean, fast orientations trend NNE from the Aegean back-arc basin to Anatolia, with little apparent signature of the North Anatolian Fault [e.g., *Biryol et al*., 2010]. Also in this case, a smooth increase in delay times is found when moving toward the trench. The fit between stretching direction and *SKS* there has also been interpreted in terms of back-arc extension [*Kreemer et al*., 2004; *Jolivet et al*., 2009].

The orientation of the trench parallel features is complex and generally positioned along the high-velocity anomalies, likely associated with subducted lithosphere (Figure 8a). Beneath the Apennines, Alps, and Atlas, the patterns of fast axes follow the orientation of the mountain chains. Beneath the Apennines, we find a decrease in delay time in the central Apennines. In this region, the orientation of the anisotropy has been related to the trench parallel flow of mantle material beneath the slab induced by its retrograde motion [*Margheriti et al*., 2003], whereas the variations in delay time have been interpreted as being due to a larger vertical component of shear beneath the central Apennines [*Lucente and Margheriti*, 2008]. Close to subduction zones, it remains unclear whether the anisotropy signal is derived from the subslab mantle [*Margheriti et al*., 2003] or from the slab itself, as proposed for other regions [*Faccenda et al*., 2008], and the multiple possible causes of subduction zone-associated anisotropy are reviewed by *Long and Becker* [2010] and *Long* [2013].

Figure 8. (a) Azimuthal anisotropy from shear wave splitting superimposed on uppermost mantle seismic tomography. Red to blue sticks indicate *SKS* splitting measurements from the compilations by *Wuestefeld et al*. [2009] and *Becker et al*. [2012], updated as of August 2013 [e.g., *Barruol and Souriau*, 1995; *Barruol et al*., 1998, 2004, 2011; *Hatzfeld et al*., 2001; *Barruol and Granet*, 2002; *Margheriti et al*., 2003; *Sandvol et al*., 2003; *Civello and Margheriti*, 2004; *Schmid et al*., 2004; *Diaz et al*., 2006, 2010; *Lucente et al*., 2006; *Plomerová et al*., 2006; *Baccheschi et al*., 2007; *Buontempo et al*., 2008; *Evangelidis et al*., 2011; *Kovács et al*., 2012; *Miller et al*., 2013], with orientation showing the "fast axes" and color coding for delay time. Background color is a smoothed version of the regional model by *Piromallo and Morelli* [2003], embedded in, and anomalies scaled up, to the global model by *Simmons et al*. [2007], where velocity anomalies were averaged within the depth range of 100 and 400 km. Superimposed plate boundaries (in black) are from *Bird* [2003], and dark green contours are smoothed topography in 500 m contour spacing for positive elevation only. (b) *SKS* splitting from Figure 8a but averaged on $1 \times 1°$ bins; gray sticks show equivalent *SKS* splitting derived by full waveform synthetics from the v_{SV} surface wave model of *Debayle and Ricard* [2013], derived using the method discussed by *Becker et al*. [2012]; gray wedges and double sticks indicate expected (one standard deviation) variation of fast axes and delay times with back azimuth. (c) Mantle flow in the Mediterranean. Dark green vectors are surface plate velocities from the NNR-MORVEL56 model [*Argus et al*., 2011] in a Eurasia-fixed reference frame; plate boundaries are as in *Bird* [2003] and shown with black heavy lines. Red vectors indicate the inferred motion of the mantle at 250 km depth with respect to the surface using a circulation model of *Hager and O'Connell* [1981] type with plate motions and density inferred from the SAVANI model of *Auer et al*. [2014].

Beneath the Hellenides and the Aegean, the delay times are smaller and orientations turn from NW-SE, parallel to the belt, to NNE in the back-arc area. This has also been interpreted as related to the complex southwestward migration of the retreating slab [*Brun and Sokoutis*, 2010]. Indeed, regional studies indicate a layered anisotropy in the Aegean Sea that may be related to the fabric within the mantle and in the lower crust [*Kreemer et al*., 2004; *Endrun et al*., 2011].

The foreland regions, for example, the Adria microplate between Italy and Balkans are distinct. Here the anisotropy azimuths progressively rotate from trench parallel—NW-SE—beneath the Apennines toward a NS orientation. At the NE corner of the Adria plate, *SKS* fast azimuths turn again to NE direction. This fabric has been interpreted as related to the overprinting of mantle flow induced by the retrograde motion of the slab in combination with an older inherited NS fabric within the lithosphere [*Plomerová et al*., 2006; *Baccheschi et al*., 2007].

There are other, smaller scale features, showing trench-perpendicular *SKS* azimuths within subduction windows or at the edge of slabs (Figure 8a). This applies, for example, in the Sicily channel, at the western corner of the Calabrian slab, where *SKS* fast axes turn to NS and then EW in the Tyrrhenian Sea [*Civello and Margheriti*, 2004]. Another example is northeast Morocco, along the northwest African coast, where *SKS* turn to a NE trending direction [*Diaz et al*., 2010]. This pattern is found at the eastern edge of the high-seismic velocity anomaly under the Alboran Sea and has been interpreted as being related to the perturbation of mantle flow at the edge of a slab [*Faccenna et al*., 2004; *Diaz et al*., 2012; *Miller et al*., 2013; *Alpert et al*., 2013]. Anisotropy may image the inflow of subslab mantle material within the subduction window itself, attaining a toroidal pattern around the edge of the slab [*Civello and Margheriti*, 2004; *Funiciello et al*., 2006; *Piromallo et al*., 2006; *Faccenna et al*., 2004, 2005; *Jolivet et al*., 2013; *Alpert et al*., 2013]. As was argued by *Faccenna et al*. [2013] for the Middle East/Hellenic slab setting and the Afar plume, southern Morocco may be another site where upper mantle flow is affected by plume influx and slab segmentation [e.g., *Duggen et al*., 2009]. *SKS* and local *S* splitting for Morocco indicate that such flow from the Canaries may be channeled by lithospheric heterogeneity on scales of the Atlas mountains [*Miller and Becker*, 2014], and the NW African craton [*Alpert et al*., 2013].

The patterns of azimuthal anisotropy from an averaged representation of the *SKS* results shown in Figure 8a can be further compared with azimuthal anisotropy from surface waves (Figure 8b). The latter have relatively poor lateral resolution but provide an independent estimate of anisotropy, and lend themselves easier to exploration of depth dependence. Figure 8b shows results from the Rayleigh wave (v_{SV}) model of *Debayle and Ricard* [2013], interpreted in terms of equivalent shear wave splitting using the full waveform approach of *Becker et al*. [2012]. Back azimuthal variations, as shown in Figure 8b as gray wedges, can then be used as some indication of the variations of anisotropy with depth.

The comparison between surface and body wave-based anisotropy shows a general match of expected delay time amplitudes. Older, global surface wave models did generally underestimate the *SKS* delay times [*Montagner et al*., 2000; *Wuestefeld et al*., 2009; *Becker et al*., 2012], implying that there is now convergence in terms of the general amplitudes of inferred azimuthal anisotropy. While local fast azimuths are often not matched that well between the surface and body wave models, the surface wave estimates for the Mediterranean do provide a large-scale average of the general features as could be inferred by further smoothing of *SKS* results [cf. *Becker et al*., 2012]. In particular, consistent patterns include a modification of a general NEE orientation of fast axes by central and eastern Mediterranean features (presumably related to the Tyrrhenian and Hellenic slab associated flow). Moreover, the surface wave-based anisotropy indicates large back azimuthal complexity underneath the eastern Mediterranean Sea (not well imaged by *SKS*).

Figure 8c shows a comparison of surface velocities (from NNR-MORVEL56 [*Argus et al*., 2011]) in a Eurasia-fixed reference frame and relative mantle flow velocities at 250 km depth (blue and red vectors, respectively). The latter are computed using a simplified *Hager and O'Connell* [1981] approach (no lateral viscosity variations) by prescribing plate velocities and converting seismic velocity anomalies from tomography (the SAVANI model of *Auer et al*. [2014]). We scale this model to density with a constant scaling factor and apply a simplified viscosity profile. Computations are performed with the HC software [*Milner et al*., 2009], and details are explored below. However, based on this example, it can be seen that the Mediterranean mantle may be expected to display a complex flow field [*Faccenna and Becker*, 2010], where the "sublithospheric mantle is leading the plate" in several regions, and surface velocities are in places reversed from deep

currents [cf. *Hager and O'Connell*, 1981; *Long and Becker*, 2010]. On the largest scales, one may infer that the shearing that is implied by the relative velocities between surface and deep mantle, rather than surface velocities in some absolute reference frame, provide a better, first-order explanation of the broad anisotropy patterns [cf. *Becker et al*., 2014].

The quantitative interpretation of anisotropy will be further investigated in section 9 where we will show detailed comparisons with predictions of LPO development and synthetic splitting based on mantle flow models.

5. Tectonic Evolution of the Mediterranean

Several kinematic models describe the tectonic evolution of the Mediterranean [*Dewey et al*., 1973; *Biju-Duval et al*., 1977; *Tapponnier*, 1977; *Dercourt et al*., 1986, 1993; *Malinverno and Ryan*, 1986; *Savostin et al*., 1986; *Dewey et al*., 1989; *Patacca et al*., 1993; *Gueguen et al*., 1998; *Faccenna et al*., 1997; *Wortel and Spakman*, 2000; *Mazzoli and Helman*, 1994; *Jolivet and Faccenna*, 2000; *Rosenbaum et al*., 2004; *Jolivet et al*., 2003; *Handy et al*., 2010; *Carminati et al*., 2012].

There is a substantial agreement between different kinematic models during the Tertiary [*Savostin et al*., 1986; *Dercourt et al*., 1986; *Dewey et al*., 1989; *Ricou*, 1994; *Mazzoli and Helman*, 1994; *Jolivet and Faccenna*, 2000; *Rosenbaum and Lister*, 2002], while the Cretaceous velocity field and the motions of Iberia are more disputed [e.g., *Olivet*, 1996; *Rosenbaum and Lister*, 2002; *Capitanio and Goes*, 2006; *Handy et al*., 2010].

The reconstruction in Figure 9 is based on the original model by *Jolivet and Faccenna* [2000], further revised using more recent data compilations [*Jolivet et al*., 2003; *Jolivet and Brun*, 2010; *Horváth and Faccenna*, 2011]. It is illustrated in five stages at 35, 23, 15, 10, and 5 Ma. The position of the trench is estimated on the basis of the amount of back-arc extension (the red line underlines the active portion of the trench) computed by first subtracting the oceanic crust and then restoring the thickness of the continental crust to that of the shoulders. This gives a minimum amount of extension since the crust on the shoulder itself may have been significantly thinned. Paleomagnetic data provide an important constraint for the block rotation timing, constrained by paleodeclinations. We assumed that Adria's motions are coherent with that of Africa, in line with the lack of relevant differential rotation [*Channell et al*., 1990].

The overall plate tectonic evolution of the Mediterranean in the Tertiary is dominated by the collision of the Adria plate, in the center of the Mediterranean, along the Alps. The asymmetry of the Adria plate, whose size increases eastward, produces asymmetry in the subduction system (Figure 9). This system consists of two large trenches, flanking the Alpine collision, the Liguro-Provençal/Tyrrhenian on one side and the Hellenic on the other side. Both slabs started to retreat at ~30–35 Ma, although a minor older rollback phase ~45 Ma of the Hellenic Trench is attested to by the Rhodope extension [*Brun and Sokoutis*, 2010]. Much of the complexity we see today in the Mediterranean is due to the inherited paleogeography. The presence of small oceanic basins and continental blocks in the Tethyan realm produced intermittent phase of subduction and collision (Figure 9). A remnant of this land-locked old oceanic lithosphere is now preserved only in the Ionian abyssal plain [e.g., *Speranza et al*., 2012].

The Cenozoic tectonic evolution of the Mediterranean region can be summarized in three successive stages:

1. Before ~30–35 Ma (Figure 9a), the subduction of the African Plate below Eurasia led to a compressional regime in the upper plate along most of the convergent margin. This led to the formation of mountain belts such as the Betic Rif orogen, the Dinarides, and the Hellenides. Subduction of the European lithosphere below Apulia-Adria induced the formation of the Alps and Carpathians. During this period, the crust of the upper plate was thickened by thrust faulting stacking and crustal material underwent high pressure–low temperature (HP-LT) and even ultrahigh pressure-LT metamorphism. In particular, Alpine-type chains formed with similar evolutions from west to east, involving a first stage of oceanic obduction and subduction, followed by subduction of the thinned continental crust of the lower plate, and shortening coeval with exhumation of the subducted crust. Considerable amounts of shortening are documented in the Alps, the Apennines, and the Dinarides-Hellenides.
2. After 30–35 Ma (Figures 9b and 9c), the tectonic regime changed in all back-arc regions, where extension took over after compression. Trenches started to retreat at rates of few cm/yr with increasing velocity through Miocene time. This extensional regime led to collapse of the previously thickened orogenic wedges and exhumation of high-temperature metamorphic domes below shallow-dipping extensional shear zones.

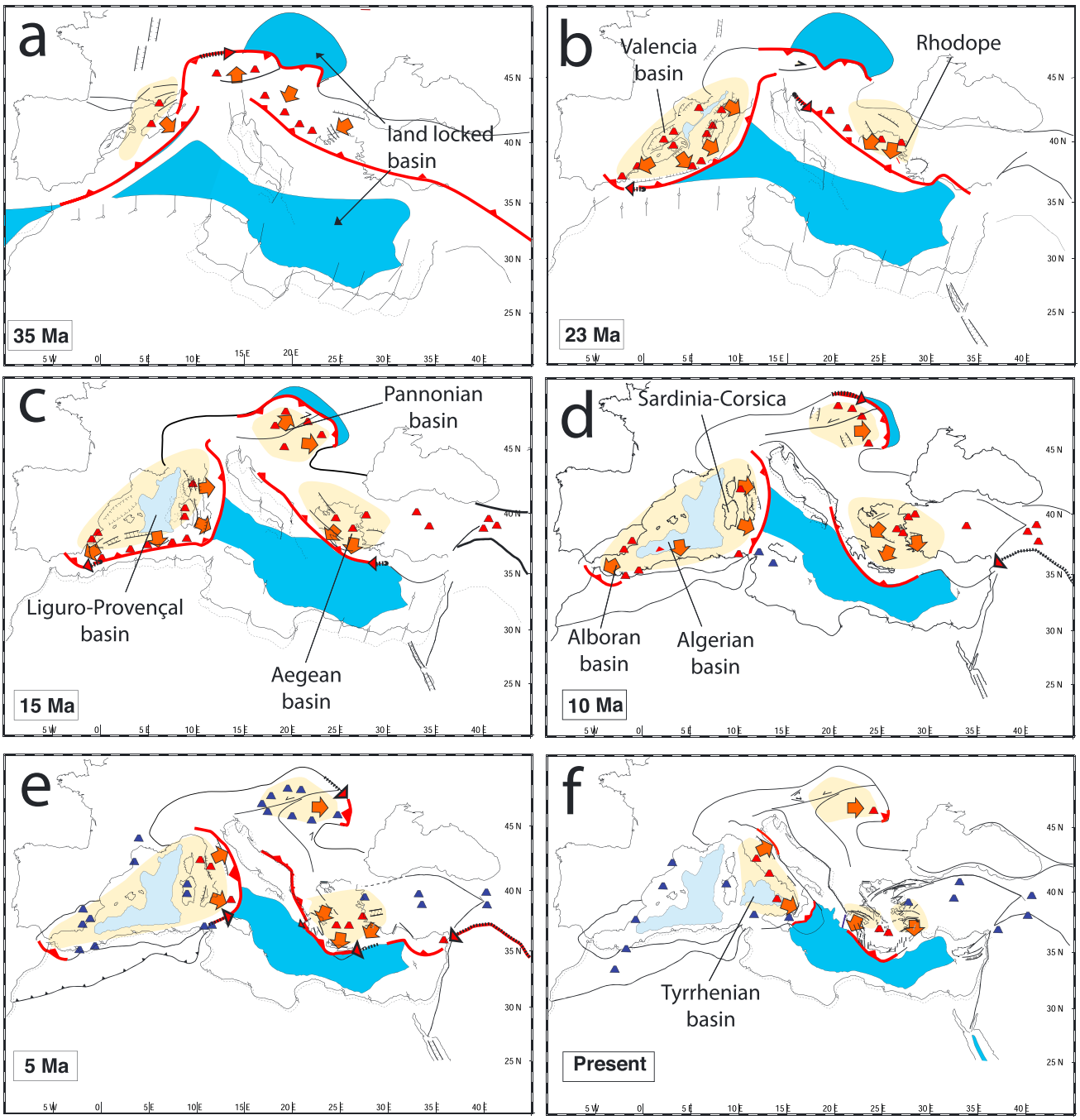

Figure 9. Evolution of the Mediterranean region in five steps. Red lines indicate active subduction. Red and blue volcanoes indicate calcalkaline and anorogenic, respectively. Yellow region: extension area, arrows: stretching direction.

Within subduction zones, a HP-LT metamorphic regime still prevails and blueschists continue to form and exhume while high-temperature domes exhume in the back-arc regions.

3. After the Miocene (Figures 9d–9f), trench retreat is associated with a progressive bending and arching, tightening and eventually lateral tearing of the subducted slabs took place at different times in the Alps, Dinarides, Hellenides, Alboran, and the Tyrrhenian. This is well attested by the presence of discontinuity along the trench and by formation along the arc of flexural basin of different ages [*Royden et al.*, 1987]. In several regions, Tyrrhenian, Aegean, and Alboran, the lateral tears separate the subducting lithosphere from the stiff and buoyant continental plate, leading to an acceleration of trench retreat and

surge of Na-alkaline anorogenic volcanism. The progressive decrease in the size of active portion of the trench eventually caused the end of subduction.

Looking at the Mediterranean as a whole, it appears that the Alps had a distinct evolution with respect to the surrounding regions. Sustained by the slow continuous motion of Adria, the Alpine orogenic wedge is only slightly affected by extension, which occurred much later, after 15 Ma. The Alps display a more continuous tectonometamorphic evolution compared to the Aegean, the Tyrrhenian, and the Alboran domains. The western Alps in particular show a stable *p-T* regime throughout their evolution, with a single cold *p-T* gradient from the Late Cretaceous to the Miocene [e.g., *Jolivet et al*., 2003]. Moreover, when the other convergence zones record the abrupt change of tectonic regime from contractional to extensional, the Western Alps show more active propagation of thrusts toward Europe and backthrusting on Adria develops in the Southern Alps. This behavior can be explained by boundary conditions in that the Alps have been situated always in front of the NNW moving Adriatic continental plate. Therefore, compression prevailed all the time. However, there are indications that the 35 to 30 Ma time interval was a period of major tectonic reorganization in the Alps, too. Namely, the Periadriatic intrusive activity occurred in late Eocene to early Miocene time [e.g., *Schmid et al*., 2013]. The pattern of sedimentation in the foreland basin also changed drastically during this period, and an increased sediment influx of shallow marine and then continental molasses (coarse continental deposits) replaced the flysch deposition (deep marine continental slope deposits) with an increase of the sediment influx [*Sinclair*, 1997; *Kuhlemann and Kempf*, 2002; *Kuhlemann et al*., 2002].

In contrast, the gravitational potential energy increase associated with the thickened crust was limited by eastward escape of an internal Alpine orogenic wedge [*Horváth et al*., 2006; *Ustaszewski et al*., 2008], facilitated by the subduction of the land-locked Late Cretaceous Tethyan basin in the Carpathian embayment (Figure 9) [*Schmid et al*., 2008]. The internal Alpine wedge welded together in the middle Miocene with a second orogenic wedge that was detached from the internal side of the Dinarides to form the present Pannonian Basin [e.g., *Horváth et al*., 2006; *Stojadinovic et al*., 2012; *Ustaszewski et al*., 2010]. The timing of the main events of this complex back-arc basin development are well constrained by stratigraphy of synrift and postrift strata, extension and subduction-related magmatic rocks, and thermochronology of exhumed metamorphic complexes [*Konecny et al*., 2002; *Schefer et al*., 2011; *Stojadinovic et al*., 2012; *Scharf et al*., 2013]. The consistent patterns of synrift sedimentation, fast exhumation, stretching of the continental crust, and the associated widespread silicic volcanism suggest that extrusion commenced at ~ 22 to 20 Ma and peak activity lasted to ~12 to 11 Ma. The retreat of the trench continued with decreased rate until the present.

The central Mediterranean region represents perhaps the largest back-arc province in the Mediterranean. Here there is agreement both on the timing and amount of extension. The first stage of back-arc extension is bracketed between ~32–30 Ma and ~16–15 Ma [*Cherchi and Montandert*, 1982; *Gorini et al*., 1994; *Burrus*, 1984; *Seranne*, 1999] and is accompanied by the ~ 40° clockwise rotation of the Sardinian-Corsica block [*Gattacceca and Speranza*, 2002], leading to the opening of the Liguro-Provençal basin. In this region, synrift deposition started 10–12 Ma on the eastern Sardinia shelf and Calabria margin [*Kastens et al*., 1988; *Sartori*, 1990; *Mattei et al*., 2002]. Consequently, localized spreading centers (at 4–5 Ma, Vavilov basin, and at 2 Ma, Marsili basin in the Tyrrhenian area) [*Sartori*, 1990] formed at very fast rate [*Nicolosi et al*., 2006]. Extension in the Tyrrhenian has currently stopped, or significantly slowed down to a fraction of that rate [*D'Agostino and Selvaggi*, 2004; *Serpelloni et al*., 2007]. The volcanic arc migrated southeastward from the Provençal and Sardinia margin, where calcalkaline suites erupted from 38 to 32 Ma up to 13 Ma [*Beccaluva et al*., 1989; *Lustrino et al*., 2009, 2011], to the Tyrrhenian basin at ~ 5 Ma (5–2 Ma), reaching its present-day position in the Eolian Island (Figure 2) [*Beccaluva et al*., 1989; *Kastens et al*., 1988; *Argnani and Savelli*, 1999]. In Sardinia and in the Southern Tyrrhenian, a new phase of magmatic activity occurred during the Pliocene with the eruption of alkaline to tholeitic suites [e.g., *Faccenna et al*., 2005; *Lustrino and Wilson*, 2007; *Carminati et al*., 2012].

The timing and amount of extension in the Aegean-Algerian and Alboran Sea is more disputed. For the Aegean Sea, the amount of extension is considered to be ~400–500 km, and most of the reconstructions are based upon paleomagnetic data and core complex exhumation history. *Faccenna et al*. [2003] estimate ~400 km of extension partitioned between ~ 300 km in the last 15 Ma and ~100 km between 30 Ma and 10 Ma. *Van Hinsbergen and Schmid* [2012] provide a similar estimate. A larger estimate of ~ 700 km extension has been proposed by *Jolivet and Brun* [2010]. The age of the first back-arc extension is still disputed. In early interpretations, it was supposed to start as late as 13 Ma [*Le Pichon and Angelier*, 1981] or even 5 Ma [*McKenzie*, 1978]. However, faulting in sedimentary basins suggested earlier ages in the middle Miocene [*Mercier et al*., 1976]. The earliest unconformable

marine deposits in extensional basins date from the base of the Miocene (Aquitanian 23–20 Ma), they are found in Naxos and Evia, Aegean Sea [*Guernet*, 1971; *Angelier et al*., 1978; *Katsikatsos et al*., 1981; *Sanchez-Gomez et al*., 2002; *Kuhlemann et al*., 2004]. The base of the Miocene could then be considered as the earliest possible date for extension in the Cyclades within the Aegean Sea [*Ring et al*., 2010]. Yet extension in the Greek Rhodope [*Brun and Sokoutis*, 2007] and large-scale normal faulting in the Bulgarian Rhodope [*Burchfield et al*., 2003] show that extension starts in middle Eocene in the north Aegean. The simultaneous starting in middle Eocene of extension in the Rhodope and of exhumation of high-pressure metamorphic rocks in the Cyclades led *Brun and Faccenna* [2008] to propose that the process of high-pressure rock exhumation was extensional and driven by gravity (slab rollback).

Paleomagnetic rotations [*Kissel and Laj*, 1988] and thermochronology data (see review by *Jolivet and Brun* [2010]) indicate an acceleration of extensional processes at ~15 Ma. An extensional displacement of ~700 km since the middle Eocene implies a mean displacement rate of 1.7 cm/yr. An independent data set is provided by the space-time distribution of magmatic products in the Aegean region. These show a clear southward displacement at a fairly constant rate of 2–3 cm/yr from 35 Ma to the present. Before that period, the magmatic arc had been quite stable in the northern Aegean and the Balkans since the Late Cretaceous. This suggests that slab rollback has indeed started some 30–35 Ma ago, which fits the timing of exhumation and *p-T-t* evolution of metamorphic domes in the Northern Cyclades. Although the displacement of the magmatic arc seems at first order to proceed at a quite constant rate since the Late Eocene [*Jolivet et al*., 1998], the displacement rate has likely varied through time with acceleration since the middle Miocene to reach the present-day values close to 2.5 cm/yr in Crete [*McClusky et al*., 2000]. In contrast, early displacement rates were likely rather low in Eocene-Oligocene time, i.e., significantly less than 1.0 cm/yr [*Brun and Sokoutis*, 2010].

The age of extension is poorly constrained in the Algerian basin, North Africa. In the Valencia trough, the westward continuation of the Provençal basin, extension occurred between ~26 and ~16 Ma [*Vergés and Sàbat*, 1999], following the clockwise rotation of the Balearic Islands and the extension of the Kabylie belt [*Parés et al*., 1992]. A few million years later extension shifted in the Algerian basin and should have occurred before ~6–7 Ma, when Messinian evaporites were deposited on the oceanic crust [*Vergés and Sàbat*, 1999], and after the compressional episode in the Balearic archipelago ended ([*Vergés and Sàbat*, 1999], ~15–12 Ma). The volcanic arc migrated southward following the trench system. Calcalkaline volcanism, 25–13 Ma in age, first occurred in the Valencia trough and migrated southward to the North African coast. In northern Algeria, subduction-related volcanic activity spanned from ~16 to 10 Ma, first with the eruption of low-K arc tholeiites and then with the emplacement of granitoids and acidic lavas with a strong crustal signature [*Maury et al*., 2000; *Fourcade et al*., 2001].

Further to the west, extension affected the orogenic wedge of the Alboran domain (i.e., surrounding Alboran Sea). The ages of synrift sediments and radiometric dating indicate that extension in the Alboran region started at ~27–25 Ma [*Comas et al*., 1999]. Extension was associated with a thermal event, as revealed by magmatism and by the clustering of most radiometric ages around ~22–18 Ma [*Platt and Whitehouse*, 1999; *Zeck*, 1999; *Platt et al*., 2013]. The amount of extension and the vergence of the subduction process in this region are also disputed. *Faccenna et al*. [2004] estimate ~200 km of extension, based on the thickness of the crust in the Alboran Sea [*Torné et al*., 2000] or even less [*Carminati et al*., 2012]. *Spakman and Wortel*'s [2004] estimate is almost double that. The processes at work in this tight arc are highly disputed. Some models predict that Alboran extension is due to a lithospheric mantle Rayleigh-Taylor instability, resulting in a radial collapse of the orogen at the surface [*Platt et al*., 2003; *Molnar and Houseman*, 2004]. Others relate the extension to lithospheric delamination or to slab rollback [*Lonergan and White*, 1997; *Faccenna et al*., 2004; *Spakman and Wortel*, 2004], or propose a south-dipping subduction or a switch from south-dipping to north-dipping subduction [*Verges and Fernandez*, 2012].

In the Anatolia-Aegea region, a major strike-slip fault, the North Anatolian Fault (NAF), started to form in the middle-late Miocene in eastern Anatolia [*Sengor et al*., 2005]. Whether it started as a wide shear zone already running from east Turkey to the Aegean Sea, or if it propagated westward to reach the Aegean domain 5–6 Ma ago, is debated [*Armijo et al*., 1999; *Flerit et al*., 2004]. Also disputed is the relation between the Aegean extension, nowadays localized in the Corinth Rift and on western Anatolia, and the Anatolia motion. Present-day geodetic velocities show that the Aegean domain moves faster southwestward than the rest of Anatolia (Figure 3) and the current compression along the East Anatolian Fault is almost negligible [*Reilinger et al*., 1997].

6. Discussion

The Mediterranean may represent a comprehensive test site to investigate the potential connection between deep mantle processes and shallow tectonics. In the previous sections, we reviewed the present-day state of deformation as deduced from active faults, seismicity, and geodetic velocity fields. We also provide information on the structure of the crust and mantle as deduced from seismological investigations, such as seismic tomography and anisotropy. We review the geological evolution of the Mediterranean over the last 35 Ma, to illustrate how the subduction system evolved in space and time. A number of questions result, such as: what controls the style of subduction in the Mediterranean and the formation of the arc-back-arc system? Is the motion of microplates, i.e., Adria, Aegea, and Anatolia, related to lithospheric dynamics and plate convergence or to deep mantle dynamics, instead? Is there a signature of mantle convection, i.e., dynamic topography, on the topography evolution of the Mediterranean?

The second part of the paper will outline attempts to answer these questions. We start by comparing tectonic reconstruction with tomography to validate the two sets of data, in particular regarding the amount of subduction (section 7). We will then review the large amount of models proposed so far to explain the velocity of subduction and the style of deformation of the region (section 8). We will then present convection models to probe the relation between the Anatolia, Adria, and Aegea motions and mantle convection (section 9), as well as the match between the predicted pattern of mantle convection and the anisotropy data (section 10), and lastly discussing the origin of the topographic features in the Mediterranean (section 11).

7. Tectonic Reconstructions and Seismic Tomography

Because of the slow convergence and the land-locked frame [*Le Pichon*, 1982], the Mediterranean represents an ideal site to assess the accuracy of the consistency between tomographic models and tectonic reconstructions. Fast seismic anomalies along convergent margins are usually interpreted as traces of cold subducted lithosphere in the mantle, providing constraints on the geological reconstructions of the subsumed basins [e.g., *Ricard et al*., 1993; *Hafkenscheid et al*., 2006]. To validate this interpretation, it is possible to compare the volume of fast seismic anomalies in the mantle with those of the subducted lithosphere as constrained by geological reconstructions. Such analysis for the Mediterranean region has been published by *De Jonge et al*. [1994], *Wortel and Spakman* [2000], *Spakman and Wortel* [2004], *Faccenna et al*. [2003, 2004], *van Hinsbergen et al*. [2005], *Hafkenscheid et al*. [2006], *Capitanio et al*. [2009], and *Jolivet and Brun* [2010]. The analysis consists in the comparison of the amount of convergence between underthrusting plate and the overlying arc with tomography, for example, along given sections. The total subduction estimate is the sum of the amount of convergence between plates plus the amount of trench retreat, which is the amount of back-arc extension when erosion at trench is negligible. Here the Adriatic Plate is assumed to be a coherent promontory of Africa [*Dewey et al*., 1989; *Channell et al*., 1990]. We will describe the results along representative sections of the convergent margins in the Southern and Northern Tyrrhenian, Aegean Sea, Algerian Sea, Alboran, Pannonian, and the Alps. The strike of the sections is parallel to the back-arc maximum stretching direction, which is assumed parallel to the subduction direction (Figure 10).

The subduction estimates over the Cenozoic amounts to ~1000 km in both the southern Tyrrhenian Sea and the Aegean Sea. This amount, however, is differently partitioned. Trench rollback is the largest portion in the southern Tyrrhenian Sea, up to 80%, instead in the Aegean Sea plate convergence accommodated 60% of subduction. In the Algerian Sea, the estimated amount of subduction is ~600 km, decreasing in the Alps to ~500 km, and to ~400 km in Alboran. Figure 10 shows such a comparison along the sections with the PM0.5 tomographic model and the estimate resulting in a reasonable match for the upper mantle slab in the Aegean Sea [*Faccenna et al*., 2003; *van Hinsbergen et al*., 2005] and in the southern Tyrrhenian, where ~1000–1200 km of subduction can be detected. Large misfits are found in the Alboran and the Algerian domains, where tomography images a longer slab (~800 and 1000 km, respectively) than subduction estimates would indicate [*Faccenna et al*., 2004; *Bezada et al*., 2013]. This may be due to an underestimated amount of extension [*van Hinsbergen et al*., 2014] or delamination of the continental lithosphere, or because the sinking material underwent significant stretching (see, e.g., *Li et al*. [2009] for the western Tien Shan). In the Alps, the observed slab mass (~300 to ~150 km from Central and Western Alps, respectively) is instead smaller than subduction estimates, interpreted as a recent slab breakoff episode [*Piromallo and Faccenna*, 2004].

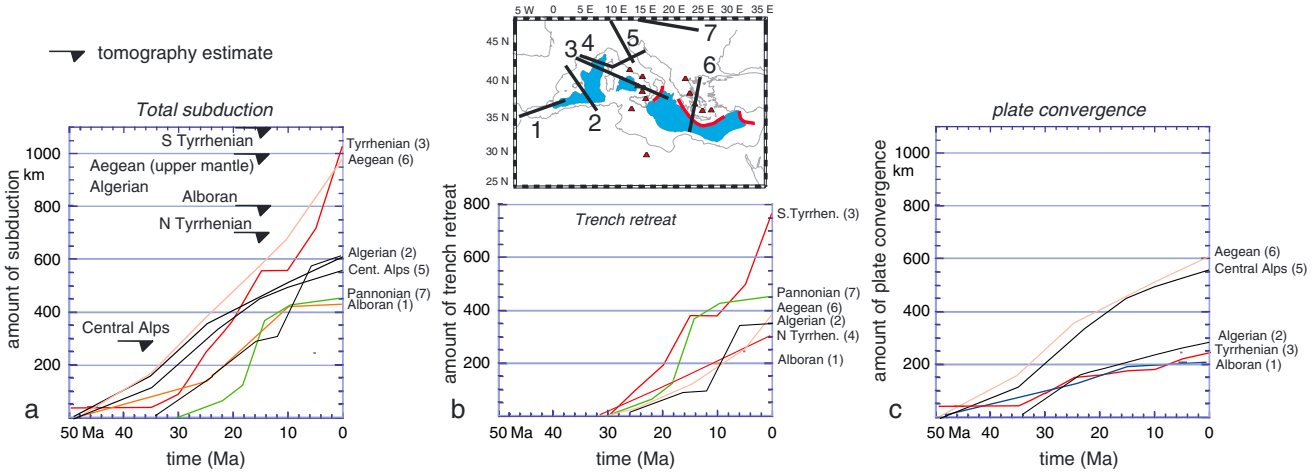

Figure 10. Estimates of the amount of subduction in time along section running perpendicular to the stretching direction for the Alboran, Algeria, South and North Tyrrhenian, Alps, Pannonian, and Aegean. (a) Total amount of subduction, (b) trench retreat, and (c) plate convergence. Kinematics are from *Dewey et al.*'s [1989] model, assuming Adria motion coherent with Africa. Black arrows on Figure 10a shows estimate from the PM0.5 tomography model.

8. The Subduction Velocity

The comparison between tectonics and tomographic models provides additional constraints on the dynamics of subduction. The subduction velocity can be defined as the sum of the back-arc motion (equal to trench retreat) and the subducting plate's convergence velocity [e.g., *Becker and Faccenna*, 2009]. Although the Aegean and the central Mediterranean subduction zones have different tectonic evolutions, they had roughly the same amount of overall subduction during the Tertiary, mostly constrained by the Africa-Eurasian plate convergence, with an average velocity of ~3 cm/yr during the last 30 Ma.

In the central Mediterranean, the directional evolution of the subduction system has been strongly time dependent and irregular while the convergence velocity was always constant and rather slow (i.e., around 0.5 cm/yr; Figure 9). Back-arc extension increased since inception at 30 Ma, peaking between 21 Ma and 16 Ma at ~ 3 cm/yr. Back-arc extension almost vanished between 16 and 10 Ma to increase again during the Vavilov-Marsili (Tyrrhenian Sea area) spreading episode [*Kastens et al.*, 1988; *Nicolosi et al.*, 2006]. As the net convergence rate was extremely low at that time, back-arc extension provides a direct estimate of the subduction velocity. In the Aegean, back-arc extension started also at ~ 35–30 Ma, accelerating by ~ 15 Ma to rates of ~ 2 cm/yr. Margin migration increased likely during the last 5 Myr to the present-day rollback velocity of 3.6 cm/yr [*Reilinger et al.*, 2006]. The convergence velocity here was higher than in the central Mediterranean as the strike of the trench was almost perpendicular to the relative motion of Africa with respect to Eurasia (Figure 9).

The average velocity of the subduction system decreases westward to ~ 2 cm/yr, along the Algerian margin, and to ~ 1 cm/yr, in the Alboran domain (Figure 10). This is likely the result of two conditions, the narrowing of the readily subductable oceanic lithosphere [e.g., *Guillaume et al.*, 2010] and the decrease in convergence on this end of the convergence zone. The same average velocity is estimated along the Alpine system, which undergoes forced underthrusting imposed by the Adria plate motions. The Pannonian system shows a trend similar to the central Mediterranean (Figure 10). Fundamental questions arise from this analysis that concern the controls on the onset of back-arc extension and the velocity of subduction.

8.1. Onset of Back-Arc Extension

Three possible mechanisms have been proposed to explain the onset of back-arc extension in the Mediterranean. The first considers the general change of boundary conditions for subduction and proposes the widespread onset of back-arc extension, from the Alboran to the Aegean, as a result of the decrease in the African Plate absolute motions [*Silver et al.*, 1998; *Jolivet and Faccenna*, 2000; *Reilinger and McClusky*, 2011]. As indicated by numerical [e.g., *Enns et al.*, 2005; *Capitanio et al.*, 2010; *Stegman et al.*, 2010] and experimental work [e.g., *Funiciello et al.*, 2004; *Bellahsen et al.*, 2005; *Schellart*, 2005], slab rollback in an isolated (e.g., without any external forcing) system is the result of an imbalance between subduction and subducting plate advance

[e.g., *Elsasser*, 1971; *Molnar and Atwater*, 1978]. In other words, when the subducting plate velocity toward the trench differs from the vertical sinking velocity driven by the slab mass, i.e., the slab pull velocity, convergence is partly accommodated by trench motions. The "natural" sinking velocity of the slab will be the Stokes velocity mediated by slab bending effects depending on rheology [e.g., *Conrad and Hager*, 1999; *Capitanio et al*., 2007; *Stegman et al*., 2010; *Ribe*, 2010]. When sinking is faster than plate advance, the difference is accommodated by trench retreat, whereas the opposite case will lead to trench advance. A decrease in the Africa-Eurasia convergence may have produced trench retreat of Mediterranean subduction zones, producing the collapse of the Alpine-Mediterranean belt first and back-arc extension later. The general slowing down of Nubia-Eurasia system has been recently revised and confirmed [from *McQuarrie et al*., 2003; *ArRajehi et al*., 2010]. *Reilinger and McKlusky* [2011] suggest indeed a correlation between plate convergence and internal deformation in the Mediterranean at ~24 Ma and ~11 Ma.

The second mechanism is related to the local dynamics of subduction. In the central Mediterranean, the spontaneous retreat during the early stage of subduction is invoked to explain the back-arc extension. Reconstructions show that at ~30 Ma, an incipient (~150 km) slab was already subducted in the upper mantle. This may have triggered a "spontaneous" subduction system [*Faccenna et al*., 2001b]. Numerical [e.g., *Becker et al*., 1999] and analog experiments [e.g., *Faccenna et al*., 1999] confirm that 150–200 km of subducted material may provide sufficient pull force to overcome resistance on a subduction fault and to bend the slab at trench. In the central Mediterranean context, the slowing down of the Africa-Eurasia convergence velocity probably had a minor effect in the subduction zone, being trench direction parallel to the relative convergence. Therefore, in this area, trench rollback is of course inherently linked to the amount of accumulated slab mass in the system needed to efficiently start self-consistent subduction. While this model for a developing slab might apply to the central Mediterranean, it cannot be invoked for the Eastern Mediterranean, where a long-term subduction was already ongoing. The Hellenic Trench started its southward migration only around ~30 Ma, opening the Aegean Sea in its wake, while the rest of the Eurasian margin, further east, remained stable.

The third process that may have triggered trench rollback in the Mediterranean could be related to the dissection of slabs during subduction, i.e., breakoff and tearing. This mechanism may be efficient to trigger back-arc extension as it may redistribute the force concentrating slab pull along a restricted portion of the trench [*Carminati et al*., 1998; *Wortel and Spakman*, 1992, 2000; *Buiter et al*., 2002; *Faccenna et al*., 2005; *Guillaume et al*., 2010]. A rotation of the slab and therefore of the plate boundary would follow, controlling the tectonics as in the case of the Aegean or Apennines. The effect of slab ruptures has also been invoked for the subsequent evolution of the Hellenic Trench, where lithospheric tears favor stress focusing and rupture propagation [*Govers and Wortel*, 2005; *Jolivet et al*., 2013]. Lastly, the presence of an eastward mantle flow with respect to the lithosphere has been advocated as another possible cause of the fast retreat of the west-dipping Tyrrhenian slab [*Doglioni et al*., 1999, 2007; *Panza et al*., 2007; *Carminati et al*., 2012].

8.2. Plate Convergence Versus Back-Arc Extension

The central Mediterranean and Aegean subduction histories show a similar amount of subduction, although partitioned in a different manner between convergence velocity and trench rollback. On average, the subduction velocity during the last ~30 Ma was ~ 3 cm/yr. Assuming little effects of plate bending for simplicity, from simple scaling relations for Stokes flow, assuming a density contrast between lithosphere and ambient mantle for a well-developed slab, such velocities can be obtained for old oceanic lithosphere using a mantle viscosity of ~ 10^{21} Pa s, although such estimates, of course, depend on the buoyancy, which would yield smaller velocities for younger oceanic or continental lithospheres [e.g., *Capitanio et al*., 2007; *Royden and Husson*, 2006, 2009].

Estimates of subduction velocities are affected by uncertainties on the age and amount of deformation of the upper plate, which provide information on the trench migration. However, in the Mediterranean, the evolution of each back-arc basin is robust and thus provides useful constraints.

A key factor controlling the evolution of the Mediterranean subduction zones is the presence of inherited heterogeneities of the lithosphere, which produced significant spatial variations in the buoyancy and strength of the subducted lithosphere. This peculiarity enhanced stepwise strain localization and the development of slab tear episodes where oceanic lithosphere was laterally juxtaposed to continental one. As

a consequence, the subducting lithosphere has been progressively fragmented, forming isolated, narrow, and fast retreating oceanic slabs close to collisional zones [e.g., *Guillaume et al*., 2013]. The lateral change from subduction to collision likely enhanced active back-arc rifts associated with rapidly rotating fore arcs [*Wallace et al*., 2009].

The subduction of continental blocks can also play an important role in trench dynamics [*Brun and Faccenna*, 2008; *Husson et al*., 2009; *Bialas et al*., 2010; *Tirel et al*., 2013; *Magni et al*., 2013]. Because slab dip is a function of slab buoyancy, the consumption of continental lithosphere decreases the subduction rate [*Molnar and Gray*, 1979; *Faccenna et al*., 2001a, 2001b; *Capitanio et al*., 2010], thus increasing the slab dip [*Royden and Husson*, 2006]. During continental subduction, as for the case of the northern Apennines, the crust may be scraped off from the mantle favoring delamination and hence back-arc extension. If the block size is small enough ($<$ 500 km), the continental lithosphere may be completely consumed, leading to the resumption of oceanic subduction and with a sudden increase on subduction rate and trench retreat [*Royden and Husson*, 2006; *Brun and Faccenna*, 2008]. The geological record of trench retreat in the Aegean suggests such a mechanism for the origin of Aegean extension [*Brun and Faccenna*, 2008; *Royden and Papanikolaou*, 2011; *Tirel et al*., 2013].

In the Aegean Sea, back-arc extension and hence trench retreat and subduction velocities accelerated at ~15 Ma. The simplest explanation for that would be the entrainment of oceanic lithosphere at the trench after the consumption of the Adria block (Figure 9) [*Royden and Papanikolaou*, 2011; *Jolivet and Brun*, 2010]. As indicated by analytical solutions [*Royden and Husson*, 2006], the acceleration of the Hellenic Trench from ~1 to ~3 cm/yr is indeed matched by the estimated negative buoyancy increase of the incoming Ionian lithosphere. It has been proposed that the acceleration of the Aegean slab could have been favored by the formation of a lateral tear under southwest Turkey, separating the Ionian oceanic lithosphere from the buoyant continental lithosphere subducting at that time beneath Anatolia (Figure 9c) [*van Hinsbergen et al*., 2010; *Jolivet et al*., 2013]. A similar but younger process occurred at the boundary between the Ionian Sea and the Adria plate on the western side of the Hellenic Trench. This may be have guided the propagation of the North Anatolian Fault in the Aegean Sea [*Royden and Papanikolaou*, 2011; *Jolivet et al*., 2013; *Guillaume et al*., 2013].

In the central Mediterranean, the overall increase in the subduction rate along the southern Tyrrhenian transect (Figure 10) is explained, to first order, by the increased amount of subducted material. However, the episodic back-arc extension and the stalling phase between the opening of the Liguro-Provençal and the Tyrrhenian Sea, between ~16 and 10 Ma, is still debated. Two main models have been proposed. The first accounts for the entrainment of a buoyant continental platform at the trench [*Malinverno and Ryan*, 1986; *Gattacceca and Speranza*, 2002] (not shown in Figure 9). The other proposed model invokes the key role of the lateral tearing of the Ionian slab from the buoyant African lithosphere to the west (Figure 9d) [*Carminati et al*., 1998; *Faccenna et al*., 2005, 2007]. The timing of this episode is marked by the cessation of a flexural basin and the change in nature of volcanism in northern Tunisia [*Faccenna et al*., 2007]. The onset of Tyrrhenian extension is indeed well correlated with that of the formation and propagation of the tear. The reconstruction of the Tyrrhenian subducting lithosphere shows that in the middle Miocene, the slab tip should have reached the 660 km discontinuity and consequently evolved into fast rollback favored by the onset of toroidal flow around the lateral edges of a torn slab [*Faccenna et al*., 2001a]. The short-lived spreading pulses forming the Vasilov (early Pliocene; *Kastens et al*. [1988]) and the Marsili basins (early Pleistocene; *Patacca et al*. [1993] and *Nicolosi et al*. [2006]) are likely related to variable slab rollback rates synchronous with the abrupt reduction of the central Mediterranean subduction zone width during its evolution [*Guillaume et al*., 2010; *Faccenna et al*., 2011]. Onset of extension in the Pannonian Basin and the rapid retrograde motions of the Carpathian slab occurred at the same time of the fast Tyrrhenian slab retrograde motions leading to the Liguro-Provençal basin opening. In both regions, the fast episode of trench retreat vanished at ~ 15 Ma. This correspondence may be fortuitous, or it may be related to the retrograde motion of the Tyrrhenian slab that may have induced mantle flow from the Adriatic toward the northeast: this, in turn, may have fostered and accelerated the retreat of the Carpathian slab inducing back-arc extension in the Pannonian [*Horváth and Faccenna*, 2011]. The formation of a slab window in the northern Dinaric slab is well documented by a phase of crustal melting and pluton emplacement postdating the main thrusting activity [*Ustaszewski et al*., 2010]. The slab window and tear seem to be in agreement with the low-velocity zone in the seismic tomography (Figure 6), although further modeling and anisotropy data are necessary to validate this hypothesis.

9. The Motion of Anatolia, Aegea, and Adria

The deformation of the Mediterranean is ultimately related to the low convergence rate between African and Eurasian plate [*McKenzie*, 1972; *Dewey et al*., 1989]. Seismicity and geodesy show that the Mediterranean area is not uniformly deformed, but strain is concentrated in narrow bands bounding smaller plates that are moving independently from the overall convergent motion (Figures 2 and 3). The scale of those continental blocks, or microplates, may be variable, and their definition and the appropriate mechanical treatment (microplates versus thin viscous sheet), of course, depends upon the spatiotemporal scales of observation [e.g., *Nyst and Thatcher*, 2004; *Thatcher*, 2009; *Floyd et al*., 2010]. However, at least three rather large microplates can be distinguished and they show a remarkable, well-recognizable pattern in current surface motion maps (Figures 1–3). Those are Adria, Aegea, and Anatolia. There may be other blocks that have been recently described; such as the one including part of the Rif and Alboran in the westernmost Mediterranean [*Fadil et al*., 2006] or Sicily [*Serpelloni et al*., 2010] but those will not be explored further here.

9.1. The Motion of Anatolia to Aegean

The geodetically imaged motions of the Arabia-Anatolia-Aegean system show a spectacular counterclockwise rotation velocity field with respect to Eurasia [*Reilinger et al*., 2006; *Kreemer et al*., 2004; *Le Pichon and Kreemer*, 2010]. Arabia behaves as a rigid plate moving NE to NNE, producing the spreading in the Red Sea and Gulf of Aden and collision against Eurasia along the Bitlis–Zagros. While convergence in Iran is accommodated by distributed northward decrease in the relative velocity, toward the west, the Anatolian Plate moves coherently at present at an average rate of < 2 cm/yr, separated from Eurasia by the North and East Anatolian Fault [*Reilinger et al*., 2006]. To the west, the Aegean plate is moving SW at -3.3 cm/yr following the retreat of the Aegean trench [*Kreemer et al*., 2004; *Reilinger et al*., 2006]. Overall, the system has a circular velocity pattern, accelerating toward the Aegean trench, about a pole determined for Anatolia-Eurasia motions located north of the Nile Delta [see also *Le Pichon and Kreemer*, 2010].

Several studies analyzed the kinematics of the Mediterranean region to capture the dynamics of the system, addressing questions regarding the motion of Anatolia and Arabia or why the Hellenic Trench retreats so fast. One model proposes that the motion of Anatolia results from a westward extrusion of the plate from the collisional zone [*McKenzie*, 1970; *Tapponnier*, 1977]. Geodetic evidence shows that Anatolia currently moves westward faster than the northern Arabia shortening velocity [*Reilinger et al*., 2006]. Hence, the Anatolia motion cannot be related to the push from the collisional zone. The velocity increase toward the trench suggests that either the buoyancy of the system under gravitational potential energy [*Hatzfeld et al*., 1997; *Jolivet*, 2001] or the subducting slab, or both, are driving the Aegean-Anatolia system. The southwestward acceleration of the geodetic velocity and the negligible compression along the Eastern Anatolian Fault suggest that the Hellenic slab system may play a relevant role as the main current driver, exerting a suction on the upper plate to drag Anatolia-Aegea toward the trench [*Le Pichon*, 1982; *Faccenna et al*., 2006; *Le Pichon and Kreemer*, 2010], even though the presence of an extensional plate boundary between Anatolia and Aegean argues against an independent motion of Anatolia with respect to the Aegean.

The slab pull model, however, can hardly explain the motion of Arabia. It may be related to slab pull exerted by the Makran system [*Bellahsen et al*., 2003; *Reilinger and McKlusky*, 2011], given that the slab beneath eastern Anatolia-Bitlis-Zagros is probably inactive and detached [*Keskin*, 2003, 2007; *Sengör et al*., 2003, 2008; *Hafkenscheid et al*., 2006; *Faccenna et al*., 2006], but the remaining portion of oceanic slab is quite small. Geological and volcanological indications suggest that the slab beneath Anatolia-Bitlis may have broken around the upper Miocene, however, likely produced a significant reorganization of the system [*Reilinger and McKlusky*, 2011; *Cosentino et al*., 2012; *Faccenna et al*., 2013]. It has also been proposed that the acceleration of trench retreat of the Hellenic slab may be due to the extra load of the broken Anatolia portion of the slab [*Faccenna et al*., 2006]. More recently, it has been suggested that mantle drag related to a large-scale convection cell could efficiently pull continental plates toward collisional zones, thus favoring indentation [*Alvarez*, 2010] and lateral escape [*Le Pichon and Kreemer*, 2010; *Becker and Faccenna*, 2011; *Faccenna et al*., 2013]. This model also agrees with previous studies that suggested that Arabia is dynamically tilted by mantle convection toward the Persian Gulf [*Daradich et al*., 2003; *Forte et al*., 2010; *Moucha and Forte*, 2011].

Despite the extensive prior efforts, basic questions on plate driving forces in the eastern Mediterranean remain unsolved [*Le Pichon and Kreemer*, 2010]. For example, it is unclear how or if the large-scale convection

cell associated with the African deep mantle plume relates to the smaller scale one associated with the pull of the Aegean slab, and what causes intraplate volcanism in the Middle East. Moreover, the relative contributions of crustal thickening during collision and active mantle upwelling, whether associated with lithospheric delamination or removal or not, in the construction of high plateaus in collisional belts remains unresolved. Although linked with the Mediterranean dynamics, the cause of Arabia's motion will be not further discussed here, limiting our discussion to the motion of microplates within the Mediterranean.

Following the discussion above, we can define three processes as potentially responsible for the motion of Anatolia. The first is the indentation of the Arabian Plate that created high terrain in eastern Anatolia whose excess gravitational energy (per unit area) can power westward movement of Anatolia relative to Eurasia. The second is the downward pull of the Hellenic slab on the overlying region, which reduces potential energy there, creates an eastward gradient in potential energy and produces return flow that may efficiently drag the upper plate trenchward [*Le Pichon*, 1982; *Faccenna et al*., 2006; *Le Pichon and Kreemer*, 2010]. The third is a basal drag applied by sublithospheric mantle flow to Anatolia and may be coupled with the second one in a convecting cell [*Le Pichon and Kreemer*, 2010; *Faccenna et al*., 2013].

To quantify the influences of these contributions, we compute the instantaneous mantle flow from seismic tomography by converting velocity anomalies to temperature [e.g., *Hager et al*., 1985; *Lithgow-Bertelloni and Silver*, 1998; *Moucha and Forte*, 2011]. We solve the Stokes equation for incompressible flow in a global, spherical shell using a finite-element approach [*Zhong et al*., 2000]. In such an approach, velocity amplitudes (controlling, e.g., microplate motions and formation of LPO anisotropy) will scale, to first order, with the local density anomaly divided by the ambient mantle viscosity, and stress quantities will depend on density anomalies alone, to first order [e.g., *Gurnis et al*., 2000].

We test several, geologically motivated models of lateral viscosity variations and several density models. The boundary conditions of the mantle flow computations are shear stress free at all or most of the surface, allowing for dynamically consistent plate motions guided by weak zones prescribed at plate boundaries [*Ricard and Vigny*, 1989; *Zhong et al*., 2000]. The modeling details are discussed in *Faccenna and Becker* [2010], whose approach involves prescribing the motions of large, "external" plates such as Africa and Arabia, only leaving the Mediterranean plates free to move, and in *Becker and Faccenna* [2011], who modeled completely "dynamically consistent" plate motions. The motivation for the partially constrained motion models is to increase the regional kinematic realism given uncertainties such as density variations underneath the African Plate. Results for all models are presented for a regional zoom-in of the global models around the Mediterranean. All velocities are rotated into a Eurasia-fixed reference frame by subtracting the velocities of a best fit rigid plate motion with axis of rotation as obtained from fitting the surface velocities within that plate.

The reference density structure for the mantle is based on several tomography models, with fast anomalies within inferred continental keels removed above 300 km to correct for shallow compositional effects [*Boschi et al*., 2010]. We use a Rayleigh number of $3.4 \cdot 10^8$ (defined as in *Zhong et al*. [2000]) with temperature scaled such density anomalies go with shear wave velocity anomalies as $(\mathrm{d} \ln \rho)/(\mathrm{d} \ln V_S) = 0.2$. This constant scaling is adopted for simplicity; it does not take depth-dependent mineral physics relationships into account [e.g., *Forte*, 2007] nor do we allow for compositional anomalies besides continental keels. However, such complications should mainly affect the amplitude but not the geometry of mantle flow.

Density models can also be inferred for slabs alone, based on deep seismicity and/or inferred past subduction [e.g., *Hager*, 1984; *Ricard et al*., 1993; *Lithgow-Bertelloni and Richards*, 1998], or by mixed models that explore the respective roles of slabs versus tomography and edge forces [e.g., *Becker and O'Connell*, 2001; *Conrad and Lithgow-Bertelloni*, 2002; *Ghosh et al*., 2010; *Stadler et al*., 2010]. Here we consider upper mantle models that are entirely or partially based on slabs inferred from the *Engdahl et al*. [1998] seismicity based, regionalized upper mantle (RUM) slab geometry of *Gudmundsson and Sambridge* [1998], following *Ghosh et al*. [2010]. No crustal density anomalies or other effects leading to lithospheric driving forces due to gravitational potential energy variations, besides those imaged by tomography, are considered.

We use a Newtonian viscous rheology with background viscosities for the lithosphere (depth $z < 100$ km), upper mantle (100 km $< z <$ 660 km), and lower mantle ($z >$ 660 km) of $5 \cdot 10^{22}$, 10^{21}, and $5 \cdot 10^{22}$ Pa s, respectively. Within the lithosphere, relative viscosities are 0.01 for weak zones along plate boundaries, defined as in *Becker and Faccenna* [2011]. This simple model achieves a good general match to global plate

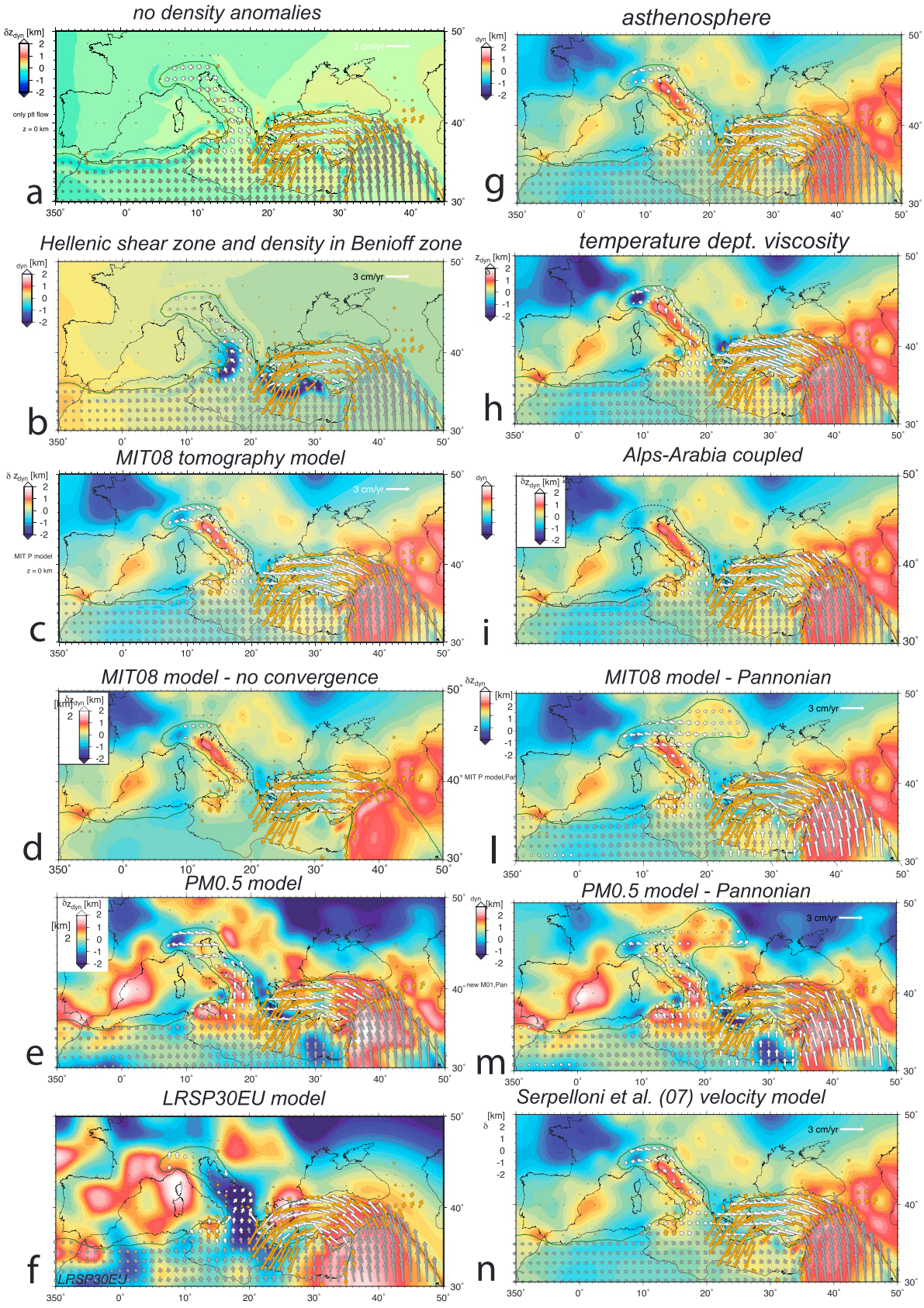

Figure 11

velocities and the geoid [*Becker et al*., 2006a; *Miller and Becker*, 2012], and we explore additional lateral viscosity variations as described below. The mantle flow model results for the region are then evaluated in the light of the present-day geodetic velocity fields by comparing predicted horizontal surface motions with seismic anisotropy (see section 9) and with dynamic topography (see section 10).

Model *a* (Figure 11a) shows results from the Africa-prescribed motion approach of *Faccenna and Becker* [2010], focusing on the motion of Anatolia and Adria (white arrows) only under the convergence velocity produced by the imposed motion of Arabia and Nubia toward Eurasia [*DeMets et al*., 2010]. The result of this simple model shows that Anatolia is moving toward the west at a rate which is ~ 60% slower than the geodetic one while the Aegean microplate motion is not matched at all. The motion of Anatolia here is simply due to the Arabia push.

Adding density anomalies (Model *b*; Figure 11b) along the Calabria and Aegean subduction zones increases the motion of Anatolia and of Aegea and the direction of the Aegean plate is better reproduced. To test the role of mantle drag, we computed circulation models based on different tomography models. Here we show results from three models, which can be compared with other two *S* wave model shown in *Boschi et al*. [2010]. Model *c* (Figure 11c) shows the results adopting the MITP08 model [*Li et al*., 2008]. Anatolia motion in this model is even faster than the geodetic velocity, indicating that mantle drag due to the upwelling in the Middle East and downwelling in the north Aegean is driving Anatolia westward. This is also quite clearly shown by model *d* (Figure 11d) where Anatolia is still moving, though at a reduced rate, when overall convergence between Africa/Arabia and Eurasia is set to zero. These calculations indicate that the motion of Anatolia results from the combined action of three main processes, as rigid escape toward the west produced by plate convergence, return flow driven by the retreating the Hellenic slab and the drag exerted by the convecting mantle [*Faccenna et al*., 2013].

Comparison with other *P* wave models [*Piromallo and Morelli*, 2003] shows basically the same results (Figure 11e). Conversely, the motion of Aegean is well reproduced by the LRSP30EU *S* wave model [*Boschi et al*., 2009, 2010] that nicely produces velocity turning into a more NE-SW direction, although it does not match the westward acceleration (Figure 11f). This may be possibly due to the fact that our model does not include the gravitational potential energy forcing stored in the crust that may be relevant in the Aegean system [*Le Pichon*, 1982].

Lastly, model tests show that the mantle flow pattern is rather stable and is more sensitive to the location of the plate boundaries than to the assumed general rheology. For example, models are only slightly sensitive to the presence or absence of an asthenosphere low-viscosity layer (Figure 11g) and the addition of temperature-dependent viscosity only slightly accelerates the velocity field but does not influence the overall pattern (Figure 11h).

The result of these simple tests shows the following that:

1. The westward motion of Anatolia with respect to Eurasia can be reproduced correctly only when accounting for the contribution of slab pull and the return flow from the retreating Hellenic slab that likely drag the upper plate trenchward, in conjunction with a mantle upwelling in the Middle East and with the shortening produced by the Arabia collision. The pattern of mantle anisotropy represents a relevant test to better understand the style of mantle flow and will be discussed in the following paragraph.
2. The motion of the Aegean plate can be correctly reproduced by suction exerted by the retreating Hellenic slab but it requires an additional contribution, probably the gravitational potential energy stored in the Aegea and Anatolia lithosphere.

9.2. The Motion of Adria

The Adria region (Figure 1) is a relatively aseismic area encircled by active orogenic belts [*McKenzie*, 1972; *Channell and Horvath*, 1976; *Channell et al*., 1979; *Anderson and Jackson*, 1987]. Stratigraphic and paleomagnetic studies have described the kinematics of Adria as a promontory of the African Plate [*Channell et al*., 1979]. The reconstruction of past relative plate positions [*Dewey et al*., 1989; *Mazzoli and Helman*, 1994; *Rosenbaum and Lister*, 2002; *Capitanio and Goes*, 2006] and the absence of relevant differential paleomagnetic

Figure 11. (a–n) Microplate motions and dynamic topography for different density models and plate boundary configurations using the approach of *Faccenna and Becker* [2010]. White vectors indicate predicted, gray-prescribed plate motions, and orange vectors are interpolated GPS observations (all in best fit Eurasia-fixed reference frame). Background color is the dynamically induced topography by mantle flow. Weak zone geometry indicated by lines. See *Faccenna and Becker* [2010] and *Boschi et al*. [2010] for details.

rotations of Adria with respect to Africa in the Tertiary [*Channell et al*., 1979; *van der Voo*, 1993; *Rosenbaum et al*., 2004] support this hypothesis. Present-day deformation patterns, as revealed by both seismological and geodetic studies, however, point out that Adria current motions are independent of both Eurasia and Africa. Despite these efforts, the boundary between Africa and Adria plate is still poorly defined, and different locations have been proposed so far in the southern part [*Anderson and Jackson*, 1987], along the Apulia Escarpment [*Battaglia et al*., 2004; *Serpelloni et al*., 2005], or by considering diffuse deformation in the Ionian Sea [*Goes et al*., 2004; *Stein and Sella*, 2005].

In a Eurasian reference frame, Adria's velocity is almost perpendicular to that of Nubia (Figures 1 and 2), with its speed increasing southward, matching the counterclockwise rotation of a rigid plate with a rotation pole in the Po Plain [*Calais et al*., 2003; *Battaglia et al*., 2004; *Serpelloni et al*., 2005]. This rotation well describes the motion of the northern part of Adria (north of Apulia promontory), which may be separated from a southern block along a E-W trending active fault zone, the mid-Adriatic shear zone, located roughly along the 41°N parallel [*Westaway*, 1990; *Calais et al*., 2003; *Oldow et al*., 2002; *Battaglia et al*., 2004; *Favali et al*., 1993, *D'Agostino et al*., 2008]. South of this fault zone, it is possible to identify another microplate, which includes the southern Adriatic block with Apulia promontory, the Ionian Sea and, possibly, the Hyblean region in southern Sicily [*D'Agostino et al*., 2008]. This southern block rotates clockwise around a pole positioned off Cyrenaica and is separated from Africa by the Sicily channel extensional zone [*Westaway*, 1990; *Argnani*, 1990; *Torelli et al*., 1995]. The kinematics of those two oppositely rotating blocks has been related to the Eurasia-Nubia plate convergence [*D'Agostino et al*., 2008].

Mantle flow models show also that the Adria plate can move independently from Africa [*Ismail-Zadeh et al*., 2010; *Faccenna and Becker*, 2010]. In these models, Adria's motion is related to a combination of plate convergence and mantle dynamics (Figure 11). Considering the close position of the oppositely dipping Hellenic and Calabria subduction zones, it appears difficult to transmit rigidly the motion from Africa to Adria. The neck of the Adria plate between the Hellenic and Calabrian trench is too narrow. In addition, Adria is probably laterally too firmly anchored by the opposite verging subducting slabs to be able to move coherently with Africa. In particular, mantle flow tests (Figure 11) show that the motion of Adria is influenced by mantle circulation and that the microplate does not behave rigidly (questioning the microplate concept). The northern side, Po Plain, is, in fact, moving with respect to Eurasia toward the west, driven by the pull of the western Alps slab (Figure 11). The central part, conversely, is pulled toward the east by the cold sinker associated with the Aegean slab (Figures 11c and 11e). This is better shown by model without convergence (Figure 11d) where southern Adria is moving much closer to what is observed from geodesy. Probably a more realistic solution is obtained by considering the Alpine collisional boundary as inactive and removing the weak zone there (Figure 11i). In this case, the expected surface velocity is closer to what is observed, especially explaining the eastward motion of the central Adria plate. Changing the convergence velocity model (Figure 11n, *Serpelloni et al*. [2007]) or the plate boundary by including also the Pannonian Basin and the Carpathians, conversely, does not produce a relevant change in the Adria motion both for the MITP08 and PM0.5 models (Figures 11l and 11m).

The results of this set of model runs for the Adria plate suggest an alternative model to that of crustal block interactions [*D'Agostino et al*., 2008] that involves an active role from the subducting slab. In this model, the eastward motion with respect to Eurasia observed in the central Adriatic zone is independent from plate convergence and is generated by the pull of the Dinaric-Aegean slab. This portion of the subducting slab is indeed seismically active. Its activity may be also related to the partial cessation of activity of the central Apennines subduction zone. Further test would be necessary to better quantify the role of these active processes in the central Mediterranean.

10. Mantle Flow and Seismic Anisotropy

Another constraint for mantle flow is provided by seismic anisotropy which in the upper mantle most likely reflects the alignment of intrinsically anisotropic, single crystals of olivine into lattice-preferred orientation (LPO) under mantle flow [e.g., *Silver*, 1996; *Montagner*, 1998; *Ben-Ismail and Mainprice*, 1998; *Savage*, 1999; *Long and Becker*, 2010]. This motivates quantitative comparisons between inferences from geodynamic models and seismological measurements, for example, of shear wave splitting [e.g., *Hall et al*., 2000; *Blackman et al*., 2002; *Behn et al*., 2004; *Becker et al*., 2006b].

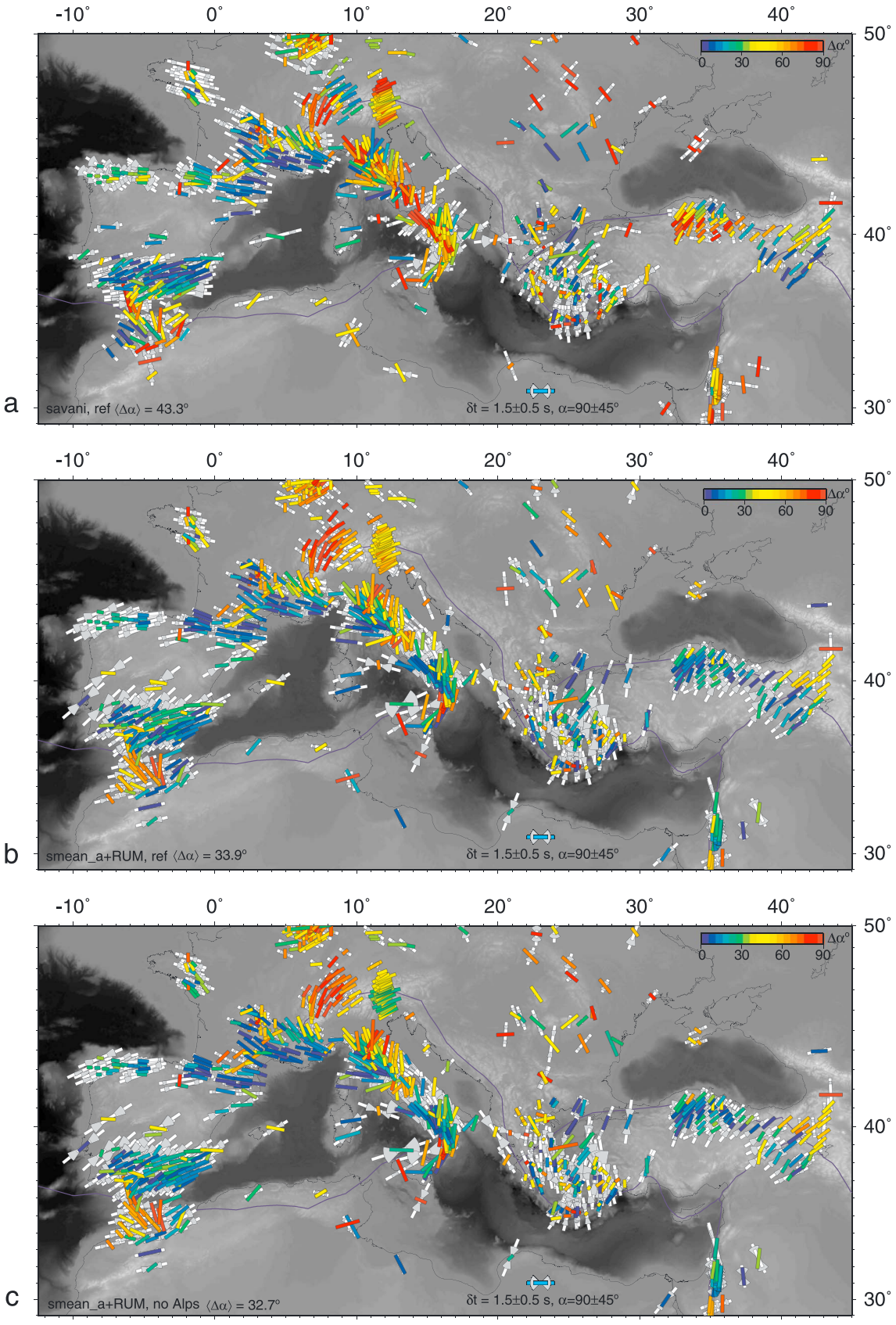

Figure 12

Here our approach consists of assuming that flow is steady state, for simplicity (cf. tests for time dependence in *Becker et al*. [2003]), for the few Ma needed to achieve saturated textures. We follow tracer particles in the global mantle circulation models we construct until stable LPOs, as predicted by the mineral physics theory of *Kaminski et al*. [2004], are reached at each desired location [*Becker et al*., 2006a]. Then, we assign pressure- and temperature-dependent elastic tensors to the resulting 3-D model of elastic anisotropy from 50 to 410 km depth. From this, we compute synthetic seismograms assuming lateral homogeneity on Fresnel zone lengths (~ 100 km) using a full waveform method for synthetic seismograms from which the expected splitting can be computed for arbitrary back azimuths [*Becker et al*., 2006b]. However, here we will only consider station-averaged splits and mainly discuss our models in terms of the average angular misfit, $\langle \Delta\alpha \rangle$, of apparent fast axes for all available nonnull splitting measurements.

Large-scale, global numerical computations now allow exploration of a significant part of parameter space of anisotropy formation at resolutions down to ~ 20 km, while treating the general ingredients of Stokes flow modeling, density, and viscosity models, as variable parameters. This allows fitting regional anisotropy and global metrics such as plate motions and the geoid [*Miller and Becker*, 2012; *Faccenna et al*., 2013]. All of the models considered for modeling seismic anisotropy have fully self-consistently moving plate motions, following the modeling approach of *Becker and Faccenna* [2011].

When modeling shear wave splitting observations, the best published regional fast azimuth misfits are of order ~20° and variations of model parameters provide inferences on the dynamics which affect mantle flow and anisotropy in the region [e.g., *Behn et al*., 2004; *Becker et al*., 2006b; *Miller and Becker*, 2012; *Alpert et al*., 2013]. However, in a previous work on the Middle East system [*Faccenna et al*., 2013], we found that the match to anisotropy in tectonically complex regions is sensitive to the details of choices regarding weak zones. As expected from the complex plate kinematics explored in the previous section, the same holds true when considering *SKS* data in the Mediterranean from Figure 8 (except *Kovács et al*.'s [2012], data, not available to us at the time), explored in Figure 12. Instead of trying to aim for the "best" model in terms of global azimuthal anisotropy misfit, we show three cases that illustrate the effects of density anomalies and viscosity variations.

Figure 12a shows the predictions for induced plate motions and internal flow as driven by the SAVANI model (Figure 6) and the reference weak zone geometry (also compare with Figures 8c and 11). The large-scale trends in the western region of Spain and France fit moderately well with this model. However, Italy and central Anatolia are not. If we replace the fast upper mantle structure in tomography by slabs as inferred from seismicity in the Tyrrhenian and Hellenic region (RUM model of *Gudmundsson and Sambridge* [1998]), the predictions are improved (Figure 12b), and the mean misfit of $\langle \Delta\alpha \rangle$ reduced from ~43° to 34°. The localized sinkers underneath Tyrrhenian and the Hellenic Sea lead to quite widespread inward flow (slab suction) in those regions, which appears to be required by the *SKS* splitting. In the central-western Mediterranean, this flow is probably induced by the rollback motion of the Calabrian slab [*Lucente et al*., 2006] matching properly the extensional direction [*Jolivet et al*., 2009]. Perhaps surprisingly, the area that is apparently affected by this suction is large and extends over Spain-North Africa and France for the Tyrrhenian case. It is remarkable that trench parallel directions observed beneath the Apennines are also predicted by the pull of the Tyrrhenian slab, giving an alternative solution to earlier suggestions of trench local mechanisms, and highlighting the nonuniqueness of slab anisotropy observations [cf. *Long*, 2013]. Similar considerations hold for Anatolia-Bitlis fabric that is predominantly matched by the pull and rollback-induced flow of the Hellenic slab, confirming our previous model [*Faccenna et al*., 2013].

This anisotropy modeling result also emphasizes the role of slab fragments for small-scale convection within the Mediterranean domain [cf. *Faccenna and Becker*, 2010]. It indicates that large-scale models such as SAVANI fail to image the required fine-scale structure that is now accessible to geodynamic modeling in light of data-rich environments such as the Mediterranean. However, employing higher resolution models such as PM0.5 did not improve the fit significantly compared to Figure 12b, which perhaps indicates that more

Figure 12. Comparison between synthetic and observed (as in Figure 8a but without the *Kovács et al*.'s [2012] data set) *SKS* splitting. Background gray wedges with white sticks indicate flow model predictions of fast azimuth and delay times including their standard deviations from full waveform back azimuth scans (in analogy to the surface wave synthetic *SKS* splitting in Figure 8b). Colored sticks are the splitting observations, colored by the local azimuth misfit, $\Delta\alpha$, with mean misfit values for the whole model domain (841 observations) indicated in the legend. (a) Reference weak zone geometry, mantle density inferred from the SAVANI model of *Auer et al*. [2014]. (b) Density in mantle inferred from a combination of the SMEAN composite model in the lower mantle, and low wave speed anomalies from SMEAN plus slab structure inferred from RUM in the upper mantle [cf. *Ghosh et al*., 2010; *Miller and Becker*, 2012]. (c) Density as in Figure 12b, but omitting the weak zone around the Alpine chain [cf. *Faccenna and Becker*, 2010]. All modeling choices are as in *Faccenna et al*. [2013], see there for details.

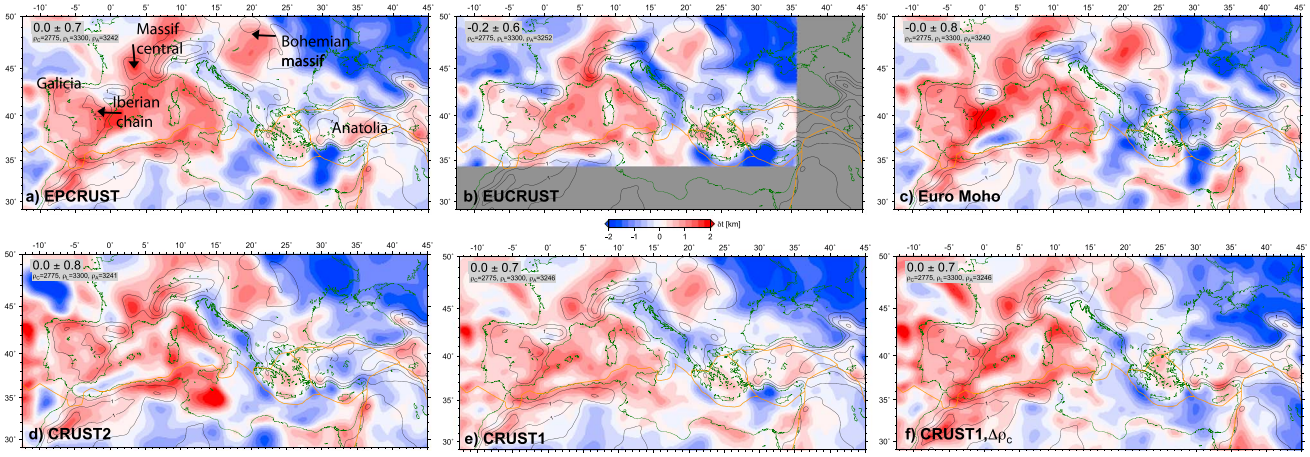

Figure 13. Estimates of the residual topography obtained by subtracting Airy compensated models of crustal structure from the observed (long-wavelength smoothed) topography for the different crustal models of Figure 5. Orange plate boundaries are from *Bird* [2003], dark contours are smoothed actual topography in 750 m intervals for positive bathymetry only. Inset shows density values used for the crust, lithosphere (constant thickness of 100 km), and asthenosphere, respectively, optimized by minimizing the residual for each model. (a–e) EPCRUST, EUCRUST, Euro Moho, CRUST2.0, and CRUST1.0 crustal thickness variations, respectively. (f) CRUST1.0 thickness and average lateral crustal density variations.

regional data should be added to multiscale shear wave tomography models that can benefit from the good surface near constraints available from surface waves.

Figure 12c illustrates the role of weak zones [cf. *Faccenna and Becker*, 2010]. Removing the whole Alps domain, i.e., considering the collisional zone as "locked," does lead to an improvement in the fit to *SKS* in the eastern, but not the western Alps that remain poorly fit. This trench pattern is actually poorly fit by those regional models and may require significant lithospheric contributions related to the orogenic pattern [*Meissner et al*., 2002]. Such lithospheric, perhaps frozen-in, fabrics are not considered here in our exploration of asthenospheric anisotropy due to convection. Regional model refinement can also improve fits by modifying density structures, as was done, for example, by *Alpert et al*. [2013] for the Alboran region. However, we shall refrain from such further refinements here.

In summary, the comparison between mantle flow model and anisotropy support the idea that the large-scale, quasi-symmetric, pattern of mantle flow in the Mediterranean is induced by the two retreating slabs, the Calabrian and the Hellenic ones. This influences the mantle strain pattern on areas wider than previously thought. Our results also support the idea that upper mantle is playing an active role on the microplate motion of the Mediterranean region.

11. Isostatic Versus Dynamic Topography

Geomorphological and geodetic data show that within several Mediterranean regions, the topography is ever changing, and at quite rapid rates. This is not only the case along plate boundaries, where variation of crustal thickness is expected, but also in regions far from plate boundaries.

Remarkable features in the Mediterranean are represented by the significant ($>$ 0.8 mm/yr) uplift rates registered along several orogenic belts, such as the Alps and the central Apennines. Moderate uplift rates (0.5 ± 0.2 mm/yr) are registered over northern Spain, in the Central system, Iberian chain, Valencia trough, the Atlas, along the Catalan Coastal range [*Janssen et al*., 1993; *Lewis et al*., 2000; *Gaspar-Escribano et al*., 2004; *Cloetingh et al*., 2002; *Teixell et al*., 2005; *Casas-Sainz and de Vicente*, 2009; *Millller and Becker*, 2013; *Scotti et al*., 2013], and over Central-Southern Anatolia [*Cosentino et al*., 2012] (Figure 3c). Subsidence is distributed over most of the basins in and around the Mediterranean, but particularly in these locales, the geodetic signal may be affected or amplified by anthropic effects such as compaction due to gas and water pumping (e.g., Po Plain and northern Apennines [*Carminati et al*., 2003a, 2003b]) (Figure 3c). The origin of the variation of the topography and of the topography itself is complex, as may be related to different processes acting at different levels, from the surface to the deep mantle.

Our contribution here is to discuss if the topography signal of some part of the Mediterranean can be attributed only to its isostatic contribution, resulting from the buoyancy of the crustal and mantle lithosphere layer, or if there is an additional contributions from deep mantle source. This deeper contribution is related to the stress generated at the base of the lithosphere by the flow produced by density variation in the Earth's mantle. This produces a "dynamic topography" signal on the surface [*Hager et al*., 1985]. A possible way to approach the problem of the "static" versus dynamic topography is to compute the expected elevation of a given lithosphere column, assuming it to be in Airy isostatic equilibrium, and to compare that with its elevation. The difference between its elevation and the one estimate from isostatic equilibrium is commonly defined as "residual topography" (Figure 13). Eventually, the residual topography can be compared with a model dynamic topography (Figure 14). Integrating in time observation and the modeling can provide further constraints to the model [e.g., *Gurnis et al*., 2000; *Daradich et al*., 2003; *Moucha and Forte*, 2011].

The expected elevation (e) of a lithospheric column assuming it to be in Airy isostatic equilibrium with respect to a reference level (H, usually taken as average ridge elevation, here -2.6 km) is given by the lithosphere buoyancy, composed of a crustal layer with a thickness (l_c) and density (ρ_c) overlying a mantle lithosphere with a thickness (l_l) and density (ρ_l), floating over an asthenosphere of density (ρ_a).

$$e = (f_1 l_c + f_2 l_m) - H \tag{1}$$

where

$$f_1 = (\rho_a - \rho_c)/\rho_a \text{ and } f_2 = (\rho_a - \rho_l)/\rho_a \tag{2}$$

Due to the composition of continental crust, $-f_2$ is usually 1 order of magnitude lower than f_1, and so the contribution of the crust to elevation is more than the double than that of the lithospheric mantle contribution. Therefore, the effect of crustal variation is more relevant than that of the lithosphere mantle, and this is fortunate given our poor knowledge on the depth of the lithosphere-asthenosphere boundary with respect to that of the Moho. The estimates of the isostatic topography suffer from the poorly constrained buoyancy parameter of the lithosphere. As we have seen, the crustal structure around the Mediterranean is only partly established (Figure 5). The main difference between the different models is in the Middle East and in western Anatolia, where EuroMoho and EPCrust show thickening up to ~40 km or more, whereas CRUST1.0 (which contains an average of the regional models) and Eucrust is always at ~30–35 km. Recent receiver function studies show that CRUST1.0 and Eucrust model are perhaps more appropriate than other models [*Karabulut et al*., 2013; *Vanacore et al*., 2013]. Other differences between models are found on orogenic belts, such as the Apennines, Pyrenees, or the western Alps, where crustal thickness variation of up to ~10 km. The crustal density is also a rather poorly constrained parameter, being dependent on the knowledge of the thickness of the sedimentary column and on the composition of the lower crust.

The residual topography shown in Figure 13 is inferred from different crustal models as shown in Figure 5 by correcting the observed topography for the expected isostatic topography. All topography estimates have short wavelength structure removed by convolution with a Gaussian smoothing kernel of 6σ width of 250 km. All models assume a constant lithosphere thickness of 100 km and a reference density of 2775 kg/m^3 and 3250 kg/m^3, for the crust and the lithospheric mantle, respectively. For one model, we allow for lateral variations in crustal density as inferred from the column averages of CRUST1.0. The asthenospheric density value is set to minimize the residual in order to attribute the maximum possible topography variations to isostasy, and best fit values range from 3202 to 3210 kg/m^3.

With exception of the Pyrenees belt, all crustal models show a positive residual topography for Iberia, with variable amplitude (Figure 13). The maximum of the residual is observed in the Iberian chain and in Galicia. The Pyrenees shows a slightly negative or null signal, suggesting a nearly Airy isostatic equilibrium. Positive residual topography is observed in Anatolia, particularly in the EuCrust07 model for the West Anatolia [cf. *Boschi et al*., 2010]. Recent receiver function studies confirm this model, thus indicating that Anatolia is more elevated than expected from isostasy [*Komut et al*., 2012; *Karabulut et al*., 2013; *Vanacore et al*., 2013]. All the models also show a broad region of positive residual topography extending from the Western Alps, Massif Central to the Bohemian massif. The western Alps, the Apennines, the Tell, and the Atlas also have a positive sign. In those regions, however, the crustal structure is complex [*Piana Agostinetti and Amato*, 2009] or, as for the case of North Africa, as of yet poorly constrained. Negative anomalies are found in the deep Mediterranean basins. In those cases, the correction should account for the age-dependent density

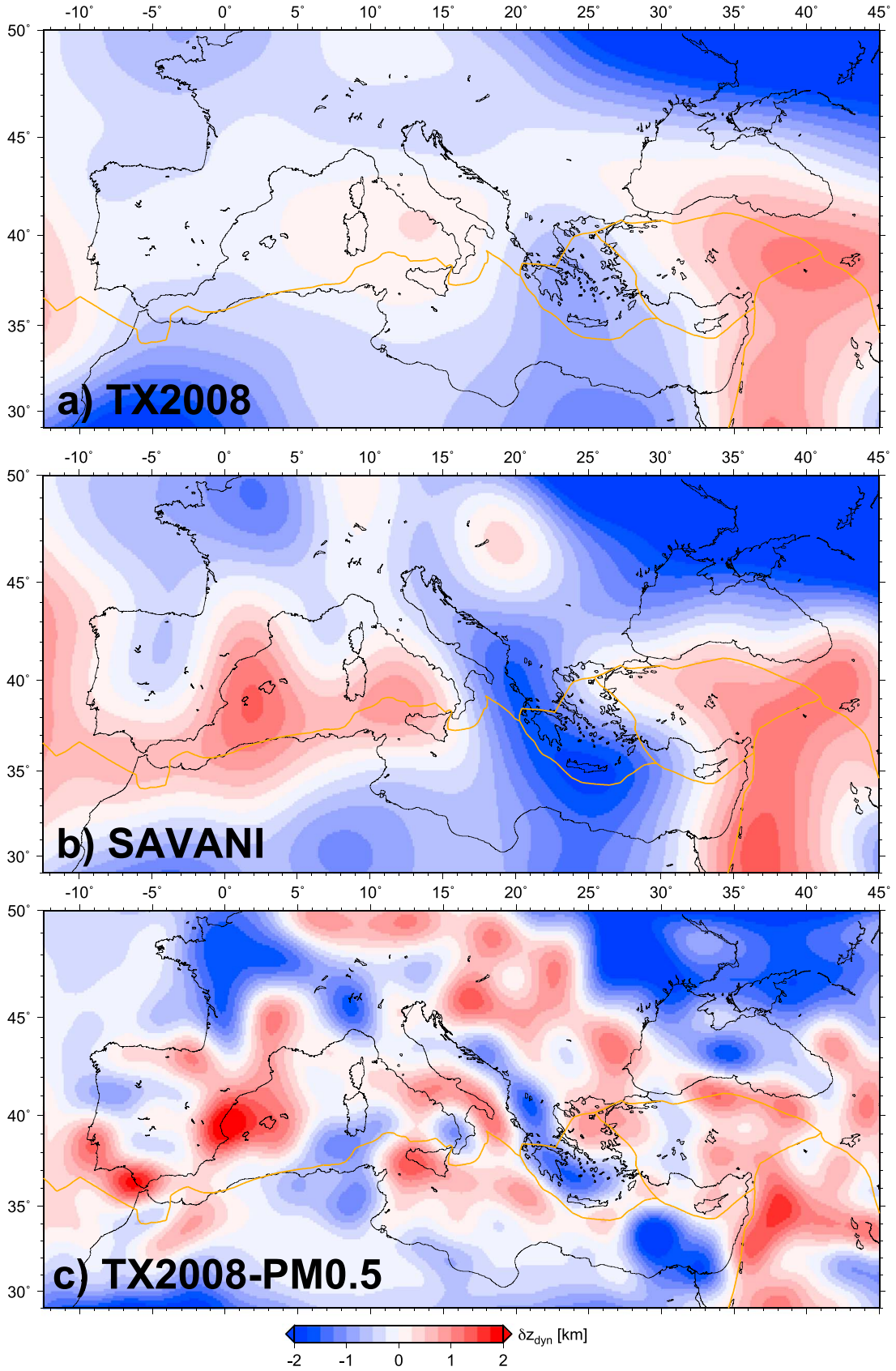

Figure 14

structure of the oceanic lithosphere, probably Jurassic in age [*Speranza et al*., 2012]. Negative topography anomalies are also in the Po Plain, along the Dinarides, the Hellenides, and in the Black Sea-East European platform. There, one may again explore a lithospheric origin of the residual topography such as due to relatively thicker, older continental lithosphere [e.g., *Artemieva*, 2007].

The origin of the residual topography shown in Figure 14 could be due to different effects. They may be related due to a variation on lithospheric thickness [cf. *Gvirtzman and Nur*, 2001; *Artemieva*, 2007]. For example, to explain the elevation and recent uplift of Iberia would require a loss of ~30 km of mantle lithosphere. Given our loose constraints on the lithosphere asthenosphere boundary, this model can be hardly tested. In any case, this lithospheric thickness variation may be considered as a viable solution in areas of recent deformation or near plate boundary [*Göğüş and Pysklyweck*, 2008; *Komut et al*., 2012], but it hardly applies to intraplate region as Iberia.

The other possible source of elevation may be related to far-field stress, producing lithospheric folding and undulation whose wavelength depends upon the elastic thickness and/or the presence of decoupling layer [*Cloetingh et al*., 2002]. For the same case of Iberia, it has been proposed that the alternation of basins and ridges may at least be partially explained by this effect.

The third possible explanation for the residual topography is related to mantle convection. Convective flow may produce vertical stresses at the base of the lithosphere producing a transient "dynamic" topography signal. The normal stresses generated by viscous flow due to density anomalies within the top ~500 km of the mantle are used to infer the instantaneous surface deflection [*Ricard et al*., 1984; *Richards and Hager*, 1984]. The dynamic topography signal can be transient and lead to uplift and subsidence, as opposed to the present-day out of isostatic equilibrium states, if the plate moves relative to the density anomalies, or vice versa. It is expected to produce undulations of the surface topography with amplitude of few hundreds of meters and wavelength of hundreds of kilometers [*Braun*, 2010; *Flament et al*., 2013].

Here we estimate the dynamic topography from instantaneous mantle flow computations from the radial tractions acting upon a free-slip surface boundary condition in an incompressible Newtonian fluid spherical annulus that has only radial viscosity variations, for simplicity. These approximations allow for a semianalytical approach to estimate global mantle flow based on spectral methods [*Ricard et al*., 1984; *Richards and Hager*, 1984]. Density models are again constructed by scaling the velocity anomalies from seismic tomography to temperature.

The dynamic topography models shown here (Figure 14) are based on different tomographic models and can be then compared with residual topography. Preliminary analysis shows that shear wave tomography models can fit both horizontal geodetic data over microplates and the residual topography map better than the body wave model, because the latter have generally poorer resolution in the shallowest layers of the mantle [*Boschi et al*., 2010].

Here we estimate dynamic topography from TX2008 [*Simmons et al*., 2009], SAVANI [*Auer et al*., 2014], and PM0.5 ([*Piromallo and Morelli*, 2003]; embedded into TX2008). Global models that do not incorporate refined regional data sets, such as TX2008 (Figure 14a), show the first-order structure of the Mediterranean, as a broad negative anomaly due to the presence of the slab beneath the Hellenic, a marked positive anomaly beneath the Middle East-Anatolia and in the Tyrrhenian-central Apennines. Also, SAVANI (Figure 14b) shows a more focused negative anomaly beneath the Hellenic region and northern France and Middle East-Anatolia positive anomaly. In addition, this model shows a positive anomaly in the central Mediterranean back-arc region extending from eastern Iberia-Valencia, Liguro-Provençal, and Tyrrhenian basin. The reason for this signal is simply that all of those regions are underlain by a shallow low velocity anomaly (Figure 6a).

The body wave models show a smaller scale, pattern of negative/positive anomaly basically confirming the SAVANI model. TX2008-PM0.5 model shows a negative anomaly along the Hellenic arc and in northern

Figure 14. Predictions of dynamic topography from inferred surface deflections as caused by the present-day mantle flow. Computations use HC [*Milner et al*., 2009] to explore simplified rheologies with only radial viscosity variations leading to imprecise plate motions. Density scaling uses (a) the global *S* wave model TX2008 [*Simmons et al*., 2009], (b) SAVANI by *Auer et al*. [2014], and (c) PM0.5 [*Piromallo and Morelli*, 2003] embedded in TX2008, as in the background of Figure 8a.

France. It also confirms the presence of a positive anomaly beneath eastern Iberia-Valencia trough and in the Middle East Anatolia. In addition, it shows a positive anomaly of smaller size in the Sicily channel, central Apennines-Apulia, Massif Central, and northern Greece. Smaller negative anomalies appear in correspondence of subducting slab such as beneath the western Alps, Calabria, and North Africa. Large negative residual topography over the stable Eurasia region may be related to an increase of that mantle lithosphere thickness [*Artemieva*, 2007].

From the comparison between residual and dynamic topography (Figures 13 and 14), it is possible to draw the following considerations:

1. Dynamic topography shows a positive signal over east Iberia, in the Valencia trough. This anomaly matches fairly well the residual topography. Geological indication also shows an episode of post-Pliocene uplift of the entire region of few hundreds of meters and few millions of years after the end of the main tectonic event [*Janssen et al*., 1993; *Scotti et al*., 2013]. Our analysis indicate that the origin of this doming event may be well explained by mantle upwelling but other possible causes as mantle lithosphere thinning or large-scale folding can be equally considered. Same considerations hold for the Pannonian Basin.
2. Confirming previous indication [*Faccenna and Becker*, 2010; *Komut et al*., 2012], we also show that part of the positive residual signal over Anatolia and Middle East may be related to mantle upwelling, as suggested by geological indications [*Cosentino et al*., 2012].
3. The Hellenides and Peloponnese show negative dynamic topography which matches the residual topography, suggesting that the pull of the Hellenic slab may be produce dynamic and detectable subsidence [*Husson*, 2006];
4. Negative residual topography in the Adria region is supported by SAVANI and from TX2008-PM05 suggesting a dynamic contribution from the Alpine slab as proposed by *Shaw and Pysklywec* [2007].

Quantifying the dynamic topography signal further requires a more detailed analysis. However, the comparison between residual and dynamic topography and geomorphological data indicates that the role of mantle flow on shaping surface topography over the Mediterranean is important. The most clear signals are, not surprisingly, represented by the negative dynamic topography over the Hellenides slab and, perhaps more surprisingly, the positive signal over Anatolia and Iberia [*Faccenna and Becker*, 2010; *Boschi et al*., 2010]. In both those two anomalously high areas, geomorphological data indicate that those regions have uplifted recently at rate of 0.5–1 mm/yr [*Scotti et al*., 2013; *Cosentino et al*., 2012] of few hundreds of meters. The amplitude of the processes may be variable depending on the chosen crustal or tomographic model, but it may be in the order of some hundreds of meters.

12. Outlook and Final Remarks

The result of the analysis of the structure and evolution of the Mediterranean can be summarized in few relevant points.

1. The past and present velocity field of the Mediterranean is only subordinately guided by the plate convergence. Back-arc spreading, now active only in the Aegean, has been episodic and punctuated by pulses of fast extension. The speed of the microplates, Anatolia, Aegea, and Adria, is and has been faster than plate convergence. The internal dynamic of the system, i.e., subduction process, rather than plate convergence exerts a primary role on Mediterranean tectonics.
2. The structure of the Mediterranean crust and mantle is rather well illuminated and robust at long-wavelength scale. The comparison between different tomography models highlights the presence of high-velocity anomalies in correspondence of the deep inclined seismic zone of the Aegean and Calabria, stagnating in the transition zone. Large low-velocity anomalies dominate the back-arc regions on the slabs side. Mantle anisotropy is well aligned to the stretching direction of back-arc basins but extends also outside them (i.e., Spain and France on the West and Anatolia-Bitlis to the East) whereas a predominantly trench parallel pattern of anisotropy is observed beneath the subduction zones.
3. The amount of subduction estimated by Tertiary tectonic reconstruction is in good agreement with what estimated from seismic tomography. The velocity of subduction and its retrograde motion can be reproduced by a simple physical model of slab sinking in a viscously stratified mantle. However, the presence of heterogeneities in the subducting material and the consequent slab deformation largely influence the style of subduction.

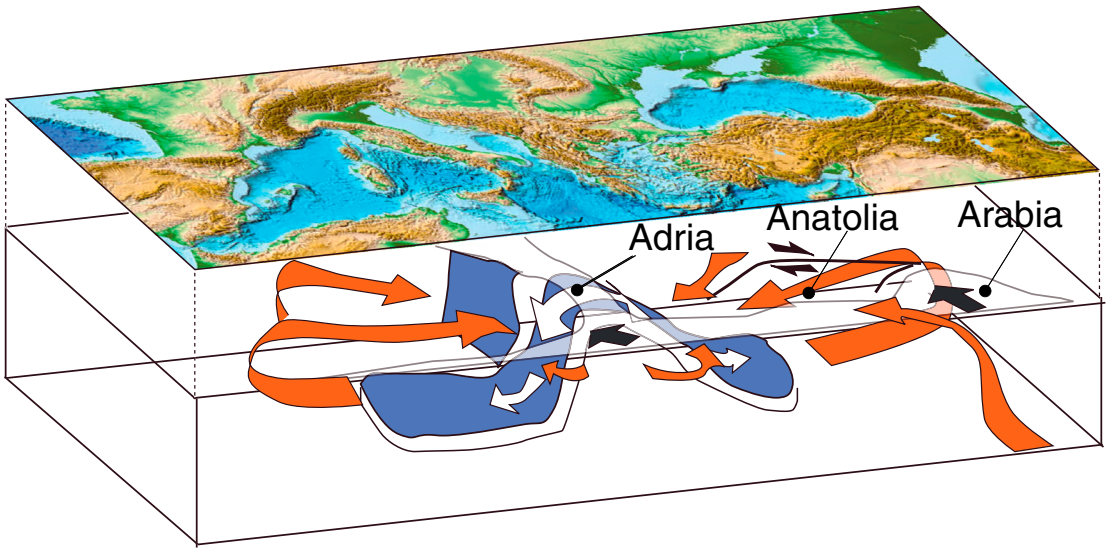

Figure 15. Cartoon showing the hypothetical pattern of mantle convection presently active in the Mediterranean (modified from *Faccenna and Becker* [2010]).

4. Simulation of the present-day pattern of mantle flow shows small-scale convection cells confined between the base of the lithosphere and the transition zone. This style of convection is expected to produce a recognizable signal on the surface in terms of horizontal and vertical motion. We explore the model sensitivity field varying input data, i.e., tomographic models, weak zones distribution, and rheological profiles. We validate the numerical simulations using the present-day motion of the microplates, seismic anisotropy, and dynamic topography.
5. Our best interpretation of the mantle flow beneath the Mediterranean is summarized in Figure 15. The central Mediterranean represents the main "catchment area": both the Hellenic and Calabria slabs are sinking there, consuming the last remnant of old lithosphere beneath the Ionian Sea. At transition zone depth, high-velocity material stagnates beneath the back-arc regions, as a result of the retrograde motion of the slab. At shallow upper mantle levels, back-arc regions are dominated by low-velocity anomalies rooted in the transition zone on the margin of the high-velocity bodies. We interpret this signal as due to an upper mantle scale return flow, induced by the subducting slabs favoring upwelling of mantle to shallower depths. In this view, the return flow of the Calabrian subduction is represented by a zone of upwelling positioned beneath the Valencia trough/eastern Spain/Massif Central. The return flow of the Hellenic slab is beneath the northern Hellenides/Anatolia. This is supported also by *SKS* fast polarization azimuth which, in the back-arc region, is parallel to the extensional direction and is well aligned with what expected from the suction flow exerted by retreating slab. Numerical simulation also shows that the motion of Anatolia is partly due to drag exerted by the subduction-related mantle flow. In addition to this first-order pattern, there is a number of small convection cells positioned on the side of the slab as shown by anisotropy and geological studies (i.e., Sicily channel for Calabria, SW Turkey for the Hellenic slab, and SW African cost of Morocco for the Alboran slab) and interpreted as toroidal flow around slab edges.
6. Comparison between residual and dynamic topography and morphological evidences indicates that at least a fraction of the topography signal over specific Mediterranean areas cannot be explained by isostatic equilibrium. There is a negative topography signal related to the subduction zones. Its surface topographic effect has been described in the Tyrrhenian and Aegean Sea but its scale and amplitude still need to be constrained. Similarly, it is possible to interpret the high topography of some undeformed regions, such as eastern Spain/Massif Central to the West or the Anatolia plateau to the East, as partly due to the upwelling return flow. Further analysis is required to properly quantify the static and dynamic component of topography; for example, constraints on the structure of the crust and of the lithosphere are essential to better assess its isostatic equilibrium.

In summary, we consider the Mediterranean as a key site where the linkage between mantle dynamics and surface processes can be analyzed in detailed. Our conclusions are only preliminary but show that understanding deformation over mobile belts requires the knowledge of mantle dynamics. Further studies and

more sophisticated modeling are necessary to test some of the ideas presented here. A main future step would be to reconstruct back in time the pattern of mantle convection over geological time scale with high resolution, including the interplay between convection and conduction and the modifications of crustal thickness (thickening or thinning) that may become relevant for the distribution of lithosphere body forces.

Glossary

Azimuthal anisotropy: a simplified case of elastic anisotropy with hexagonal symmetry axis in the horizontal such that vertically polarized shear waves propagate with velocity *v*_{SV1} along the "fast azimuth" compared to *v*_{SV2} along the slow azimuth at 90°.

Backarc: the region positioned behind the volcanic arc on the opposite side of the subduction zone (i.e., toward the upper plats). The tectonic regime of the back-arc area can be compressional, extensional, strike-slip, or neutral depending on the relative motion between the trench and the upper plate.

Capable fault: a fault potentially able to generate surface deformations including coseismic deformations.

Dynamic topography: continental or oceans topographic deflection due to the stress generated by mantle convection at the base of the lithosphere. It is transient as it varies with mantle flow.

Extrusion: or escape describes the motion of continental material away from collision zone related to forces due to continental buoyancy.

Fabric: The fabric of rocks describes the spatial and geometric configuration of all the elements that make it up, at microscopic scale. It is generally adopted to describe the structure on a metamorphic rocks.

Flysch: a sequence of sedimentary rocks deposited in a deep marine facies in the foreland basin of a growing orogen. They consist of repeated sedimentary cycles with upward fining of the sediments.

Foredeep: a basin related to the bending and flexure at trench of the downgoing slab close to an orogenic belt.

Fresnel zone: the three-dimensional, cone-shaped region along an idealized raypath that approximates the region where Earth's structure most influences seismograms at a given period as used for seismic measurements, expected to be ~100–200 km in the upper mantle.

Lattice-preferred orientation (LPO): also as crystallographic preferred orientation describes the nonrandom alignment of mineral grains as a consequence of rock deformation, here used in terms of macroscopic anisotropy resulting from alignment of intrinsically anisotropic minerals such as olivine under mantle flow.

Microplate: rigid tectonic plate significantly smaller than the surrounding ones. No size threshold exists to define microplates.

Mobile belts: elongated continental margin plate boundaries that exhibit long-lived deformation history along continental margin. They contrast the stability of cratons.

Molasses: Sedimentary continental deposits filling foredeep basin. They derive from the erosion of the rising mountain belt.

Oblique convergence: the nonorthogonal relative motion of plates at plate boundary (subduction zone).

Orocline: a curved orogenic belt bent after its formation.

Radial anisotropy: a simplified case of elastic anisotropy with hexagonal symmetry axis in the vertical such that horizontally polarized shear waves propagate with velocity *v*_{SH} that is different from that for vertically polarized shear waves traveling with *v*_{SV}.

Receiver function analysis: a technique to isolate, on three-component seismograms, the signal from *P*-to-*S* teleseismic waves converted at interfaces beneath the seismometer (receiver). The amplitudes of the arrivals in a receiver function depend on the incidence angle of the impinging *P* wave and the size of the velocity contrasts generating the conversions. The arrival times of the converted phase depend on the depth of the velocity contrast, the *P* and *S* velocity between the contrast and the surface, and the *P* wave incidence angle. The relative amplitudes of the later arrivals and their frequency content depend on the sharpness of the velocity transition.

Residual topography: the nonisostatic component of topography. It can be obtained by subtracting from the actual topography the expected topography assuming isostatic equilibrium.

Seismic moment: a measure of the size of an earthquake based on the fault rupture area, the average amount of slip, and the force required to overcome the friction coupling the rocks that were displaced by seismic faulting.

Seismic tomography: A technique that uses the recordings at seismic stations of seismic waves to derive three-dimensional images of Earth's interior in terms of seismic parameters (wave speed, attenuation).

Subduction zone coupling: friction between the two sides of a subduction interface and related short-term (interseismic) slip rate.

Synrift: Deposits filling an extensional basin during its opening phase. It contrasts with postrift deposits that accumulate after the main extensional phase.

Tectonic inversion: reactivation of a structure or a basin under a different tectonic regime. More common is the positive tectonic inversion to indicate an extensional basins or normal faults reactivated under compression.

Trench rollback: also as slab rollback, the backward/oceanward motion of the trench with respect to the upper plate.

Acknowledgments
C.F. thanks the University of Southern California (USC) for supporting his visit at USC where this paper was written. We would like to thank the reviewers, Editor Fabio Florindo, and in particular Peter Molnar for the thoughtful revision and discussion.

The Editor on this paper was Fabio Florindo. He thanks Peter Molnar and three anonymous reviewers for their review assistance on this manuscript.

References

Alchalbi, A., M. Daoud, F. Gomez, S. McClusky, R. Reilinger, M. A. Romeyeh, A. Alsouod, R. Yassminh, B. Ballani, and R. Darawcheh (2010), Crustal deformation in northwestern Arabia from GPS measurements in Syria: Slow slip rate along the northern Dead Sea Fault, *Geophys. J. Int.*, *180*(1), 125–135.

Alpert, L. A., M. S. Miller, T. W. Becker, and A. A. Allam (2013), Structure beneath the Alboran from geodynamic flow models and seismic anisotropy, *J. Geophys. Res. Solid Earth*, *118*, 4265–4277, doi:10.1002/jgrb.50309.

Altamimi, Z., X. Collilieux, and L. Métivier (2011), ITRF2008: An improved solution of the international terrestrial reference frame, *J. Geod.*, *85*, 457–473.

Altamimi, Z., L. Métivier, and X. Collilieux (2012), ITRF2008 plate motion model, *J. Geophys. Res.*, *117*, B07402, doi:10.1029/2011JB008930.

Alvarez, W. (2010), Protracted continental collisions argue for continental plates driven by basal traction, *Earth Planet. Sci. Lett.*, *296*(3), 434–442.

Alvarez, W., T. Cocozza, and F. C. Wezel (1974), Fragmentation of the Alpine orogenic belt by microplate dispersal, *Nature*, *248*, 309–314, doi:10.1038/248309a0.

Anderson, H. A., and J. A. Jackson (1987), Active tectonics of the Adriatic region, *Geophys. J. R. Astron. Soc.*, *91*, 937–983.

Angelica, C., A. Bonforte, G. Distefano, E. Serpelloni, and S. Gresta (2013), Seismic potential in Italy from integration and comparison of seismic and geodetic strain rates, *Tectonophysics*, doi:10.1016/j.tecto.2013.07.014, in press.

Angelier, J., G. Glaçon, and C. Muller (1978), Sur la présence et la position tectonique du Miocène inférieur marin dans l'archipel de Naxos (Cyclades, Grèce), *C. R. Acad. Sci. Paris*, *286*, 21–24.

Argand, E. (1924), La tectonique de l'Asie. Comp.Rend. 13e congrés geol. intern. Bruxelles, 1922., vol. 1, pp. 171–372.

Argnani, A. (1990), The strait of Sicily rift zone: Foreland deformation related to the evolution of a back-arc basin, *J. Geodyn.*, *12*, 311–331.

Argnani, A., and C. Savelli (1999), Cenozoic volcanism and tectonics in the southern Tyrrhenian Sea: Space-time distribution and geodynamic significance, *J. Geodyn.*, *27*(4–5), 409–432.

Argnani, A., E. Serpelloni, and C. Bonazzi (2007), Pattern of deformation around the central Aeolian Islands: Evidence from multichannel seismics and GPS data, *Terra Nova*, *19*(5), 317–323, doi:10.1111/j.1365-3121.2007.00753.x.

Argus, D. F., R. G. Gordon, and C. DeMets (2011), Geologically current motion of 56 plates relative to the no-net-rotation reference frame, *Geochem. Geophys. Geosyst.*, *12*, Q11001, doi:10.1029/2011GC003751.

Armijo, R., B. Meyer, A. Hubert, and A. Barka (1999), Westward propagation of the North Anatolian fault into the northern Aegean: Timing and kinematics, *Geology*, *27*, 267–270.

ArRajehi, A., et al. (2010), Geodetic constraints on present day motion of the Arabian Plate: Implications for Red Sea and Gulf of Aden rifting, *Tectonics*, *29*, TC3011, doi:10.1029/2009TC002482.

Artemieva, I. M. (2007), Dynamic topography of the East European craton: Shedding light upon lithospheric structure, composition and mantle dynamics, *Global Planet. Change*, *58*(1), 411–434.

Auer, L., L. Boschi, T. W. Becker, T. Nissen-Meyer, and D. Giardini (2014), Savani: A variable-resolution whole-mantle model of anisotropic shear-velocity variations based on multiple datasets, *J. Geophys. Res. Solid Earth*, *119*, doi:10.1002/2013JB010773.

Baccheschi, P., L. Margheriti, and M. S. Steckler (2007), Seismic anisotropy reveals focused mantle flow around the Calabrian slab (Southern Italy), *Geophys. Res. Lett.*, *34*, L05302, doi:10.1029/2006GL028899.

Barka, A., and R. Reilinger (1997), Active tectonics of the Eastern Mediterranean region: Deduced from GPS, neotectonic and seismicity data, *Ann. Geofis.*, *40*, 587–610.

Barrier, E., N. Chamot-Rooke, G. Giordano, A. Morelli, and J. F. Brouillet, (2004) Seismicity and tectonics map of the Mediterranean, scale 1:10,000,000 at the center of the Map) Commission for the Geological Map of the World, 2004, Paris, France.

Barruol, G., and M. Granet (2002), A Tertiary asthenospheric flow beneath the southern French Massif Central indicated by upper mantle seismic anisotropy and related to the west Mediterranean extension, *Earth Planet. Sci. Lett.*, *202*(1), 31–47, doi:10.1016/S0012-821X(02)00752-5.

Barruol, G., and A. Souriau (1995), Anisotropy beneath the Pyrenees Range from teleseismic shear wave splitting: Results from a test experiment, *Geophys. Res. Lett.*, *22*(4), 493–496, doi:10.1029/94GL03225.

Barruol, G., A. Souriau, A. Vauchez, J. Diaz, J. Gallart, J. Tubia, and J. Cuevas (1998), Lithospheric anisotropy beneath the Pyrenees from shear wave splitting, *J. Geophys. Res.*, *103*, 30,039–30,053, doi:10.1029/98JB02790.

Barruol, G., A. Deschamps, and O. Coutant (2004), Mapping upper mantle anisotropy beneath SE France by SKS splitting indicates Neogene asthenospheric flow induced by Apenninic slab roll-back and deflected by the deep Alpine roots, *Tectonophysics*, *394*(1–2), 125–138, doi:10.1016/j.tecto.2004.08.002.

Barruol, G., M. Bonnin, H. Pedersen, G. H. R. Bokelmann, and C. Tiberi (2011), Belt-parallel mantle-flow beneath a halted continental collision: The Western Alps, *Earth Planet. Sci. Lett.*, *302*, 429–438.

Bassin, C., G. Laske, and G. Masters (2000), The current limits of resolution for surface wave tomography in North America, *Eos Trans. AGU*, *81*, F897.

Battaglia, M., M. H. Murray, E. Serpelloni, and R. Bürgmann (2004), The Adriatic region: An independent microplate within the Africa-Eurasia collision zone, *Geophys. Res. Lett.*, *31*, L09605, doi:10.1029/2004GL019723.

Beccaluva, L., P. Brotzu, G. Macciotta, L. Morbidelli, G. Serri, and G. Traversa (1989), Cenozoic tectono-magmatic evolution and inferred mantle sources in the Sardo-Tyrrhenian area, in *The Lithosphere in Italy: Advances in Science Research*, edited by A. Boriani et al., pp. 229–248, Accademia Nazionale dei Lincei, Roma.

Becker, T. W. (2012), On recent seismic tomography for the western United States, *Geochem. Geophys. Geosyst.*, *13*, Q01W10, doi:10.1029/2011GC003977.

Becker, T. W., and C. Faccenna (2009), A review of the role of subduction dynamics for regional and global plate motions, in *Subduction Zone Geodynamics*, edited by S. Lallemand and F. Funiciello, pp. 3–34, Springer, Berlin, Germany.

Becker, T. W., and C. Faccenna (2011), Mantle conveyor beneath the Tethyan collisional belt, *Earth Planet. Sci. Lett.*, *310*(3), 453–461.

Becker, T. W., and R. J. O'Connell (2001), Predicting plate velocities with mantle circulation models, *Geochem. Geophys. Geosyst.*, *2*(12), 1060, doi:10.1029/2001GC000171.

Becker, T. W., C. Faccenna, R. J. O'Connell, and D. Giardini (1999), The development of slabs in the upper mantle: Insights from experimental and laboratory experiments, *J. Geophys. Res.*, *104*(B7), 15,207–15,226, doi:10.1029/1999JB900140.

Becker, T. W., J. B. Kellogg, G. Ekström, and R. J. O'Connell (2003), Comparison of azimuthal seismic anisotropy from surface waves and finite-strain from global mantle circulation models, *Geophys. J. Int.*, *155*, 696–714.

Becker, T. W., S. Chevrot, V. Schulte-Pelkum, and D. K. Blackman (2006a), Statistical properties of seismic anisotropy predicted by upper mantle geodynamic models. *J. Geophys. Res.*, *111*, B08309, doi:10.1029/2005JB004095.

Becker, T. W., V. Schulte-Pelkum, D. Blackman, J. B. Kellogg, and R. J. O'Connell (2006b), Mantle flow under the western United States from shear wave splitting, *Earth Planet. Sci. Lett.*, *247*, 235–251.

Becker, T. W., B. Kustowski, and G. Ekström (2008), Radial seismic anisotropy as a constraint for upper mantle rheology, *Earth Planet. Sci. Lett.*, *267*, 213–237.

Becker, T. W., S. Lebedev, and M. D. Long (2012), On the relationship between azimuthal anisotropy from shear wave splitting and surface wave tomography, *J. Geophys. Res.*, *117*, B01306, doi:10.1029/2011JB008705.

Becker, T. W., C. P. Conrad, A. J. Schaffer, and S. Lebedev (2014), Origin of azimuthal seismic anisotropy in oceanic plates and mantle, *Earth Planet. Sci. Lett.*, doi:10.1016/j.epsl.2014.06.014.

Behn, M. D., C. P. Conrad, and P. G. Silver (2004), Detection of upper mantle flow associated with the African superplume, *Earth Planet. Sci. Lett.*, *224*, 259–274.

Bellahsen, N., C. Faccenna, F. Funiciello, L. Jolivet, and J. M. Daniel (2003), Why did Arabia separate from Africa? Insights from 3-D laboratory experiments, *Earth Planet. Sci. Lett.*, *216*(3), 365–381.

Bellahsen, N., C. Faccenna, and F. Funiciello (2005), Dynamics of subduction and plate motion in laboratory experiments: Insights into the "plate tectonics" behavior of the Earth, *J. Geophys. Res.*, *110*, B01401, doi:10.1029/2004JB002999.

Ben-Avraham, Z., M. Lazar, U. Schattner, and S. Marco (2005), The Dead Sea Fault and its effect on civilization, in *Lecture Notes in Earth Sciences: Perspectives in Modern Seismology*, edited by F. Wenzel, pp. 147–170, Springer Verlag, Heidelberg.

Ben-Ismaïl, W., and D. Mainprice (1998), A statistical view of the strength of seismic anisotropy in the upper mantle based on petrofabric studies of Ophiolite and xenolith samples, *Tectonophysics*, *296*, 145–157.

Bennett, R. A., S. Hreinsdóttir, G. Buble, T. Bašić, E. Bačić, M. Marjanović, G. Casale, A. Gendaszek, and D. Cowan (2008), Eocene to present subduction of southern Adria mantle lithosphere beneath the Dinarides, *Geology*, *36*(1), 3, doi:10.1130/G24136A.1.

Bennett, R. A., et al. (2012), Syn-convergent extension observed using the RETREAT GPS network, northern Apennines, Italy, *J. Geophys. Res.*, *117*, B04408, doi:10.1029/2011JB008744.

Bezada, M. J., E. D. Humphreys, D. R. Toomey, M. Harnafi, J. M. Dávila, and J. Gallart (2013), Slab rollback in the westernmost Mediterranean unambiguously revealed by new upper mantle tomography, *Earth Planet. Sci. Lett.*, *368*, 51–60.

Bialas, R. W., F. Funiciello, and C. Faccenna (2010), Subduction and exhumation of continental crust: Insights from laboratory models, *Geophys. J. Int.*, *184*, 43–64, doi:10.1111/j.1365-246X.2010.04824.x.

Bianca, M., C. Monaco, L. Tortorici, and L. Cernobori (1999), Quaternary normal faulting in southeastern Sicily (Italy): A seismic source for the 1693 large earthquake, *Geophys. J. Int.*, *139*, 370–394.

Biju-Duval, B., J. Dercourt, and X. Le Pichon (1977), From the Tethys ocean to the Mediterranean seas: A plate tectonic model of the evolution of the western Alpine system, in *International Symposium on the Structural History of the Mediterranean Basins*, edited by B. Biju-Duval and L. Montander, Split 1976, pp. 143–164, Edition Technip, Paris.

Bijwaard, H., W. Spakman, and E. R. Engdahl (1998), Closing the gap between regional and global travel time tomography, *J. Geophys. Res.*, *103*, 30,055–30,078, doi:10.1029/98JB02467.

Billi, A., D. Presti, C. Faccenna, G. Neri, and B. Orecchio (2007), Seismotectonics of the Nubia plate compressive margin in the south-Tyrrhenian region, Italy: Clues for subduction inception, *J. Geophys. Res.*, *112*, B08302, doi:10.1029/2006JB004837.

Billi, A., R. Funiciello, L. Minelli, C. Faccenna, G. Neri, B. Orecchio, and D. Presti (2008), On the cause of the 1908 Messina tsunami, Southern Italy, *Geophys. Res. Lett.*, *35*, L06301, doi:10.1029/2008GL033251.

Billi, A., L. Minelli, B. Orecchio, and D. Presti (2010), Constraints to the cause of three historical tsunamis (1908, 1783, and 1693) in the Messina Straits region, Sicily, southern Italy, *Seismol. Res. Lett.*, *81*, 907–915.

Billi, A., C. Faccenna, O. Bellier, L. Minelli, G. Neri, C. Piromallo, D. Presti, D. Scrocca, and E. Serpelloni (2011), Recent tectonic reorganization of the Nubia-Eurasia convergent boundary heading for the closure of the western Mediterranean, *Bull. Soc. Geol. Fr.*, *182*, 279–303.

Bird, P. (2003), An updated digital model of plate boundaries, *Geochem. Geophys. Geosyst.*, *4*(3), 1027, doi:10.1029/2001GC000252.

Biryol, C. B., G. Zandt, S. L. Beck, A. A. Ozacar, H. E. Adiyaman, and R. C. Gans (2010), Shear wave splitting along a nascent plate boundary: The North Anatolian fault zone, *Geophys. J. Int.*, *181*, 1201–1213.

Blackman, D. K., H.-R. Wenk, and J. M. Kendall (2002), Seismic anisotropy of the upper mantle: 1. Factors that affect mineral texture and effective elastic properties, *Geochem. Geophys. Geosyst.*, *3*(9), 8601, doi:10.1029/2001GC000248.

Boccaletti, M., and G. Guazzone (1974), Remnant arcs and marginal basins in the Cainozoic development of the Mediterranean, *Nature*, *252*, 18–21.

Bokelmann, G., E. Qorbani, and I. Bianchi (2013), Seismic anisotropy and large-scale deformation of the Eastern Alps, *Earth Planet. Sci. Lett.*, *383*, 1–6.

Boschi, L., B. Fry, G. Ekström, and D. Giardini (2009), The European upper mantle as seen by surface waves, *Surv. Geophys.*, *30*, 463–501, doi:10.1007/s10712-009-9066-2.

Boschi, L., C. Faccenna, and T. W. Becker (2010), Mantle structure and dynamic topography in the Mediterranean Basin, *Geophys. Res. Lett.*, *37*, L20303, doi:10.1029/2010GL045001.

Brandmayr, E., R. Raykova, M. Zuri, F. Romanelli, C. Doglioni, and G. Panza (2010), The lithosphere in Italy: Structure and seismicity, in *The Geology of Italy: Tectonics and Life Along Plate Margins*, edited by M. Beltrando et al., vol. 36, paper 1, Journal of the Virtual Explorer, Electronic Edition, Clear range, Australia, ISSN 1441–8142, doi:10.3809/jvirtex.2010.00224.

Braun, J. (2010), The many surface expressions of mantle dynamics, *Nat. Geosci.*, *3*, 825–833, doi:10.1038/ngeo1020.
Brun, J. P., and C. Faccenna (2008), Exhumation of high-pressure rocks driven by slab rollback, *Earth planet. Sci. Lett.*, *272*, 1–7, doi:10.1016/j.epsl.2008.02.038.
Brun, J. P., and D. Sokoutis (2007), Kinematics of the southern Rhodope core complex (North Greece), *Int. J. Earth Sci.*, *96*(6), 1079–1099.
Brun, J. P., and D. Sokoutis (2010), 45 m.y. of Aegean crust and mantle flow driven by trench retreat, *Geology*, *38*(9), 815–818, doi:10.1130/G30950.1.
Buiter, S. J. H., R. Govers, and M. J. R. Wortel (2002), Two-dimensional simulations of surface deformation caused by slab detachment, *Tectonophysics*, *354*, 195–210.
Buontempo, L., G. H. R. Bokelmann, G. Barruol, and J. Morales (2008), Seismic anisotropy beneath southern Iberia from SKS splitting, *Earth Planet. Sci. Lett.*, *273*(3–4), 237–250, doi:10.1016/j.epsl.2008.06.024.
Burchfiel, B., R. King, A. Todosov, V. Kotzev, N. Durmurdzanov, T. Serafimovski, and B. Nurce (2006), GPS results for Macedonia and its importance for the tectonics of the Southern Balkan extensional regime, *Tectonophysics*, *413*, 239–248, doi:10.1016/j.tecto.2005.10.046.
Burrus, J. (1984), Contribution to a geodynamic synthesis of the Provençal basin (north-western Mediterranean), *Mar. Geol.*, *55*, 247–269.
Calais, E., C. DeMets, and J. M. Nocquet (2003), Evidence for a post-3.16-Ma change in Nubia–Eurasia–North America plate motions?, *Earth Planet. Sci. Lett.*, *216*(1–2), 81–92, doi:10.1016/S0012-821X(03)00482-5.
Capitanio, F. A., and S. Goes (2006), Mesozoic spreading kinematics: Consequences for Cenozoic Central and Western Mediterranean subduction, *Geophys. J. Int.*, *165*, 804–816.
Capitanio, F. A., G. Morra, and S. Goes (2007), Dynamic models of downgoing plate-buoyancy driven subduction: Subduction motions and energy dissipation, *Earth Planet. Sci. Lett.*, *262*, 284–297.
Capitanio, F. A., C. Faccenna, and R. Funiciello (2009), Opening of Sirte Basin: Result of slab avalanche?, *Earth Planet Sci. Lett.*, *285*(1–2), 210–216.
Capitanio, F. A., G. Morra, S. Goes, R. F. Weinberg, and L. Moresi (2010), India–Asia convergence driven by the subduction of the Greater Indian continent, *Nat. Geosci.*, *3*(2), 136–139.
Carey, S. W. (1955), The orocline concept in geotectonics-Part I, *Pap. proc. R. Soc. Tasmania*, *89*, 255–288.
Carminati, E., M. J. R. Wortel, W. Spakman, and R. Sabadini (1998), The role of slab detachment processes in the opening of the western-central Mediterranean basins: Some geological and geophysical evidence, *Earth Planet. Sci. Lett.*, *160*, 651–665.
Carminati, E., C. Doglioni, and D. Scrocca (2003a), Apennines subduction- related subsidence of Venice (Italy), *Geophys. Res. Lett.*, *30*(13), 1717, doi:10.1029/2003GL017001.
Carminati, E., G. Martinelli, and P. Severi (2003b), Influence of glacial cycles and tectonics on natural subsidence in the Po Plain (northern Italy): Insights from ^{14}C ages, *Geochem. Geophys. Geosyst.*, *4*(10), 1082, doi:10.1029/2002GC000481.
Carminati, E., M. Lustrino, and C. Doglioni (2012), Geodynamic evolution of the central and western Mediterranean: Tectonics vs. igneous petrology constraints, *Tectonophysics*, Mediterranean, *Earth Planet. Sci. Lett.*, *257*, 200–214.
Casas-Sainz, A. M., and G. de Vicente (2009), On the tectonic origin of Iberian topography, *Tectonophysics*, *474*, 214–235, doi:10.1016/j.tecto.2009.01.030.
Channell, J. E. T., and F. Horvath (1976), The African/Adriatic promontory as a paleogeographical premise for Alpine orogeny and plate movements in the Carpatho-Balkan region, *Tectonophysics*, *35*, 71–101.
Channell, J. E. T., B. D'Argenio, and F. Horvath (1979), Adria, the African promontory, in Mesozoic Mediterranean paleogeography, *Earth Sci. Rev.*, *15*(3), 213–292.
Channell, J. E. T., J. S. Oldow, R. Catalano, and B. D'Argenio (1990), Paleomagnetically determined rotations in the western Sicilian fold and thrust belt, *Tectonics*, *9*, 641–660, doi:10.1029/TC009i004p00641.
Chardon, C., and O. Bellier (2003), Geological boundary conditions of the 1909 Lambesc (Provence, France) earthquake: Structure and evolution of the Trévaresse ridge anticline, *Bull. Soc. Geol. Fr.*, *174*, 497–510.
Cherchi, A., and L. Montandert (1982), Oligo-Miocene rift of Sardinia and the early history of the western Mediterranean basin, *Nature*, *298*, 736–739.
Civello, S., and L. Margheriti (2004), Toroidal mantle flow around the Calabrian slab (Italy) from SKS splitting, *Geophys. Res. Lett.*, *31*, L10601, doi:10.1029/2004GL019607.
Cloetingh, S., E. Burov, F. Beekman, B. Andeweg, P. Andriessen, D. Garcia-Castellanos, V. Muñoz, and R. Vegas (2002), Lithospheric folding in Iberia, *Tectonics*, *21*(5), 1041–1067, doi:10.1029/2001TC901031.
Comas, M. C., J. P. Platt, J. I. Soto, and A. B. Watts (1999), The origin and tectonic history of the Alboran basin: Insights from leg 161 results, *Proc. Ocean Drill. Program Sci. Results*, *161*, 555–579.
Conrad, C. P., and B. H. Hager (1999), Effects of plate bending and fault strength at subduction zones on plate dynamics, *J. Geophys. Res.*, *104*, 17,551–17,571, doi:10.1029/1999JB900149.
Conrad, C. P., and C. Lithgow-Bertelloni (2002), How mantle slabs drive plate tectonics, *Science*, *298*, 207–209.
Cosentino, D., T. F. Schildgen, P. Cipollari, C. Faranda, E. Gliozzi, N. Hudáčková, and M. R. Strecker (2012), Late Miocene surface uplift of the southern margin of the Central Anatolian Plateau, Central Taurides, Turkey, *Geol. Soc. Am. Bull.*, *124*(1–2), 133–145.
D'Agostino, N., and G. Selvaggi (2004), Crustal motion along the Eurasia-Nubia plate boundary in the Calabrian Arc and Sicily and active extension in the Messina Straits from GPS measurements, *J. Geophys. Res.*, *109*, B11402, doi:10.1029/2004JB002998.
D'Agostino, N., D. Cheloni, S. Mantenuto, G. Selvaggi, A. Michelini, and D. Zuliani (2005), Strain accumulation in the southern Alps (NE Italy) and deformation at the northeastern boundary of Adria observed by CGPS measurements, *Geophys. Res. Lett.*, *32*, L19306, doi:10.1029/2005GL024266.
D'Agostino, N., A. Avallone, D. Cheloni, E. D'Anastasio, S. Mantenuto, and G. Selvaggi (2008), Active tectonics of the Adriatic region from GPS and earthquake slip vectors, *J. Geophys. Res.*, *113*, B12413, doi:10.1029/2008JB005860.
D'Agostino, N., E. D'Anastasio, A. Gervasi, I. Guerra, M. R. Nedimović, L. Seeber, and M. Steckler (2011), Forearc extension and slow rollback of the Calabrian Arc from GPS measurements, *Geophys. Res. Lett.*, *38*, L17304, doi:10.1029/2011GL048270.
Dando, B. D. E., G. W. Stuart, G. A. Houseman, E. Hegedüs, E. Brückl, and S. Radovanović (2011), Teleseismic tomography of the mantle in the Carpathian-Pannonian region of central Europe, *Geophys. J. Int.*, *186*, 11–31.
Daradich, A., J. X. Mitrovica, R. N. Pysklywec, S. D. Willett, and A. M. Forte (2003), Mantle flow, dynamic topography, and rift-flank uplift of Arabia, *Geology*, *31*, 901–904.
De Jonge, M. R., and M. J. R. Wortel (1990), The thermal structure of the Mediterranean upper mantle: A forward modelling approach, *Terra Nova*, *2*, 609–616.
De Jonge, M. R., M. J. R. Wortel, and W. Spakman (1994), Regional scale tectonic evolution and the seismic velocity structure of the lithosphere and upper mantle: The Mediterranean region, *J. Geophys. Res.*, *99*(B6), 12,091–12,108, doi:10.1029/94JB00648.

Debayle, E., and Y. Ricard (2013), Seismic observations of large-scale deformation at the bottom of fast-moving plates, *Earth Planet. Sci. Lett.*, *376*, 165–177.
DeMets, C., R. G. Gordon, and D. F. Argus (2010), Geologically current plate motions, *Geophys. J. Int.*, *181*(1), 1–80, doi:10.1111/j.1365-246X.2009.04491.x.
Dercourt, J., et al. (1986), Geological evolution of the Tethys belt from the Atlantic to the Pamirs since the Lias, *Tectonophysics*, *123*, 241–315.
Dercourt, J., L. E. Ricou, and B. Vrielynck (Eds.) (1993), *Atlas Téthys, Palaeoenvironmental Maps*, Elsevier, New York.
Dévèrchere, J., et al. (2005), Active thrust faulting offshore Boumerdés, Algeria, and its relations to the 2003 M_w 6.9 earthquake, *Geophys. Res. Lett.*, *32*, L04311, doi:10.1029/2004GL021646.
Devoti, R., A. Esposito, G. Pietrantonio, A. R. Pisani, and F. Riguzzi (2011), Evidence of large scale deformation patterns from GPS data in the Italian subduction boundary, *Earth Planet. Sci. Lett.*, *311*(3–4), 1–12, doi:10.1016/j.epsl.2011.09.034.
Dewey, J. F. (1980), Episodicity, sequence and style at convergent plate boundaries: pp. 553–573, in *The Continental Crust and its Mineral Deposits*, *Geol. Assoc. Can. Spec. Paper 20,* edited by D. W. Strangeway, 804 pp., Geol. Assoc. Canada, St. Jhon, Canada.
Dewey, J. F., W. C. Pitman III, W. B. F. Ryan, and J. Bonnin (1973), Plate tectonics and the evolution of the Alpine system, *Geol. Soc. Am. Bull.*, *84*, 3137–3180.
Dewey, J. F., W. C. Pitman, W. B. F. Ryan, and J. Bonnin (1975), Plate tectonics and the evolution of the Alpine system: Discussion and reply, *Geol. Soc. Am. Bull.*, *86*(5), 719–720, doi:10.1130/0016-7606(1975)86<719:PTATEO>2.0.CO;2.
Dewey, J. F., M. L. Helman, E. Turco, D. H. W. Hutton, and S. D. Knott (1989), Kinematics of the western Mediterranean, in *Alpine Tectonics*, *Geol. Soc. Spec. Publ.,* vol. 45, edited by M. P. Coward, D. Dietrich, and R. G. Park, pp. 265–283, Geol. Soc. of London, U. K.
Di Stefano, R., E. Kissling, C. Chiarabba, A. Amato, and D. Giardini (2009), Shallow subduction beneath Italy: Three-dimensional images of the Adriatic-European-Tyrrhenian lithosphere system based on high-quality *P* wave arrival times, *J. Geophys. Res.*, *114*, B05305, doi:10.1029/2008JB005641.
Di Stefano, R., I. Bianchi, M. G. Ciaccio, G. Carrara, and E. Kissling (2011), Three-dimensional Moho topography in Italy: New constraints from receiver functions and controlled source seismology, *Geochem. Geophys. Geosyst.*, *12*, Q09006, doi:10.1029/2011GC003649
Diaz, J., J. Gallart, M. Ruiz, J. A. Pulgar, C. Lopez-Fernandez, and J. M. Gonzalez-Cortina (2006), Probing seismic anisotropy in North Iberia from shear wave splitting, *Phys. Earth Planet. Inter.*, *158*(2–4), 210–225, doi:10.1016/j.pepi.2005.12.011.
Diaz, J., J. Gallart, A. Villasenor, F. Mancilla, A. Pazos, D. Cordoba, J. A. Pulgar, P. Ibarra, and M. Harnafi (2010), Mantle dynamics beneath the Gibraltar Arc (western Mediterranean) from shear-wave splitting measurements on a dense seismic array, *Geophys. Res. Lett.*, *37*, L18304, 10.1029/2010GL044201.
Diaz, J., D. Pedreira, M. Ruiz, J. A. Pulgar, and J. Gallart (2012), Mapping the indentation between the Iberian and Eurasian plates beneath the Western Pyrenees/Eastern Cantabrian Mountains from receiver function analysis, *Tectonophysics*, *570*, 114–122, doi:10.1016/j.tecto.2012.07.005.
Doglioni, C., E. Gueguen, P. Harabaglia, and F. Mongelli (1999), On the origin of W-directed subduction zones and applications to the western Mediterranean, *Geol. Soc. Spec. Publ.*, *156*, 541–561.
Doglioni, C., E. Carminati, M. Cuffaro, and D. Scrocca (2007), Subduction kinematics and dynamic constraints, *Earth Sci. Rev.*, *83*, 125–175, doi:10.1016/j.earscirev.2007.04.001.
Doglioni, C., et al. (2012), The tectonic puzzle of the Messina area (Southern Italy): Insights from new seismic reflection data, *Sci. Rep.*, *2*, 970, doi:10.1038/srep00970.
Duggen, S., K. A. Hoernle, F. Hauff, A. Kluegl, M. Bouabdellah, and M. Thirlwall (2009), Flow of Canary mantle plume material through a sublithospheric corridor beneath Africa to the Mediterranean, *Geology*, *37*, 283–286.
Elsasser, W. (1971), Sea-floor spreading as convection, *J. Geophys. Res.*, *76*, 1101–1112, doi:10.1029/JB076i005p01101.
Endrun, B., S. Lebedev, T. Meier, C. Tirel, and W. Friederich (2011), Complex layered deformation within the Aegean crust and mantle revealed by seismic anisotropy, *Nat. Geosci.*, *4*(3), 203–207, doi:10.1038/NGEO1065.
Engdahl, E. R., R. D. van der Hilst, and R. Buland (1998), Global teleseismic earthquake relocation with improved travel times and procedures for depth determination, *Bull. Seismol. Soc. Am.*, *88*, 722–743.
England, P., and R. Wortel (1980), Some consequences of the subduction of young slabs, *Earth Planet. Sci. Lett.*, *47*, 403–415.
Enns, A., T. W. Becker, and H. Schmeling (2005), The dynamics of subduction and trench migration for viscosity stratification, *Geophys. J. Int.*, *160*, 761–775.
Evangelidis, C. P., W.-T. Liang, N. S. Melis, and K. I. Kostantinou (2011), Shear wave anisotropy beneath the Aegean inferred from SKS splitting observations, *J. Geophys. Res.*, *116*, B04314, doi:10.1029/2010JB007884.
Faccenna, C., and T. W. Becker (2010), Shaping mobile belts by small-scale convection, *Nature*, *465*(7298), 602–605, doi:10.1038/nature09064.
Faccenna, C., M. Mattei, R. Funiciello, and L. Jolivet (1997), Styles of back-arc extension in the central Mediterranean, *Terra Nova*, *9*, 126–130.
Faccenda, M., L. Burlini, T. V. Geryal, and D. Mainprice (2008), Fault-induced seismic anisotropy by hydration in subducting oceanic plates, *Nature*, *455*, 1097–1100, doi:10.1038/nature07376.
Faccenna, C., D. Giardini, P. Davy, and A. Argentieri (1999), Initiation of subduction at Atlantic-type margin: Insight from laboratory experiments, *J. Geophys. Res.*, *104*, 2749–2766, doi:10.1029/1998JB900072.
Faccenna, C., F. Funiciello, D. Giardini, and P. Lucente (2001a), Episodic back-arc extension during restricted mantle convection in the central Mediterranean, *Earth Planet. Sci. Lett.*, *187*(1-2), 105–116.
Faccenna, C., T. W. Becker, F. P. Lucente, L. Jolivet, and F. Rossetti (2001b), History of subduction and back-arc extension in the central Mediterranean, *Geophys. J. Int.*, *145*, 809–820.
Faccenna, C., L. Jolivet, C. Piromallo, and A. Morelli (2003), Subduction and the depth of convection in the Mediterranean mantle, *J. Geophys. Res.*, *108*(B2), 2099, doi:10.1029/2001JB001690.
Faccenna, C., C. Piromallo, A. Crespo-Blanc, and L. Jolivet (2004), Lateral slab deformation and the origin of the western Mediterranean arcs, *Tectonics*, *23*, TC1012, doi:10.1029/2002TC001488.
Faccenna, C., L. Civetta, M. D'Antonio, F. Funiciello, L. Margheriti, and C. Piromallo (2005), Constraints on mantle circulation around the deforming Calabrian slab, *Geophys. Res. Lett.*, *32*, L06311, doi:10.1029/2004GL021874.
Faccenna, C., O. Bellier, J. Martinod, C. Piromallo, and V. Regard (2006), Slab detachment beneath eastern Anatolia: A possible cause for the formation of the North Anatolian fault, *Earth Planet. Sci. Lett.*, *242*(1), 85–97.
Faccenna, C., F. Funiciello, L. Civetta, M. D'Antonio, M. Moroni and C. Piromallo (2007), Slab disruption, mantle circulation, and the opening of the Tyrrhenian basins, in *Cenozoic Volcanism in the Mediterranean Area*, edited by L. Beccaluva, G. Bianchini, and M. Wilson, Geological Society of America Special Paper 41, pp. 153–169, AGU, Washington, D. C., doi:10.1130/2007.2418(08).
Faccenna, C., P. Molin, B. Orecchio, V. Olivetti, O. Bellier, F. Funiciello, L. Minelli, C. Piromallo, and A. Billi (2011), Topography of the Calabria subduction zone (southern Italy): Clues for the origin of Mt. Etna, *Tectonics*, *30*, TC1003, doi:10.1029/2010TC002694.

Faccenna, C., T. W. Becker, L. Jolivet, and M. Keskin (2013), Mantle convection in the Middle East: Reconciling Afar upwelling, Arabia indentation and Aegean trench rollback, *Earth Planet. Sci. Lett.*, doi:10.1016/j.epsl.2013.05.043i.

Fadil, A., P. Vernant, S. McClusky, R. Reilinger, F. Gomez, D. Sari, and M. Barazangi (2006), Active tectonics of the western Mediterranean: Geodetic evidence for rollback of a delaminated subcontinental lithospheric slab beneath the Rif Mountains, Morocco, *Geology*, *34*(7), 529–532.

Favali, P., F. Funiciello, and P. Pieri (1993), An active margin across the Adriatic Sea (central Mediterranean Sea), *Tectonophysics*, *219*, 109–117.

Flament, N., M. Gurnis, S. Williams, M. Seton, J. Skogseid, C. Heine, and R. D. Müller (2013), Topographic asymmetry of the South Atlantic from global models of mantle flow and lithospheric stretching, *Earth Planet. Sci. Lett.*, *387*, 107–119.

Flerit, F., R. Armijo, G. King, and B. Meyer (2004), The mechanical interaction between the propagating North Anatolian Fault and back-arc extension in the Aegean, *Earth Planet. Sci. Lett.*, *224*, 347–362.

Floyd, M. A., et al. (2010), A new velocity field for Greece: Implications for the kinematics and dynamics of the Aegean, *J. Geophys. Res.*, *115*, B10403, doi:10.1029/2009JB007040.

Forte, A. M. (2007), Constraints on seismic models from other disciplines—Implications for mantle dynamics and composition, in *Treatise on Geophysics*, edited by G. Schubert and D. Bercovici, pp. 805–858, Elsevier, Amsterdam.

Forte, A. M., S. Quéré, R. Moucha, N. A. Simmons, S. P. Grand, J. X. Mitrovica, and D. B. Rowley (2010), Joint seismic–geodynamic-mineral physical modelling of African geodynamics: A reconciliation of deep-mantle convection with surface geophysical constraints, *Earth Planet. Sci. Lett.*, *295*, 329–341.

Fouch, M. J., and S. Rondenay (2006), Seismic anisotropy beneath stable continental interiors, *Phys. Earth Planet. Inter.*, *158*, 292–320.

Fourcade, S., R. Capdevila, A. Ouabadi, and F. Martineau (2001), The origin and geodynamic significance of the Alpine cordierite-bearing granitoids of northern Algeria. A combined petrological, mineralogical, geochemical and isotopic (O, H, Sr, Nd) study, *Lithos*, *57*, 187–216.

Funiciello, F., C. Faccenna, and D. Giardini (2004), Role of lateral mantle flow in the evolution of subduction system: Insights from 3-D laboratory experiments, *Geophys. J. Int.*, *157*, 1393–1406.

Funiciello, F., M. Moroni, C. Piromallo, C. Faccenna, A. Cenedese, and H. A. Bui (2006), Mapping mantle flow during retreating subduction: Laboratory models analyzed by feature tracking, *J. Geophys. Res.*, *111*, B03402, doi:10.1029/2005JB003792.

Garfunkel, Z. (1981), Internal structure of the Dead Sea leaky transform (rift) in relation to plate kinematics, *Tectonophysics*, *80*, 81–108.

Gaspar-Escribano, J. M., D. Garcia-Castellanos, E. Roca, and S. A. P. L. Cloetingh (2004), Cenozoic vertical motions of the Catalan Coastal Ranges (NE Spain): The role of tectonics, isostasy, and surface transport, *Tectonics*, *23*, TC1004, doi:10.1029/2003TC001511.

Gattacceca, J., and F. Speranza (2002), Paleomagnetism of Jurassic to Miocene sediments from the Apenninic carbonate platform (southern Apennines, Italy): Evidence for a 60° counterclockwise Miocene rotation, *Earth Planet. Sci. Lett.*, *201*, 19–34.

Ghosh, A., T. W. Beckerand, and S. Zhong (2010), Effects of lateral viscosity variations on the geoid, *Geophys. Res. Lett.*, *37*, L01301, doi:10.1029/2009GL040426.

Giardini, D., and M. Velona (1991), The deep seismicity of the Tyrrhenian Sea, *Terra Nova*, *3*, 57–64.

Godey, S., R. Bossu, and J. Guilbert (2013), Improving the Mediterranean seismicity picture thanks to international collaborations, *Phys. Chem. Earth*, doi:10.1016/j.pce.2013.04.012.

Goes, S., R. Govers, and P. Vacher (2000), Shallow mantle temperatures under Europe from *P* and *S* wave tomography, *J. Geophys. Res.*, *105*, 11,153–11,169, doi:10.1029/1999JB900300.

Goes, S., D. Giardini, S. Jenny, C. Hollenstein, H. G. Kahle, and A. Geiger (2004), A recent tectonic reorganization in the south-central Mediterranean, *Earth Planet. Sci. Lett.*, *226*(3–4), 335–345, doi:10.1016/j.epsl.2004.07.038.

Göğüş, O. H., and R. N. Pysklywec (2008), Mantle lithosphere delamination driving plateau uplift and synconvergent extension in eastern Anatolia, *Geology*, *36*, 723–726, doi:10.1130/G24982A.1.

Gomez, F., G. Karam, M. Khawlie, S. McClusky, P. Vernant, R. Reilinger, R. Jaafar, C. Tabet, K. Khairand, and M. Barazangi (2007), Global positioning system measurements of strain accumulation and slip transfer through the restraining bend along the Dead Sea fault system in Lebanon, *Geophys. J. Int.*, *168*, 1021–1028, doi:10.1111/j.1365-246X.2006.03328.x.

Gorini, C., A. Mauffret, P. Guennoc, and A. Le Marrec (1994), Structure of the Gulf of Lions (northwestern Mediterranean Sea): A review, in *Hydrocarbon and Petroleum Geology of France*, edited by A. Mascle, pp. 223–243, Eur. Assoc. of Pet. Geol, Houten, Netherlands.

Govers, R., and M. J. R. Wortel (2005), Lithosphere tearing at STEP faults: Response to edges of subduction zones, *Earth Planet. Sci. Lett.*, *236*, 505–523.

Grad, M., T. Tire, and ESC Working Group (2009), The Moho depth map of the European Plate, *Geophys. J. Int.*, *176*(1), 279–292, doi:10.1111/j.1365-246X.2008.03919.x.

Gudmundsson, O., and M. Sambridge (1998), A regionalized upper mantle (RUM) seismic model, *J. Geophys. Res.*, *103*, 7121–7136, doi:10.1029/97JB02488.

Gueguen, E., C. Doglioni, and M. Fernandez (1998), On the post 25 Ma geodynamic evolution of the western Mediterranean, *Tectonophysics*, *298*(1), 259–269.

Guernet, C. (1971), Etudes géologiques en Eubée et dans les régions voisines (Grèce), Thèse d'Etat thesis, Université Paris VI, Paris.

Guidoboni E., G. Ferrari, D. Mariotti, A. Comastri, G. Tarabusi, and G. Valensise (2007), CFTI4Med, catalogue of strong earthquakes in Italy (461 B.C.-1997) and Mediterranean area (760 B.C.-1500), INGV-SGA. [Available from http://storing.ingv.it/cfti4med/.]

Guillaume, B., F. Funiciello, C. Faccenna, J. Martinod, and V. Olivetti (2010), Spreading pulses of the Tyrrhenian Sea during the narrowing of the Calabrian slab, *Geology*, *38*, 819–822.

Guillaume, B., L. Husson, F. Funiciello, and C. Faccenna (2013), The dynamics of laterally variable subductions: Laboratory models applied to the Hellenides, *Solid Earth*, *4*, 179–200, doi:10.5194/se-4-179-2013.

Gurnis, M., J. X. Mitrovica, J. Ritsema, and H.-J. van Heijst (2000), Constraining mantle density structure using geological evidence of surface uplift rates: The case of the African superplume, *Geochem. Geophys. Geosyst.*, *1*, 1020, doi:10.1029/1999GC000035.

Gutenberg, B., and C. F. Richter (1954), *Seismicity of the Earth and Associated Phenomena*, 310 pp., Princeton Univ. Press, Princeton, N. J.

Gvirtzman, Z., and A. Nur (2001), Residual topography, lithospheric structure and sunken slabs in the central Mediterranean, *Earth Planet. Sci. Lett.*, *187*(1), 117–130.

Hafkenscheid, E., M. J. R. Wortel, and W. Spakman (2006), Subduction history of the Tethyan region derived from seismic tomography and tectonic reconstructions, *J. Geophys. Res.*, *111*, B08401, doi:10.1029/2005JB003791.

Hager, B. H. (1984), Subducted slabs and the geoid: Constraints on mantle rheology and flow, *J. Geophys. Res.*, *89*, 6003–6015, doi:10.1029/JB089iB07p06003.

Hager, B. H., and R. J. O'Connell (1981), A simple global model of plate dynamics and mantle convection, *J. Geophys. Res.*, *86*, 4843–4867, doi:10.1029/JB086iB06p04843.
Hager, B. H., R. W. Clayton, M. Richards, R. P. Comer, and A. M. Dziewonski (1985), Lower mantle heterogeneity, dynamic topography and the geoid, *Nature*, *313*(6003), 541–545.
Hall, C., K. M. Fischer, E. M. Parmentier, and D. K. Blackman (2000), The influence of plate motions on three-dimensional back arc mantle flow and shear wave splitting, *J. Geophys. Res.*, *105*, 28,009–28,033, doi:10.1029/2000JB900297.
Handy, M., S. M. Schmid, R. Bousquet, E. Kissling, and D. Bernoulli (2010), Reconciling plate-tectonic reconstructions of Alpine Tethys with the geological-geophysical record of spreading and subduction in the Alps, *Earth Sci. Rev.*, *102*, 121–158.
Hatzfeld, D., J. Martinod, G. Bastet, and P. Gautier (1997), An analog model for the Aegean to describe the contribution of gravitational potential energy, *J. Geophys. Res.*, *102*, 649–659, doi:10.1029/96JB02594.
Hatzfeld, D., E. Karagianni, I. Kassaras, A. Kiratzi, E. Louvari, H. Lyon-Caen, K. Makropoulos, P. Papadimitriou, G. Bock, and K. Priestley (2001), Shear wave anisotropy in the upper mantle beneath the Aegean related to internal deformation, *J. Geophys. Res.*, *106*, 30,737–30,753, doi:10.1029/2001JB000387.
Hollenstein, C., M. D. Müller, A. Geiger, and H. G. Kahle (2008), Crustal motion and deformation in Greece from a decade of GPS measurements, 1993–2003, *Tectonophysics*, *449*(1–4), 17–40, doi:10.1016/j.tecto.2007.12.006.
Horvath, F., and H. Berckhemer (1982), Mediterranean backarc basins, in *Alpine-Mediterranean Geodynamics*, *Geodyn. Ser.*, vol. 7, edited by H. Berckhemer and K. Hsü, pp. 141–173, AGU, Washington, D. C.
Horváth, F., and C. Faccenna (2011), Central Mediterranean mantle flow system and the formation of the Pannonian Basin, *Geophys. Res. Abstr.*, *13*, EGU2011-8894-2.
Horváth, F., G. Bada, P. Szafián, G. Tari, A. Ádám, and S. Cloetingh (2006), Formation and deformation of the Pannonian Basin: Constraints from observational data, in *European Lithosphere Dynamics*, edited by D. G. Gee and R. A. Stephenson, pp. 191–206, Geol. Soc. of London, London.
Hubert-Ferrari, A., R. Armijo, G. King, B. Meyer, and A. Barka (2002), Morphology, displacement, and slip rates along the North Anatolian fault, Turkey, *J. Geophys. Res.*, *107*(B10), 2235, doi:10.1029/2001JB000393.
Hunstad, I., G. Selvaggi, N. D'Agostino, P. England, P. Clarke, and M. Pierozzi (2003), Geodetic strain in peninsular Italy between 1875 and 2001, *Geophys. Res. Lett.*, *30*(4), 1181, doi:10.1029/2002GL016447.
Husson, L. (2006), Dynamic topography above retreating subduction zones, *Geology*, *34*(9), 741–744.
Husson, L., J. P. Brun, P. Yamato, and C. Faccenna (2009), Episodic slab rollback fosters exhumation of HP-UHP rocks, *Geophys. J. Int.*, *179*, 1292–1300, doi:10.1111/j.1365-246X.2009.04372.x.
Isacks, B., and P. Molnar (1971), Distribution of stresses in the descending lithosphere from a global survey of focal-mechanism solutions of mantle earthquakes, *Rev. Geophys. Space Phys.*, *9*, 103–174.
Ismail-Zadeh, A., A. Aoudia, and G. Panza (2010), Three-dimensional numerical modeling of contemporary mantle flow and tectonic stress beneath the Central Mediterranean, *Tectonophysics*, *482*, 226–236.
Jackson, J., and D. McKenzie (1988), The relationship between plate motions and seismic moment tensors, and rates of active deformation in the Mediterranean and Middle East, *Geophys. J.*, *93*, 45–73.
Janssen, M. E., S. Cloetingh, and E. Banda (1993), Pliocene uplift of the eastern Iberian margin: Inferences from quantitative modelling of the Valencia Trough, *Earth Planet. Sci. Lett.*, *119*, 585–597.
Jolivet, L. (2001), A comparison of geodetic and finite strain in the Aegean, geodynamic implications, *Earth Planet. Sci. Lett.*, *187*, 95–104.
Jolivet, L., and J. P. Brun (2010), Cenozoic geodynamic evolution of the Aegean region, *Int. J. Earth Sci.*, *99*, 109–138, doi:10.1007/s00531-00008-00366-00534.
Jolivet, L., and C. Faccenna (2000), Mediterranean extension and the Africa-Eurasia collision, *Tectonics*, *19*(6), 1095–1106, doi:10.1029/2000TC900018.
Jolivet, L., C. Faccenna, B. Goffé, M. Mattei, F. Rossetti, C. Brunet, F. Storti, R. Funiciello, J. P. Cadet, and T. Parra (1998), Mid-crustal shear zones in post-orogenic extension: The northern Tyrrhenian Sea case, *J. Geophys. Res.*, *103*, 12,123–12,160, doi:10.1029/97JB03616.
Jolivet, L., C. Faccenna, B. Goffé, E. Burov, and P. Agard (2003), Subduction tectonics and exhumation of high-pressure metamorphic rocks in the Mediterranean orogens, *Am. J. Sci.*, *303*, 353–409.
Jolivet, L., C. Faccenna, and C. Piromallo (2009), From mantle to crust: Stretching the Mediterranean, *Earth Planet. Sci. Lett.*, *285*(1–2), 198–209, doi:10.1016/j.epsl.2009.06.017.
Jolivet, L., et al. (2013), Aegean tectonics: Strain localisation, slab tearing and trench retreat, *Tectonophysics*, *597–598*, 1–33.
Kaminski, E., N. M. Ribe, and J. T. Browaeys (2004), D-rex, a program for calculation of seismic anisotropy due to crystal lattice preferred orientation in the convective upper mantle, *Geophys. J. Int.*, *158*, 744–752.
Karabacak, V., E. Altunel, M. Meghraoui, and H. S. Akyuz (2010), Field evidences from northern Dead Sea Fault Zone (South Turkey): New findings for the initiation age and slip rate, *Tectonophysics*, *480*, 172–182.
Karabulut, H., A. Paul, T. A. Ergun, D. Hatzfeld, D. M. Childs, and M. Aktar, (2013), Long-wavelength undulations of the seismic Moho beneath the strongly stretched Western Anatolia, *Geophys. J. Int.*, *194*(1), 450–464, doi:10.1093/gji/ggt100.
Kastens, K., J. Mascle, and ODP Leg 107 Scientific party (1988), ODP Leg in the Tyrrhenian Sea: Insight into passive margin and back-arc basin evolution, *Geol. Soc. Am. Bull.*, *100*, 1140–1156.
Katsikatsos, G., H. De Bruijn, and A. J. Van der Meulen (1981), The Neogene of the island of Euboea (Evia), a review, *Geol. Mijnbouw*, *60*, 509–516.
Keskin, M. (2003), Magma generation by slab steepening and breakoff beneath a subduction-accretion complex: An alternative model for collision-related volcanism in eastern Anatolia, Turkey, *Geophys. Res. Lett.*, *30*(24), 8046, doi:10.1029/2003GL018019.
Keskin, M. (2007), Eastern Anatolia: A hotspot in a collision zone without a mantle plume, in *Plates, Plumes, and Planetary Processes*, vol. 430, edited by G. R. Foulger and D. M. Jurdy, pp. 693–722, AGU, Geological Society of America Special Paper.
Khair, K., G. F. Karakaisis, and E. E. Papadimitriou (2000), Seismic zonation of the Dead Sea Transform Fault area, *Ann. Geophys.*, *43*, 61–79.
Kissel, C., and C. Laj (1988), The Tertiary geodynamic evolution of the Aegean arc: A paleomagnetic reconstruction, *Tectonophysics*, *146*, 183–201.
Komut, T., R. Gray, R. Pysklywec, and O. H. Göğüş (2012), Mantle flow uplift of western Anatolia and the Aegean: Interpretations from geophysical analyses and geodynamic modeling, *J. Geophys. Res.*, *117*, B11412, doi:10.1029/2012JB009306.
Konecny, V., M. Kovac, J. Lexa, and J. Sefara (2002), Neogene evolution of the Carpatho-Pannonian region: An interplay of subduction and back-arc uprise in the mantle, *EGU St. Mueller Spec. Publ. Ser.*, *1*, 105–123.

Koulali, A., D. Ouazar, A. Tahayt, R. W. King, P. Vernant, R. E. Reilinger, S. McClusky, T. Mourabit, J. M. Davila, and N. Amraoui (2011), New GPS constraints on active deformation along the Africa–Iberia plate boundary, *Earth Planet. Sci. Lett.*, *308*(1), 211–217.

Kovács, I., G. Falus, G. Stuart, K. Hidas, C. Szabó, M. F. J. Flower, E. Hegedűs, K. Posgay, and L. Zilahi-Sebess (2012), Seismic anisotropy and deformation patterns in upper mantle xenoliths from the central Carpathian–Pannonian region: Asthenospheric flow as a driving force for Cenozoic extension and extrusion?, *Tectonophysics*, *514–517*, 168–179.

Kozacı, Ö., J. Dolan, R. Finkel, and R. Hartleb (2007), Late Holocene slip rate for the North Anatolian fault, Turkey, from cosmogenic ^{36}Cl geochronology: Implications for the constancy of fault loading and strain release rates, *Geology*, *35*, 867–870.

Kozacı, Ö., J. F. Dolan, and R. C. Finkel (2009), A late Holocene slip rate for the central North Anatolian fault, at Tahtaköprü, Turkey, from cosmogenic ^{10}Be geochronology: Implications for fault loading and strain release rates, *J. Geophys. Res. 114*, B01405, doi:10.1029/2008JB005760.

Kreemer, C., N. Chamot-Rooke, and X. Le Pichon (2004), Constraints on the evolution and vertical coherency of deformation in the Northern Aegean from a comparison of geodetic, geologic and seismologic data, *Earth Planet. Sci. Lett.*, *225*, 329–346.

Kuhlemann, J., and O. Kempf (2002), Post-Eocene evolution of the North Alpine Foreland Basin and its response to Alpine tectonics, *Sediment. Geol.*, *152*, 45–78.

Kuhlemann, J., W. Frisch, B. Székely, I. Dunkl, and M. Kázmér (2002), Post-collisional sediment budget tectonic versus climatic control, *Int. J. Earth Sci.*, *91*, 818–837.

Kuhlemann, J., W. Frisch, I. Dunkl, M. Kázmér, and G. Schmiedl (2004), Miocene siliciclastic deposits of Naxos Island: Geodynamic and environmental implications for the evolution of the southern Aegean Sea (Greece), in *Detrital Thermochronology - Provenance Analysis, Exhumation, and Landscape Evolution of Mountain Belts*, *Geol. Soc. Am. Spec. Pap.*, edited by M. Bernet and C. Spiegel, pp. 51–65, Geological Society of America, Boulder, Colo.

Kuk, V., E. Prelogovic, and I. Dragicevic (2000), Seismotectonically active zones in the Dinarides, *Geol. Croat.*, *53*, 295–303.

Kurt, H., et al. (2013), Steady late Quaternary slip rate on the Cinarcik section of the North Anatolian Fault near Istanbul, Turkey, *Geophys. Res. Lett.*, *40*, 4555–4559, doi:10.1002/grl.50882.

Laske, G., G. Masters, Z. Ma, and M. Pasyanos (2013), Update on CRUST1.0 - A 1-degree global model of Earth's crust, *Geophys. Res. Abstracts*, 15, Abstract EGU2013-2658.

Le Beon, M., Y. Klinger, A. Q. Amrat, A. Agnon, L. Dorbath, G. Baer, J.-C. Ruegg, O. Charade, and O. Mayyas (2008), Slip rate and locking depth from GPS profiles across the southern Dead Sea Transform, *J. Geophys. Res.*, *113*, B11403, doi:10.1029/2007JB005280.

Le Pichon, X. (1982), *Land-Locked Ocean Basin and Continental Collision in the Eastern Mediterranean Area as a Case Example: Mountain Building Processes*, pp. 201–213, Academic Press, London.

Le Pichon, X., and J. Angelier (1981), The Aegean Sea, *Phil. Trans. Roy. Soc. London*, *300*, 357–372.

Le Pichon, X., and C. Kreemer (2010), The Miocene-to-present kinematic evolution of the eastern Mediterranean and Middle East and its implications for dynamics, *Annu. Rev. Earth Planet. Sci.*, *38*(1), 323–351, doi:10.1146/annurev-earth-040809-152419.

Lewis, C. J., J. Vergés, and M. Marzo (2000), High mountains in a zone of extended crust: Insights into the Neogene and Quaternary topographic development of north-eastern Iberia, *Tectonics*, *19*, 86–102, doi:10.1029/1999TC900056.

Li, C., R. D. van der Hilst, E. R. Engdahl, and S. Burdick (2008), A new global model for *P* wave speed variations in Earth's mantle, *Geochem. Geophys. Geosyst.*, *9*, Q05018, doi:10.1029/2007GC001806.

Li, Z. W., S. Roecker, Z. H. Li, B. Wei, H. T. Wang, G. Schelochkov, and V. Bragin (2009), Tomographic image of the crust and upper mantle beneath the western Tien Shan from the MANAS broadband deployment: Possible evidence for lithospheric delamination, *Tectonophysics*, *477*, 49–57.

Lithgow-Bertelloni, C., and M. Richards (1998), The dynamics of Cenozoic and Mesozoic plate motions, *Rev. Geophys.*, *36*, 27–78, doi:10.1029/97RG02282.

Lithgow-Bertelloni, C., and P. G. Silver (1998), Dynamic topography, plate driving forces and the African superswell, *Nature*, *395*, 269–272.

Lonergan, L., and N. White (1997), Origin of the Betic-Rif mountain belt, *Tectonics*, *16*, 504–522, doi:10.1029/96TC03937.

Long, M. D. (2013), Constrains on subduction geodynamics from seismic anisotropy, *Rev. Geophys.*, *51*, 76–112, doi:10.1002/rog.20008.

Long, M. D., and T. W. Becker (2010), Mantle dynamics and seismic anisotropy, *Earth Planet. Sci. Lett.*, *297*, 341–354.

Lucente, F. P., and L. Margheriti (2008), Subduction rollback, slab breakoff, and induced strain in the uppermost mantle beneath Italy, *Geology*, *36*(5), 375–378, doi:10.1130/G24529A.1.

Lucente, F. P., L. Margheriti, C. Piromallo, and G. Barruol (2006), Seismic anisotropy reveals the long route of the slab through the western-central Mediterranean mantle, *Earth Planet. Sci. Lett.*, *241*, 517–529.

Lustrino, M., and M. Wilson (2007), The circum-Mediterranean Cenozoic Anorogenic Igneous Province, *Earth Sci. Rev.*, *81*, 1–65.

Lustrino M., V. Morra, L. Fedele, and L. Franciosi (2009), Beginning of the Apennine subduction system in central western Mediterranean: Constraints from Cenozoic "orogenic" magmatic activity of Sardinia (Italy), *Tectonics*, *28*, TC5016, doi:10.1029/2008TC002419.

Lustrino, M., S. Duggen, and C. L. Rosenberg (2011), The Central-Western Mediterranean: Anomalous igneous activity in an anomalous collisional setting, *Earth Sci. Rev.*, *104*, 1–40.

Magni, V., C. Faccenna, J. van Hunen, and F. Funiciello (2013), Delamination vs. break-off: The fate of continental collision, *Geophys. Res. Lett.*, *40*, 285–289, doi:10.1002/grl.50090.

Malinverno, A., and W. B. F. Ryan (1986), Extension on the Tyrrhenian Sea and shortening in the Apennines as results of arc migration driven by sinking of the lithosphere, *Tectonics*, *5*, 227–245, doi:10.1029/TC005i002p00227.

Margheriti, L., F. P. Lucente, and S. Pondrelli (2003), SKS splitting measurements in the Apenninic-Tyrrhenian domain (Italy) and their relation with lithospheric subduction and mantle convection, *J. Geophys. Res.*, *108*(B4), 2218, doi:10.1029/2002JB001793.

Mattei, M., P. Cipollari, D. Cosentino, A. Argentieri, F. Rossetti, F. Speranza, and L. Di Bella (2002), The Miocene tectono-sedimentary evolution of the southern Tyrrhenian Sea: Stratigraphy, structural and palaeomagnetic data from the on-shore Amantea basin (Calabrian Arc, Italy), *Basin Res.*, *14*, 147–168.

Mauffret, A. (2007), The northwestern (Maghreb) boundary of the Nubia (Africa) plate, *Tectonophysics*, *429*, 21–44.

Maury, C., R. Fourcade, S. Coulon, C. Bellon, H. Coutelle, A. Ouabadi, and J. P. Réhault (2000), Post-collisional Neogene magmatism of the Mediterranean Maghreb margin: A consequence of slab breakoff, *C.R. Acad. Sci., Ser. IIa: Sci. Terre Planets*, *331*(3), 159–173.

Mazzoli, S., and M. Helman (1994), Neogene patterns of relative plate motion for Africa-Europe: Some implications for recent central Mediterranean tectonics, *Geol. Rundsch.*, *83*(2), 464–468.

McClusky, S., et al. (2000), Global Positioning System constraints on plate kinematics and dynamics in the eastern Mediterranean and Caucasus, *J. Geophys. Res.*, *105*, 5695–5720, doi:10.1029/1996JB900351.

McClusky, S., R. Reilinger, S. Mahmoud, D. Ben Sari, and A. Tealeb (2003), GPS constraints on Africa (Nubia) and Arabia plate motions, *Geophys. J. Int.*, *155*(1), 126–138.

McKenzie, D. P. (1970), Plate tectonics of the Mediterranean region, *Nature*, *226*, 239–43.
McKenzie, D. (1972), Active tectonics in the Mediterranean region, *Geophys. J. R. Astron. Soc.*, *30*, 109–185.
McKenzie, D. P. (1978), Active tectonics of the Alpine-Himalayan belt: The Aegean Sea and surrounding regions, *Geophys. J. R. Astron. Soc.*, *55*, 217–254.
McQuarrie, N., J. M. Stock, C. Verdel, and B. P. Wernicke (2003), Cenozoic evolution of Neotethys and implications for the causes of plate motions, *Geophys. Res. Lett.*, *30*, 2036, doi:10.1029/2003GL017992.
Meghraoui, M., and S. Pondrelli (2013), Active faulting and transpression tectonics along the plate boundary in North Africa, *Ann. Geophys.-Italy*, doi:10.4401/ag-4970.
Meghraoui, M., et al. (2003), Evidence for 830 years of seismic quiescence from palaeoseismology, archaeoseismology and historical seismicity along the Dead Sea fault in Syria, *Earth Planet. Sci. Lett.*, *210*, 35–52.
Meghraoui, M., S. Maouche, B. Chemaa, Z. Cakir, A. Aoudia, A. Harbi, P. J. Alasset, A. Ayadi, Y. Bouhada, and F. Benhamouda (2004), Coastal uplift and thrust faulting associated with the $M = 6.8$ Zemmouri (Algeria) earthquake of 21 May 2003, *Geophys. Res. Lett.*, *31*, L19605, doi:10.1029/2004GL020466.
Meissner, R., W. D. Mooney, and I. Artemieva (2002), Seismic anisotropy and mantle creep in young orogens, *Geophys. J. Int.*, *149*(1), 1–14.
Mercier, J. L., E. Carey, H. Philipand, and D. Sorel (1976), La néotectonique plio-quaternaire de l'arc egéen externe et de la Mer égée et ses relations avec seismicité, *Bull. Soc. Geol. Fr.*, *18*, 159–176.
Miller, M. S., and N. Piana Agostinetti (2012), Insights into the evolution of the Italian lithospheric structure from S receiver function analysis, *Earth Planet. Sci. Lett.*, *345*, 49–59, doi:10.1016/j.epsl.2012.06.028.
Miller, M. S., and T. W. Becker (2013), Reactivated lithospheric-scale discontinuities localize dynamic uplift of the Moroccan Atlas. *Geology*, *42*(1), 35-38, doi:10.1130/G34959.1.
Miller, M. S., A. A. Allam, T. W. Becker, J. Di Leo, and J. Wookey (2013), Constraints on the geodynamic evolution of the westernmost Mediterranean and northwestern Africa from shear wave splitting analysis, *Earth Planet. Sci. Lett.*, *375*, 234–243.
Miller, M. S., and T. W. Becker (2012), Mantle flow deflected by interactions between subducted slabs and cratonic keels, *Nat. Geosci.*, *5*, 726–730, doi:10.1038/ngeo1553.
Milner, K., T. W. Becker, L. Boschi, J. Sain, D. Schorlemmer, and H. Waterhouse (2009), The Solid Earth Research and Teaching Environment: A new software framework to share research tools in the classroom and across disciplines, *Eos Trans. AGU*, *90*, 12, doi:10.1029/2009EO120005.
Minelli, L., and C. Faccenna (2010), Evolution of the Calabrian accretionary wedge (central Mediterranean), *Tectonics*, *29*, TC4004, doi:10.1029/2009TC002562.
Mitterbauer, U., M. Behm, E. Brückl, R. Lippitsch, A. Guterch, G. R. Keller, E. Koslovskaya, E.-M. Rumpfhuber, and F. Šumanovac (2011), Shape and origin of the East-Alpine slab constrained by the ALPASS teleseismic model, *Tectonophysics*, *510*, 195–206.
Molnar, P., and T. Atwater (1978), Interarc spreading and cordilleran tectonics as alternates related to the age of subducted oceanic lithosphere, *Earth Planet. Sci. Lett.*, *41*, 330–340.
Molnar, P., and K. E. Dayem (2010), Major intracontinental strike-slip faults and contrasts in lithospheric strength, *Geosphere*, *6*, 444–467.
Molinari, I., and A. Morelli (2011), EPcrust: A reference crustal model for the European Plate, *Geophys. J. Int.*, *185*, 352–364, doi:10.1111/j.1365-246X.2011.04940.x.
Molnar, P., and D. Gray (1979), Subduction of continental lithosphere: Some constraints and uncertainties, *Geology*, *7*, 58–62.
Molnar, P., and G. A. Houseman (2004), Effects of buoyant crust on the gravitational instability of thickened mantle lithosphere at zones of intracontinental convergence, *Geophys. J. Int.*, *158*, 1134–1150.
Montagner, J.-P. (1998), Where can seismic anisotropy be detected in the Earth's mantle? In boundary layers, *Pure Appl. Geophys.*, *151*, 223–256.
Montagner, J.-P., D. A. Griot-Pommera, and J. Lave (2000), How to relate body wave and surface wave anisotropy?, *J. Geophys. Res.*, *105*, 19,015–19,027, doi:10.1029/2000JB900015.
Montone, P., M. T. Mariucci, S. Pondrelli, and A. Amato (2004), An improbe stress map for Italy and surrounding regions (central Mediterranean), *J. Geophys. Res.*, *109*, B10410, doi:10.1029/2003JB002703.
Moucha, R., and A. Forte (2011), Changes in African topography driven by mantle convection, *Nat. Geosci.*, *4*(10), 707–712.
Nicolosi, I., F. Speranza, and M. Chiappini (2006), Ultrafast oceanic spreading of the Marsili Basin, southern Tyrrhenian Sea: Evidence from magmatic anomaly analysis, *Geology*, *34*, 717–720, doi:10.1130/G22555.1.
Nocquet, J.-M. (2012), Present-day kinematics of the Mediterranean: A comprehensive overview of GPS results, *Tectonophysics*, *579*, 220–242, doi:10.1016/j.tecto.2012.03.037.
Nolet, G., R. Allen, and D. Zhao (2007), Mantle plume tomography, *Chem. Geol.*, *241*, 248–263, doi:10.1016/j.chemgeo.2007.01.022.
Nyst, M., and W. Thatcher (2004), New constraints on the active tectonic deformation of the Aegean, *J. Geophys. Res.*, *109*, B11406, doi:10.1029/2003JB002830.
Oldow, J. S., L. Ferranti, D. S. Lewis, J. K. Campbell, B. D'Argenio, R. Catalano, G. Pappone, L. Carmignani, P. Conti, and C. Aiken (2002), Active fragmentation of Adria, the north Africa promontory, central Mediterranean orogen, *Geology*, *30*, 779–782.
Olivet, J. L. (1996), Cinematique de la plaque Iberique, *Bull. Cent. Rech. Explor. Prod. Elf-Aquitaine*, *20*, 131–195.
Panza, G., R. B. Raykova, E. Carminati, and C. Doglioni (2007), Upper mantle flow in the western Mediterranean, *Earth Planet. Sci. Lett.*, *257*, 200–214.
Parés, J. M., R. Freeman, and E. Roca (1992), Neogene structural development in the Valencia trough margins from paleomagnetic data, *Tectonophysics*, *203*, 111–124.
Patacca, E., R. Sartori, and P. Scandone (1993), Tyrrhenian basin and Apennines. Kinematic evolution and related dynamic constraints, in *Recent Evolution and Seismicity of the Mediterranean Region*, pp. 161–171, Springer, Netherlands.
Peterschmitt, E. (1956), Quelque donnee nouvelles sur les seismes profond de la Mer Tyrrhenienne, *Ann. Geophys.*, *9*(3), 305–334.
Piana Agostinetti, N., and A. Amato (2009), Moho depth and V_P/V_S ratio in peninsular Italy from teleseismic receiver functions, *J. Geophys. Res.*, *114*, B06303, doi:10.1029/2008JB005899.
Piromallo, C., and C. Faccenna (2004), How deep can we find the traces of Alpine subduction?, *Geophys. Res. Lett.*, *31*, L06605, doi:10.1029/2003GL019288.
Piromallo, C., and A. Morelli (2003), *P* wave tomography of the mantle under the Alpine-Mediterranean area, *J. Geophys. Res.*, *108*(B2), 2065, doi:10.1029/2002JB001757.
Piromallo, C., A. P. Vincent, D. A. Yuen, and A. Morelli (2001), Dynamics of the transition zone under Europe inferred from wavelet cross-spectra of seismic tomography, *Phys. Earth Planet. Inter.*, *125*, 125–139, doi:10.1016/S0031-9201(01)00249-7.
Piromallo, C., T. W. Becker, F. Funiciello, and C. Faccenna (2006), Three-dimensional instantaneous mantle flow induced by subduction, *Geophys. Res. Lett.*, *33*, L08304, doi:10.1029/2005GL025390.

Platt, J. P., and M. J. Whitehouse (1999), Early Miocene high-temperature metamorphism and rapid exhumation in the Betic Cordillera (Spain): Evidence from U-Pb zircon ages, *Earth Planet. Sci. Lett.*, *171*, 591–605.
Platt, J. P., S. Allerton, A. Kirker, C. Mandeville, A. Mayfield, and E. S. Platzman (2003), The ultimate arc: Differential displacement, oroclinal bending, and vertical axis rotation in the External Betic-Rif arc, *Tectonics*, *22*(3), 1017, doi:10.1029/2001TC001321.
Platt, P., W. Behr, K. Johanesen, and J. R. Williams (2013), The Betic-Rif arc and its orogenic hinterland: A review, *Ann. Rev. Earth Planet. Sci.*, *41*, 313–357.
Plomerová, J., L. Margheriti, J. Park, V. Babuska, S. Pondrelli, L. Vecsey, D. Piccinini, V. Levin, P. Baccheschi, and S. Salimbeni (2006), Seismic anisotropy beneath the Northern Apennines (Italy): Mantle flow or lithosphere fabric?, *Earth Planet. Sci. Lett.*, *247*, 157–170.
Polonia, A., et al. (2004), Holocene slip rate of the North Anatolian Fault beneath the Sea of Marmara, *Earth Planet. Sci. Lett.*, *227*, 411–426.
Polonia, A., G. Panieri, L. Gasperini, A. Gasparotto, L. G. Bellucci, and L. Torelli (2013), Turbidite paleoseismology in the Calabrian Arc Subduction Complex (Ionian Sea), *Geochem. Geophys. Geosyst.*, *14*, 112–140, doi:10.1029/2012GC004402.
Pondrelli, S., C. Piromallo, and E. Serpelloni (2004), Convergence vs. retreat in Southern Tyrrhenian Sea: Insights from kinematics, *Geophys. Res. Lett.*, *31*, L06611, doi:10.1029/2003GL019223.
Presti, D., A. Billi, B. Orecchio, C. Totaro, C. Faccenna, and G. Neri (2013), Earthquake focal mechanisms, seismogenic stress, and seismotectonics of the Calabrian Arc, Italy, *Tectonophysics*, *602*, 153–175, doi:10.1016/j.tecto.2013.01.030.
Pucci, S., P. M. De Martini, and D. Pantosti (2008), Preliminary slip rate estimates for the Düzce segment of the North Anatolian fault zone from offset geomorphic markers, *Geomorphology*, *97*, 538–554, doi:10.1016/j.geomorph.2007.09.002.
Rebischung, P., J. Griffiths, J. Ray, R. Schmid, X. Collilieux, and B. Garayt (2011), IGS08: The IGS realization of ITRF2008, *GPS Solution*, doi:10.1007/s10291-011-0248-2.
Reilinger, R., et al. (2006), GPS constraints on continental deformation in the Africa-Arabia-Eurasia continental collision zone and implications for the dynamics of plate interactions, *J. Geophys. Res.*, *111*, B05411, doi:10.1029/2005JB004051.
Reilinger, R., and S. McClusky (2011), Nubia-Arabia-Eurasia plate motions and the dynamics of Mediterranean and Middle East tectonics, *Geophys. J. Int.*, *186*, 971–979, doi:10.1111/j.1365-246X.2011.05133.x.
Reilinger, R. E., S. C. McClusky, and M. B. Oral (1997), GPS measurements of present day crustal movements in the Arabia-Africa-Eurasia plate collision zone, *J. Geophys. Res.*, *102*, 9983–9999, doi:10.1029/96JB03736.
Ren, Y., G. W. Stuart, G. A. Houseman, B. Dando, C. Ionescu, E. Hegedüs, S. Radovanović, Y. Shen, and South Carpathian Project working group (2012), Upper mantle structures beneath the Carpathian-Pannonian region: Implications for the geodynamics of continental collision, *Earth Planet. Sci. Lett.*, *349–350*, 139–152.
Ribe, N. (2010), Bending mechanics and mode selection in free subduction: A thin-sheet analysis, *Geophys. J. Int.*, *180*, 559–576, doi:10.1111/j.1365-246X.2009.04460.x.
Ricard, Y., and C. Vigny (1989), Mantle dynamics with induced plate tectonics, *J. Geophys. Res.*, *94*, 17,543–17,559, doi:10.1029/JB094iB12p17543.
Ricard, Y., L. Fleitout, and C. Froidevaux (1984), Geoid heights and lithospheric stresses for a dynamic Earth, *Ann. Geophys.*, *2*, 267–286.
Ricard, Y., M. A. Richards, C. Lithgow-Bertelloni, and Y. Le Stunff (1993), Geodynamic model of mantle density heterogeneity, *J. Geophys. Res.*, *98*, 21,895–21,909, doi:10.1029/93JB02216.
Richards, M. A., and B. H. Hager (1984), Geoid anomalies in a dynamic Earth, *J. Geophys. Res.*, *89*, 5987–6002, doi:10.1029/JB089iB07p05987.
Ricou, L. E. (1994), Tethys reconstructed - plates, continental fragments and their boundaries since 260-Ma from central-America to south-eastern Asia, *Geodinamica Acta*, *7*(4), 169–218.
Ring, U., J. Glodny, T. Will, and S. Thomson (2010), The Hellenic subduction system: High-pressure metamorphism, exhumation, normal faulting, and large-scale extension, *Annu. Rev. Earth Planet. Sci.*, *38*, 45–76, doi:10.1146/annurev.earth.050708.170910.
Rosenbaum, G., and G. S. Lister (2002), Reconstruction of the evolution of the Alpine-Himalayan orogen - An introduction, *J. Virtual Explorer*, *8*, 1–2.
Rosenbaum, G., G. Lister, and C. Duboz (2004), Relative motions of Africa, Iberia and Europe during Alpine orogeny, *Tectonophysics*, *359*, 117–129.
Royden, L. (1993), The tectonic expression of slab pull at continental convergent boundaries, *Tectonics*, *12*, 303–325, doi:10.1029/92TC02248.
Royden, L., and L. Husson (2006), Trench motion, slab geometry and viscous stresses in subduction systems, *Geophys. J. Int.*, *167*, 881–905, doi:10.1111/j.1365-246X.2006.03079.x.
Royden, L., and L. Husson, (2009), Subduction with variations in slab buoyancy: Models and application to the Banda and Apennine systems, in *Subduction Zone Geodynamics*, edited by F. Funiciello and S. Lallemand, *Frontiers in Earth Sciences*, Springer-Verlag, Berlin Heidelberg, doi:10.1007/978-3-540-87974-9.
Royden, L., E. Patacca, and P. Scandone (1987), Segmentation and configuration of subducted lithosphere in Italy - An important control on thrust-belt and foredeep-basin Evolution, *Geology*, *15*, 714–717.
Royden, L. H., and D. J. Papanikolaou (2011), Slab segmentation and late Cenozoic disruption of the Hellenic arc, *Geochem. Geophys. Geosyst.*, *12*, Q03010, doi:10.1029/2010GC003280.
Sanchez-Gomez, M., D. Avigad, and A. Heiman (2002), Geochronology of clasts in allochthonous Miocene sedimentary sequences on Mykonos and Paros islands: implications for back-arc extension in the Aegean Sea, *J. Geol. Soc. London*, *159*, 45–55.
Sandvol, E., N. Turkelli, E. Zor, R. Gok, T. Bekler, C. Gurbuz, D. Seber, and M. Barazangi (2003), Shear wave splitting in a young continent-continent collision: An example from Eastern Turkey, *Geophys. Res. Lett.*, *30*(24), 8041, doi:10.1029/2003GL017390.
Saria, E., E. Calais, Z. Altamimi, P. Willis, and H. Farah (2013), A new velocity field for Africa from combined GPS and DORIS space geodetic solutions: Contribution to the definition of the African Reference Frame (AFREF), *J. Geophys. Res. Solid Earth*, *118*, 1677–1697, doi:10.1002/jgrb.50137.
Sartori, R. (1990), The main results of ODP Leg 107 in the frame of Neogene to recent geology of perityrrhenian areas, in *Proc. ODP Sci. Res*, vol. 107, edited by K. A. Kastens et al., pp. 715–730, Ocean Drilling Program, College Station, Tex.
Savage, M. K. (1999), Seismic anisotropy and mantle deformation: What have we learned from shear wave splitting?, *Rev. Geophys.*, *37*, 65–106, doi:10.1029/98RG02075.
Savostin, L. A., J.-C. Sibuet, L. P. Zonenshain, X. Le Pichon, and M.-J. Roulet (1986), Kinematic evolution of the Tethys Belt from the Atlantic Ocean to the Pamirs since Triassic, *Tectonophysics*, *123*, 1–35.
Schaefer, J. F., L. Boschi, T. W. Becker, and E. Kissling (2011), Radial anisotropy in the European mantle: Tomographic studies explored in terms of mantle flow, *Geophys. Res. Lett.*, *38*, L23304, doi:10.1029/2011GL049687.
Scharf, A., M. R. Handy, S. Favaro, S. M. Schmid, and A. Bertrand (2013), Modes of orogen-parallel stretching and extensional exhumation in response to microplate indentation and roll-back subduction (Tauern Window, Eastern Alps), *Int. J. Earth Sci.*, doi:10.1007/s00531-013-0894-4.

Schefer, S., V. Cvetkovic, B. Fügenschuh, A. Kounov, M. Ovtcharova, U. Schaltegger, and S. M. Schmid (2011), Cenozoic granitoids in the Dinarides of southern Serbia: Age of intrusion, isotope geochemistry, exhumation history and significance for the geodynamic evolution of the Balkan Peninsula, *Int. J Earth Sci.*, *100*, 1181–1206, doi:10.1007/s00531-010-0599-x.

Schellart, W. P. (2005), Influence of the subducting plate velocity on the geometry of the slab and migration of the subduction hinge, *Earth Planet. Sci. Lett.*, *231*(3).

Schivardi, R., and A. Morelli (2009), Surface wave tomography in the European and Mediterranean region, *Geophys. J. Int.*, *177*, 1050–1066, doi:10.1111/j.1365-246X.2009.04100.x.

Schmandt, B., and E. Humphreys (2010), Complex subduction and small-scale convection revealed by body-wave tomography of the western United States upper mantle, *Earth Planet. Sci. Lett.*, *297*, 435–445, doi:10.1016/j.epsl.2010.06.047.

Schmid, C., S. van der Lee, and D. Giardini (2004), Delay times and shear wave splitting in the Mediterranean region, *Geophys. J. Int.*, *159*(1), 275–290, doi:10.1111/j.1365-246X.2004.02381.x.

Schmid, S. M., D. Bernoulli, B. Fügenschuh, L. Matenco, R. Schuster, S. Schefer, M. Tischler, and K. Ustaszewski (2008), The Alpine-Carpathian-Dinaridic orogenic system: Correlation and evolution of tectonic units, *Swiss J. Geosci.*, *101*, 139–183, doi:10.1007/s00015-008-1247-3.

Schmid, S. M., A. Scharf, M. R. Handy, and C. Rosenberg (2013), The Tauern Window (Eastern Alps. Austria): A new tectonic map, with cross-sections and a tectono metamorphic synthesis. *Swiss J. Geosci.*, 175–194, doi:10.1007/s00015-013-0123-y, in press.

Scotti, V. N., P. Molin, C. Faccenna, M. Soligo, and A. Casas-Sainz (2013), The influence of surface and tectonic processes on landscape evolution of the Iberian Chain (Spain): Quantitative geomorphological analysis and geochronology, *Geomorphology*, online 29 September 2013, ISSN 0169-555X, doi:10.1016/j.geomorph.2013.09.017.

Scrocca, D., et al. (Eds.) (2003), *CROP ATLAS: Seismic Reflection Profiles of the Italian Crust*, Mem, Desc.Carta Geol. Ital, vol. 62, 193 pp., Ist. Poligrafico e Zecca dello Stato, Roma.

Selvaggi, G., and C. Chiarabba (1995), Seismicity and *P* wave velocity image of the Southern Tyrrhenian subduction zone, *Geophys. J. Int.*, *121*, 818–826.

Şengör, A. M. C., S. Özeren, T. Genç, and E. Zor (2003), East Anatolian high plateau as a mantle-supported, north-south shortened domal structure, *Geophys. Res. Lett.*, *30*(24), 8045, doi:10.1029/2003GL017858.

Sengor, A. M. C., O. Tuysuz, C. Imren, M. Sakinc, H. Eyidogan, N. Gorur, X. Le Pichon, and C. Rangin (2005), The North Anatolian Fault: A new look, *Annu. Rev. Earth Planet. Sci.*, *33*, 37–1112, doi:10.1146/Annrev.earth.32.101802.120415.

Şengör, A. M. C., M. S. Özeren, M. Keskin, M. Sakınç, A. D. Özbakır, and I. Kayan (2008), Eastern Turkish high plateau as a small Turkic-type orogen: Implications for post-collisional crust-forming processes in Turkic-type orogens, *Earth Sci. Rev.*, *90*(1–2), 1–48, doi:10.1016/j.earscirev.2008.05.002.

Seranne, M. (1999), The Gulf of Lion continental margin (NW Mediterranean) revisited by IBS: An overview, in *The Mediterranean Basins: Tertiary Extension Within the Alpine Orogen*, *Geol. Soc. Spec. Publ.,* vol. 156, edited by B. Durand et al., pp. 21–53, Geol. Soc. of London, U. K.

Serpelloni, E., M. Anzidei, P. Baldi, G. Casula, and A. Galvani (2005), Crustal velocity and strain-rate fields in Italy and surrounding regions: New results from the analysis of permanent and non-permanent GPS networks, *Geophys. J. Int.*, *161*, 861–880.

Serpelloni, E., G. Vannucci, S. Pondrelli, A. Argnani, G. Casula, M. Anzidei, P. Baldi, and P. Gasperini (2007), Kinematics of the western Africa-Eurasia plate boundary from local mechanisms and GPS data, *Geophys. J. Int.*, *169*, 1180–1200.

Serpelloni, E., R. Bürgmann, M. Anzidei, P. Baldi, B. Mastrolembo Ventura, and E. Boschi (2010), Strain accumulation across the Messina Straits and kinematics of Sicily and Calabria from GPS data and dislocation modeling, *Earth Planet. Sci. Lett.*, *298*(3–4), 347–360, doi:10.1016/j.epsl.2010.08.005.

Serpelloni, E., C. Faccenna, G. Spada, D. Dong and S. D. P. Williams (2013), Vertical GPS ground motion rates in the Euro-Mediterranean region: New evidence of velocity gradients at different spatial scales along the Nubia-Eurasia plate boundary, *J. Geophys. Res. Solid Earth*, *118*, 6003–6024, doi:10.1002/2013JB010102.

Shaw, M., and R. Pysklywec (2007), Anomalous uplift of the Apennines and subsidence of the Adriatic: The result of active mantle flow?, *Geophys. Res. Lett.*, *34*, L04311, doi:10.1029/2006GL028337.

Silver, P. (1996), Seismic anisotropy beneath the continents: Probing the depths of geology, *Annual Rev. Earth Planet. Sci.*, *24*, 385–432.

Silver, P. G., R. M. Russo, and C. Lithgow-Bertelloni (1998), Coupling of South American and African Plate motion and Plate deformation, *Science*, *279*(5347), 60–63.

Simmons, N., A. Forte, and S. P. Grand (2009), Joint seismic, geodynamic and mineral physical constraints on three-dimensional mantle heterogeneity: Implications for the relative importance of thermal versus compositional heterogeneity, *Geophys. J. Int.*, *177*, 1284–1304, doi:10.1111/j.1365-246X.2009.04133.x.

Sinclair, H. (1997), Flysch to molasses transition in peripheral foreland basin: The role of the passive margin versus slab break-of, *Geology*, *25*(12), 1123–1126.

Smith, A. (1971), Alpine deformation and the oceanic areas of the Tethys, Mediterranean and the Atlantic, *Bull. Geol. Soc. Am.*, *82*, 2039–2070.

Smith, W. H. F., and P. Wessel (1990), Gridding with continuous curvature splines in tension, *Geophysics*, *55*, 293–305.

Spakman, W. (1990), Tomographic images of the upper mantle below central Europe and the Mediterranean, *Terra Nova*, *2*, 542–553.

Spakman, W., and R. Wortel (2004), A tomographic view on Western Mediterranean geodynamics, in *The TRANSMED Atlas - The Mediterranean Region From Crust to Mantle*, edited by W. Cavazza et al., pp. 31–52, Springer, Berlin, Heidelberg.

Spakman, W., S. van der Lee, and R. D. van der Hilst (1993), Travel-time tomography of the European-Mediterranean mantle down to 1400 km, *Phys. Earth Planet. Inter.*, *79*(1–2), 3–74, doi:10.1016/0031-9201(93)90142-V.

Speranza, F., L. Minelli, A. Pignatelli, and M. Chiappini (2012), The Ionian Sea: The oldest in situ ocean fragment of the world?, *J. Geophys. Res.*, *117*, B12101, doi:10.1029/2012JB009475.

Stadler, G., M. Gurnis, C. Burstedde, L. C. Wilcox, L. Alisic, and O. Ghattas (2010), The dynamics of plate tectonics and mantle flow: From local to global scales, *Science*, *329*, 1033–1038.

Stegman, D. R., R. Farrington, F. A. Capitanio, and W. P. Schellart (2010), A regime diagram for subduction styles from 3-D numerical models of free subduction, *Tectonophysics*, *483*, 29–45, doi:10.1016/j.tecto.2009.08.041.

Stein, S., and G. Sella (2005), Pleistocene change from convergence to extension in the Apennines as a consequence of Adria microplate motion, in *The Adria Microplate: GPS Geodesy, Tectonics and Hazards*, *Nato Sci. Ser.,* edited by N. Pinter et al., pp. 21–34, Springer, Berlin, Germany.

Stich, D., E. Serpelloni, F. de Lis Mancilla, and J. Morales (2006), Kinematics of the Iberia–Maghreb plate contact from seismic moment tensors and GPS observations, *Tectonophysics*, *426*(3–4), 295–317, doi:10.1016/j.tecto.2006.08.004.

Stich, D., F. D. Mancilla, D. Baumont, and J. Morales (2005), Source analysis of the M_w 6.3 2004 Al Hoceima earthquake (Morocco) using regional apparent source time functions, *J. Geophys. Res.*, *110*, B06306, doi:10.1029/2004JB003366.

Stojadinovic, U., L. Matenco, P. A. M. Andriessen, M. Toljic, and J. P. T. Foeken (2012), The balance between orogenic building and subsequent extension during the Tertiary evolution of the NE Dinarides: Constraints from low-temperature thermochronology, *Global Planet. Change*, *103*, 19–38, doi:10.1016/j.gloplacha.2012.08.004.

Tapponnier, P. (1977), Evolution tectonique du systeme alpine en Meéditerranee: Poincement et ecrasement rigide-plastique, *Bull. Soc. Geol. Fr.*, *7*, 437–460.

Teixell, A., P. Ayarza, H. Zeyen, M. Fernandez, and M. L. Arboleya (2005), Effects of mantle upwelling in a compressional setting: The Atlas Mountains of Morocco, *Terra Nova*, *17*, 456–461.

Tesauro, M., M. K. Kaban, and S. A. P. L. Cloetingh (2008), EuCRUST-07: A new reference model for the European crust, *Geophys. Res. Lett.*, *35*, L05313, doi:10.1029/2007GL032244.

Thatcher, W. (2009), How the continents deform: The evidence from tectonic geodesy, *Ann. Rev. Earth Planet. Sci.*, *37*, 237–262.

Tirel, C., J.-P. Brun, E. Burov, M. J. R. Wortel, and S. Lebedev (2013), A plate tectonics oddity: Caterpillar-walk exhumation of subducted continental crust, *Geology*, *41*(5), 555–558, doi:10.1130/G33862.1.

Torelli, L., M. Grasso, G. Mazzoldi, D. Peis, and D. Gori (1995), Cretaceous to Neogene structural evolution of the Lampedusa shelf (Pelagian Sea, Central Mediterranean), *Terra Nova*, *7*, 200–212.

Torné, M., M. Fernandez, M. C. Comas, and J. Soto (2000), Lithospheric structures beneath the Alboran Basin: Results from three-dimensional gravity modeling and tectonic relevance, *J. Geophys. Res.*, *105*, 3209–3228, doi:10.1029/1999JB900281.

Ustaszewski, K., A. Kounov, S. M. Schmid, U. Schaltegger, E. Krenn, W. Frank, and B. Fügenschuh (2010), Evolution of the Adria-Europe plate boundary in the northern Dinarides: From continent-continent collision to back-arc extension, *Tectonics*, *29*, TC6017, doi:10.1029/2010TC002668.

Ustaszewski, K., S. M. Schmid, B. Fügenschuh, M. Tischler, E. Kissling, and W. Spakman (2008), A map-view restoration of the Alpine-Carpathian-Dinaridic system for the early Miocene, *Swiss J. Geosci.*, *101*(suppl 1), 273–294.

Valensise, L., and D. Pantosti (1992), A 125 kyr-long geological record of seismic source repeatability: The Messina Straits (southern Italy) and the 1908 earthquake ($M_s = 7½$), *Terra Nova*, *4*, 472–483.

Van der Voo, R. (1993), *Paleomagnetism of the Atlantic Thethys and Iapetus Oceans*, Cambridge Univ. Press, New York.

van Hinsbergen, D. J. J., and S. M. Schmid (2012), Map-view restoration of Aegean-west Anatolian accretion and extension since the Eocene, *Tectonics*, *31*, TC5005, doi:10.1029/2012TC003132.

van Hinsbergen, D. J. J., E. Hafkenscheid, W. Spakman, J. E. Meulenkamp, and R. Wortel (2005), Nappe stacking resulting from subduction of oceanic and continental lithosphere below Greece, *Geology*, *33*(4), 325–328.

van Hinsbergen, D. J. J., N. Kaymakci, W. Spakman, and T. H. Torsvik (2010), Reconciling the geological history of western Turkey with plate circuits and mantle tomography, *Earth Planet. Sci. Lett.*, *297*, 674–686.

van Hinsbergen, D. J. J., R. L. M. Vissers, and W. Spakman (2014), Origin and consequences of western Mediterranean subduction, rollback, and slab segmentation, *Tectonics*, doi:10.1002/2013TC003349.

Vanacore, E. A., T. Taymaz, and E. Saygin (2013), Moho structure of the Anatolian Plate from receiver function analysis, *Geophys. J. Int.*, *93*, 329–337, doi:10.1093/gji/ggs107.

Vannucci, G., S. Pondrelli, A. Argnani, A. Morelli, P. Gasperini, and E. Boschi (2004), An atlas of Mediterranean seismicity, *Ann. Geophys.*, *47*, 247–302.

Vergés, J., and F. Sàbat (1999), Constraints on the western Mediterranean kinematics evolution along a 1,000-km transect from Iberia to Africa, in *The Mediterranean Basins: Tertiary Extension Within the Alpine Orogen*, *Geol. Soc. Spec. Publ.,* vol. 156, edited by B. Duran et al., pp. 63–80, Geol. Soc. of London, U. K.

Verges, J., and M. Fernandez (2012), Tethys-Atlantic interaction along the Iberia-Africa plate boundary: The Betic-Rif orogenic system, *Tectonophysics*, *579*, 144–172.

Vernant, P., F. Nilforoushan, D. Hatzfeld, M. R. Abbassi, C. Vigny, F. Masson, and J. Chéry (2004), Present-day crustal deformation and plate kinematics in the Middle East constrained by GPS measurements in Iran and northern Oman, *Geophys. J. Int.*, *157*(1), 381–398.

Vigny, C., P. Huchon, J. C. Ruegg, K. Khanbari, and L. M. Asfaw (2006), Confirmation of Arabia plate slow motion by new GPS data in Yemen, *J. Geophys. Res.*, *111*, B02402, doi:10.1029/2004JB003229.

Wallace, L. M., S. Ellis, and P. Mann (2009), Collisional model for rapid fore-arc block rotations, arc curvature, and episodic back-arc rifting in subduction settings, *Geochem. Geophys. Geosyst.*, *10*, Q05001, doi:10.1029/2008GC002220.

Wdowinski, S.,Y. Bock, G. Baer, L. Prawirodirdjo, N. Bechor, S. Naaman Knafo, Y. Forrai, and Y. Melzer (2004), GPS measurements of current crustal movements along the Dead Sea Fault, *J. Geophys. Res.*, *109*, B05403, doi:10.1029/2003JB002640.

Westaway, R. (1990), Present-day kinematics of the plate boundary zone between Africa and Europe, from the Azores to the Aegean, *Earth Planet. Sci. Lett.*, *96*, 393–406.

Westaway, R. (2003), Kinematics of the Middle East and eastern Mediterranean updated, *Turk. J. Earth Sci.*, *12*, 5–46.

Westaway, R. (2004), Kinematic consistency between the Dead Sea Fault Zone and the Neogene and Quaternary left-lateral faulting in SE Turkey, *Tectonophysics*, *391*, 203–237.

Wortel, M. J. R., and W. Spakman (1992), Structure and dynamics of subducted lithosphere in the Mediterranean region, *Proc. K. Ned. Akad. Wet.*, *95*(3), 325–347.

Wortel, M. J. R., and W. Spakman (2000), Subduction and slab detachment in the Mediterranean-Carpathian region, *Science*, *290*, 1910–1917.

Wuestefeld, A., G. H. R. Bokelmann, G. Barruol, and J. P. Montagner (2009), Identifying global seismic anisotropy patterns by correlating shear-wave splitting and surface-wave data, *Phys. Earth Planet. Int.*, *176*, 198–212.

Zeck, H. P. (1999), Alpine kinematic evolution in the W Mediterranean: A W-ward directed subduction regime followed by slab roll-back and slab detachment, in *The Mediterranean Basin: Tertiary Extension Within the Alpine Orogen*, *Geol. Soc. Spec. Publ.,* vol. 156, edited by B. Durand et al., pp. 109–120, Geol. Soc. of London, U. K.

Zhong, S., M. T. Zuber, L. Moresi, and M. Gurnis (2000), Role of temperature-dependent viscosity and surface plates in spherical shell models of mantle convection, *J. Geophys. Res.*, *105*, 11,063–11,082, doi:10.1029/2000JB900003.

Zhu, H., E. Bozdag, D. Peter, and J. Tromp (2012), Structure of the European upper mantle revealed by adjoint tomography, *Nat. Geosci.*, *5*, 493–498, doi:10.1038/ngeo1501.